# Computational Modeling-based Discovery of Novel Classes of Anti-inflammatory Drugs that Target Lanthionine Synthetase C-like Protein 2

Pinyi Lu

Dissertation submitted to the faculty of the Virginia Polytechnic Institute and State University in partial fulfillment of the requirements for the degree of

Doctor of Philosophy
In
Genetics, Bioinformatics and Computational Biology

Josep Bassaganya-Riera, Chair
Raquel Hontecillas-Magarzo
David Bevan
Stefan Hoops

December 1, 2015
Blacksburg, VA

Keywords: Lanthionine synthetase C-like protein 2, inflammation, drug discovery, molecular modeling, *in silico* clinical trial

Computational Modeling-based Discovery of Novel Classes of Anti-inflammatory Drugs that Target Lanthionine Synthetase C-like Protein 2

Pinyi Lu

ABSTRACT

Lanthionine synthetase C-like protein 2 (LANCL2) is a member of the LANCL protein family, which is broadly expressed throughout the body. LANCL2 is the molecular target of abscisic acid (ABA), a compound with insulin-sensitizing and immune modulatory actions. LANCL2 is required for membrane binding and signaling of ABA in immune cells. Direct binding of ABA to LANCL2 was predicted *in silico* using molecular modeling approaches and validated experimentally using ligand-binding assays and kinetic surface plasmon resonance studies. The therapeutic potential of the LANCL2 pathway ranges from increasing cellular sensitivity to anticancer drugs, insulin-sensitizing effects and modulating immune and inflammatory responses in the context of immune-mediated and infectious diseases. A case for LANCL2-based drug discovery and development is also illustrated by the anti-inflammatory activity of novel LANCL2 ligands such as NSC61610 against inflammatory bowel disease in mice. This dissertation discusses the value of LANCL2 as a novel therapeutic target for the discovery and development of new classes of orally active drugs against chronic metabolic, immune-mediated and infectious diseases and as a validated target that can be used in precision medicine.

Specifically, in Chapter 2 of the dissertation, we performed homology modeling to construct a three-dimensional structure of LANCL2 using the crystal structure of LANCL1 as a template. Our molecular docking studies predicted that ABA and other PPAR γ agonists share a binding site on the surface of LANCL2.

In Chapter 3 of the dissertation, structure-based virtual screening was performed. Several potential ligands were identified using molecular docking. In order to validate the anti-inflammatory efficacy of the top ranked compound (NSC61610) in the NCI Diversity Set II, a series of *in vitro* and pre-clinical efficacy studies were performed using a mouse model of dextran sodium sulfate (DSS)-induced colitis.

In Chapter 4 of the dissertation, we developed a novel integrated approach for creating a synthetic patient population and testing the efficacy of the novel pre-clinical stage LANCL2 therapeutic for Crohn's disease in large clinical cohorts *in silico*. Efficacy of treatments on Crohn's disease was evaluated by analyzing predicted changes of Crohn's disease activity index (CDAI) scores and correlations with immunological variables were evaluated. The results from our placebo-controlled, randomized, Phase III *in silico* clinical trial at 6 weeks following the treatment shows a positive correlation between the initial disease activity score and the drop in CDAI score. This observation highlights the need for precision medicine strategies for IBD.

ACKNOWLEDGEMENT

This dissertation would have not been possible without the help, support, and guidance of my committee, colleagues, friends, family and many other people. It is with great pleasure and gratitude that I acknowledge their efforts.

Firstly, I would like to thank my PhD committee chair and my advisor Dr. Josep Bassaganya-Riera, who offered me tremendous mentoring, continuous support, and exemplary guidance throughout my doctoral training. I also thank the rest of my PhD committee members, Drs. Raquel Hontecillas-Magarzo, David Bevan, and Stefan Hoops, who have been supporting me with their expertise and resources on my research and sharing their abundant knowledge with me. Additionally, I would like to thank my Master committee members, Drs. Madhav Marathe, Josep Bassaganya-Riera, Kirk Cameron, and Calvin Ribbens, who offered me the opportunity to pursue the simultaneous Master degree of Computer Science.

I would like to thank the Genetics, Bioinformatics and Computational Biology (GBCB) program and thank Drs. David Bevan, Brett Tyler, and Ms. Dennie Munson, who have being tremendous help for me in this program, from application to graduation.

I would like to thank all my colleagues from Nutritional Immunology and Molecular Medicine Laboratory (NIMML), Center for Modeling Immunity to Enteric Pathogens (MIEP), and Virginia Bioinformatics Institute (VBI), who helped me, encouraged me, and inspired me throughout these years.

I would like to thank all my friends, especially those (Min Tang, Tian Hong, Fan Yang, and Xiaojin Sun) who helped me through the difficult times when I was suffering from health problems.

I would also like to thank the Badminton Club at VT, which made my life in Blacksburg more colorful and healthier.

Lastly, I would like to thank my family, especially my parents, Yuhong Chen and Jianguo Lu, for their love, encouragement and support during my doctoral training.

# ATTRIBUTION

Several colleagues aided in the research and writing of the papers presented as Chapter1, Chapter 2, Chapter 3, and Chapter 4 in this dissertation. Their contributions are included as follows.

Chapter 1 included my work "Lanthionine Synthetase Component C-like Protein 2: A New Drug Target for Inflammatory Diseases and Diabetes". This paper was published in 2014 in Current Drug Targets 15, no. 6 (2014): 565-572. I have permission from Bentham Science Publishers to use this chapter in my dissertation.

On Chapter 1, Dr. Raquel Hontecillas (an associate professor in Virginia Bioinformatics Institute at Virginia Tech) and Casandra W. Philipson (a PhD student in Nutritional Immunology and Molecular Medicine Laboratory at Virginia Tech), and Dr. Josep Bassaganya-Riera (a professor in Virginia Bioinformatics Institute at Virginia Tech) contributed to the manuscript writing.

Chapter 2 included my work "Molecular Modeling of Lanthionine Synthetase Component C-like Protein 2: A Potential Target for The Discovery of Novel Type 2 Diabetes Prophylactics and Therapeutics". This paper was published in 2011 in Journal of Molecular Modeling 17.3 (2011): 543-553. I have permission from Springer to use this chapter in my dissertation.

On Chapter 2, Dr. David R. Bevan (a professor in the Department of Biochemistry at Virginia Tech) and Stephanie N. Lewis (a PhD student in Dr. David R. Bevan's lab) contributed to analyzing the results. Dr. Hontecillas, and Dr. Josep Bassaganya-Riera contributed to the manuscript writing.

Chapter 3 included my work "Computational Modeling-based Discovery of Novel Classes of Anti-inflammatory Drugs that Target Lanthionine Synthetase C-like Protein 2". This paper was published in 2012 in PloS one 7.4 (2012): e34643. I have permission from PLOS to use this chapter in my dissertation.

On Chapter 3, Dr. Raquel Hontecillas, and Dr. Josep Bassaganya-Riera contributed to the manuscript writing. William T. Horne (previous lab manager in Nutritional Immunology and Molecular Medicine Laboratory at Virginia Tech), Adria Carbo (a PhD student in Nutritional Immunology and Molecular Medicine Laboratory at Virginia Tech), Monica Viladomiu (a PhD student in Nutritional Immunology and Molecular Medicine Laboratory at Virginia Tech), Mireia Pedragosa (a PhD student in Nutritional Immunology and Molecular Medicine Laboratory at Virginia Tech) contributed to performing animal studies. Dr. David R. Bevan and Stephanie N. Lewis contributed to analyzing the results.

Chapter 4 included my work "Phase III Placebo-Controlled, Randomized Clinical Trial with Synthetic Crohn's Disease Patients to Evaluate Treatment Response". This paper was under review by the book of Emerging Trends in Computational Biology, Bioinformatics, and Systems Biology–Systems & Applications, Elsevier.

On Chapter 4, Dr. Vida Abedi (an assistant professor in Virginia Bioinformatics Institute at Virginia Tech), Dr. Raquel Hontecillas, Meghna Verma (a PhD student in Nutritional Immunology and Molecular Medicine Laboratory at Virginia Tech), Gavin Vess (a undergraduate student in Nutritional Immunology and Molecular Medicine Laboratory at Virginia Tech), and Dr. Josep Bassaganya-Riera contributed to manuscript writing. Casandra W. Philipson, Adria Carbo, Andrew Leber (a PhD student in Nutritional Immunology and Molecular Medicine Laboratory at Virginia Tech), Nuria Tubau-Juni (a PhD student in Nutritional Immunology and Molecular Medicine Laboratory at Virginia Tech), Dr. Stefan Hoops (an assistant profess in Virginia Bioinformatics Institute at Virginia Tech) contributed to analyzing the results.

TABLE OF CONTENTS

# Chapter 1. Introduction--Lanthionine synthetase component C-like protein 2: A new drug target for inflammatory diseases and diabetes

**Pinyi Lu[1], Raquel Hontecillas[1], Casandra W. Philipson[1], and Josep Bassaganya-Riera[1, 2]**

Lu P, Hontecillas R, Philipson CW, Bassaganya-Riera J. Lanthionine synthetase component C-like protein 2: a new drug target for inflammatory diseases and diabetes. Current drug targets. 2014;15(6):565-72. Used with permission of Bentham Science Publishers, 2015.

[1]Nutritional Immunology and Molecular Medicine Laboratory, Virginia Bioinformatics Institute, Virginia Tech, Blacksburg, Virginia, USA, [2]Department of Biomedical Sciences and Pathobiology, Virginia-Maryland Regional College of Veterinary Medicine, Virginia Tech, Blacksburg, Virginia, USA.

CORRESPONDENCE: *To whom correspondence should be addressed at: Josep Bassaganya-Riera, Laboratory of Nutritional Immunology and Molecular Medicine Laboratory (www.nimml.org), Virginia Bioinformatics Institute, Virginia Tech, Blacksburg, VA 24061. Phone: (540) 231-7421, FAX: (540) 231-2606, and e-mail: jbassaga@vt.edu.

## 1.1 Abstract

Lanthionine synthetase component C-like protein 2 (LANCL2) is a member of the LANCL protein family, which is broadly expressed throughout the body. LANCL2 is the molecular target of abscisic acid (ABA), a compound with insulin-sensitizing and immune modulatory actions. LANCL2 is required for membrane binding and signaling of ABA in immune cells. Direct binding of ABA to LANCL2 was predicted *in silico* using molecular modeling approaches and validated experimentally using ligand-binding assays and kinetic surface plasmon resonance studies. The therapeutic potential of the LANCL2 pathway ranges from increasing cellular sensitivity to anticancer drugs, insulin-sensitizing effects and modulating immune and inflammatory responses in the context of immune-mediated and infectious diseases. A case for LANCL2-based drug discovery and development is also illustrated by the anti-inflammatory activity of novel LANCL2 ligands such as NSC61610 against inflammatory bowel disease and influenza-driven inflammation in mice. This review discusses the value of LANCL2 as a novel therapeutic target for the discovery and development of new classes of orally active drugs against chronic metabolic, immune-mediated and infectious diseases.

## 1.2 Introduction

The lanthionine synthetase C-like 2 (LANCL2) has emerged from an obscure protein expressed in brain and testes to a broadly expressed therapeutic target for chronic inflammatory, metabolic and immune-mediated diseases. LANCL2 received this name because it is the eukaryotic homologue of the prokaryotic lanthionine synthetase component C (LanC) protein (1). Prokaryotic LanC is a zinc-containing enzyme, which is also a part of the multimeric membrane associated lanthionine synthetase complex. The functions of LanC include modification and transport of peptides and producing lanthionines, the macrocyclic thioether analogs of cysteine by coordinating with specific dehydratases to facilitate intramolecular conjugation of cysteine to serine or threonine residues. Because of their potent antimicrobial activity, lanthionines are also known as lantibiotics (2, 3).

LANCL1 was the first member of the LANCL family isolated from human erythrocyte membranes (4). A related protein, LANCL2, was subsequently identified by Dr. Prohaska in various human tissues, such as brain, testis, heart, placenta, lung, liver, skeletal muscle, pancreas, thymus, and prostate (5), whose down-regulation resulted in anticancer drug resistance (6). LANCL2 is broadly expressed in human and mouse tissues, including immune cells, gastrointestinal tract and pancreas (5) (Fig. 1.1). LANCL2 overexpression increased cellular sensitivity to adriamycin, an anticancer drug, by suppressing the expression of MultiDrug-Resistance (MDR) 1 and P-glycoprotein (P-gp). Due to its original discovery in the testis, LANCL2 was also termed Testis-specific Adriamycin Sensitivity Protein (TASP) (6). Furthermore, LANCL2 plays a role in cytoskeletal reorganization and cellular movement by interacting with the actin cytoskeleton (7).

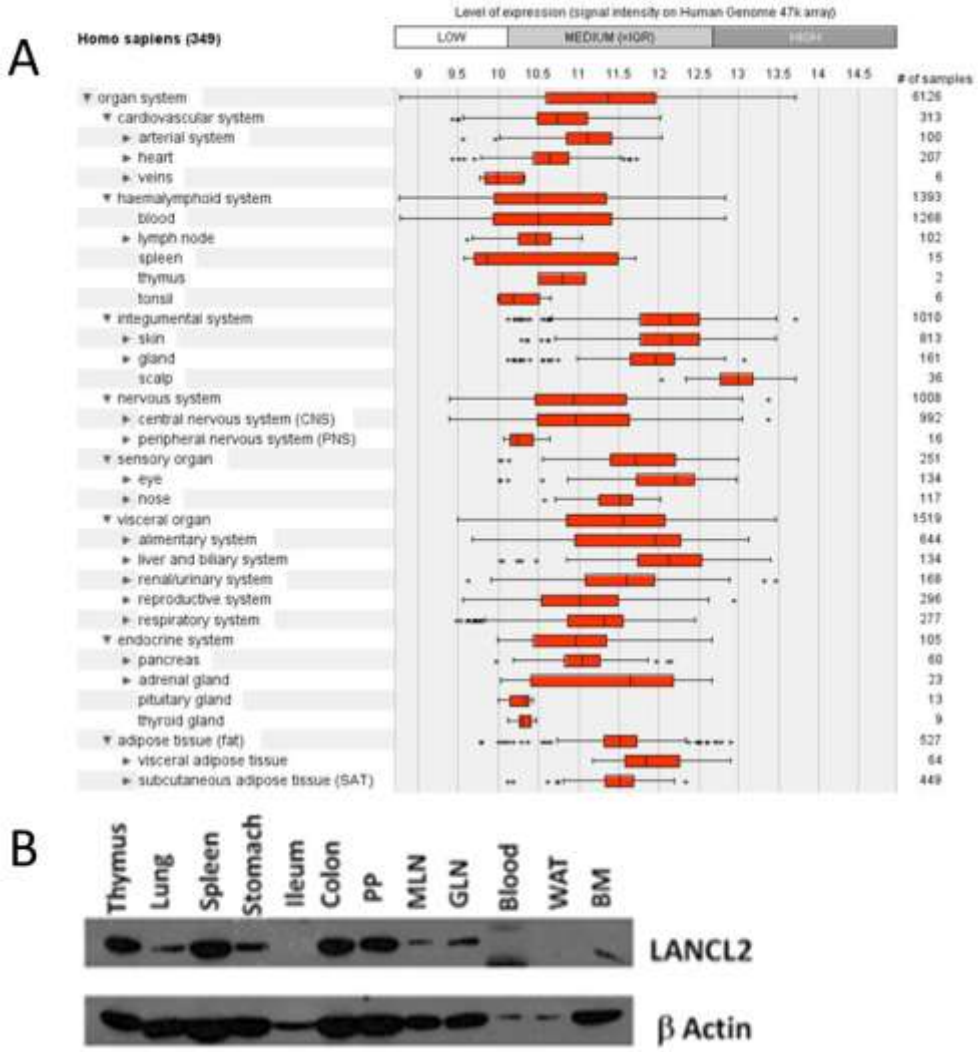


**Figure 1.1.** Lanthionine synthetase C-like 2 (LANCL2) expression in tissues of humans and mice. A. Meta-Profile analysis of LANCL2 gene expression using Geneinvesigator. The Anatomy tool was used to display how strongly LANCL2 gene is expressed in different anatomical categories in tissue level. The data is from *Homo sapiens.* Platform is Human 133_2: Human Genome 47k array. The level of expression within a tissue type is the average expression across all samples that were annotated with that particular tissue type. The number of samples is indicated on the right of the graph. The whiskers indicate the standard error of the mean. B. Pattern of expression of LANCL2 protein thymus, lung, spleen, stomach, ileum, colon, Peyer's patches (PP), mesenteric lymph nodes (MLN), gastric lymph nodes (GLN), blood, white adipose tissue (WAT) and bone marrow of mice.

LANCL2 is a membrane-associated protein required for membrane binding and signaling of abscisic acid (ABA) in granulocytes (8), suggesting that LANCL2 is the molecular target for ABA's immune modulatory actions. ABA is an isoprenoid phytohormone derived from the carotenoid biogenesis pathway discovered in the early 1960s that modulates plant responses to environmental stresses and host defense (9). The discovery of ABA biosynthesis in animal cells has generated considerable interest for its potential role as bioactive botanical, nutrient, hormone and therapeutic scaffold (10-12).

Our initial studies in mouse models of diabetes and inflammatory bowel disease (IBD) investigated the role of ABA as a potential agonist of a well-established therapeutic target for inflammation and diabetes: peroxisome proliferator-activated receptor (PPAR) γ. We demonstrated that ABA does not bind to PPAR γ. Mechanistic studies show that ABA-mediated downstream signaling requires expression of LANCL2 in immune cells (13). Indeed, we predicted for the first time that ABA binds to LANCL2 *in silico*. Moreover, by using molecular modeling approaches, the location of the potential binding site of LANCL2 for ABA was predicted (14). Direct binding of ABA to LANCL2 was also confirmed by a series of *in vitro* binding studies using human LANCL2 recombinant protein, including saturation binding, scintillation proximity assays, dot blot experiments, and affinity chromatography (15). We recently demonstrated binding of ABA to LANCL2 using kinetic surface plasmon resonance studies. Demonstration of ABA binding to LANCL2 is a key step for the discovery and development novel immune modulatory and anti-diabetic drugs that target LANCL2.

We employed an integrated translational medicine and drug discovery platform consisting of molecular modeling approaches followed by experimental validation to identify potential ligands of LANCL2. Large-scale screening of compound libraries was performed based on binding free energy between compounds and the LANCL2 binding site, thus identifying novel putative compounds for the treatment of inflammatory and chronic diseases. The follow-up functional studies show that the top ranked lead compound NSC61610, of the bis(benzimidazoyl)-terepthalanalides (BTTs) family, significantly ameliorated experimental inflammatory bowel disease (IBD) in mice (16).

The most favorable binding sites for ABA and NSC61610 are different, which indicates that LANCL2 might have multiple binding sites. ABA binds inside a pocket in LANCL2, which includes TYR279, LYS283, LYS284, PHE285, PRO291, ASN296 and SER295 (14). The predicted binding site of LANCL2 favored by NSC61610 is composed of ARG102, VAL103, TYR189, THR196, HIS410, ASP414, LEU416, GLY417, ARG422, and LEU428 (16). The existence of distinct binding sites indicates that LANCL2 might be involved in multiple signaling network and allosteric sites of LANCL2 might exist. The predicted binding pockets of the natural and synthetic ligand of LANCL2 are outlined in Figure 1.2.

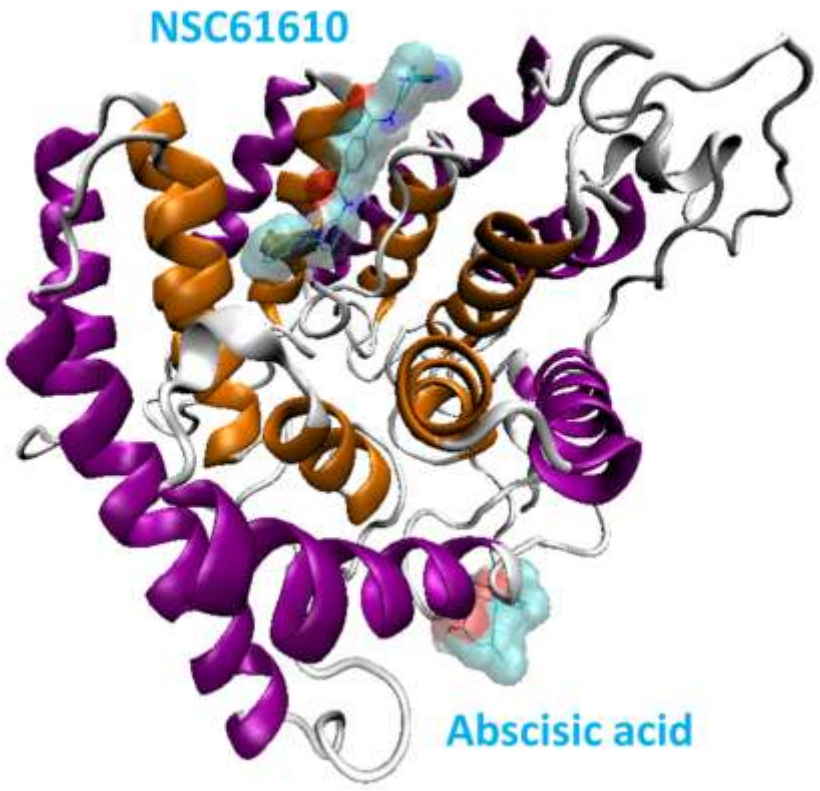


**Figure 1.2.** Energetically favorable pose for abscisic acid (ABA) and NSC61610 bound to lanthionine synthetase C-like protein 2 (LANCL2) in ribbon representation with helix layers colored in purple (outer) and orange (inner). ABA and NSC61610 are represented in line method with transparent surface. The predicted binding site of LANCL2 favored by ABA is composed of TYR279, LYS 283, LYS284, PHE285, PRO291, ASN296 and SER295. The predicted binding site of LANCL2 favored by NSC61610 is composed of ARG102, VAL103, TYR189, THR196, HIS410, ASP414, LEU416, GLY417, ARG422, and LEU428.

This review summarizes the current knowledge on LANCL2 as a potential drug target, including sequence, structure, expression patterns, function, and cellular localization. The main components of the article provide an up-to-date accounting of LANCL2 biological activities and its validation as a novel therapeutic target for human disease.

### 1.3 Sequence characterization of human LANCL2 and comparison to LANCL1

Analysis of the composite nucleotide sequence of human LANCL2 revealed a coding region of 1,353 nucleotides, starting from the first ATG in the open reading frame and coding for 450 amino acids. The 5'-UTR contains 186 nucleotides, an in-frame stop codon lies at position -105 upstream to the start codon. There are two imperfect polyadenylation signals within the 3'-UTR of 2433 nucleotides, including AATATAAA at position 1,720 and AGTAAA at position 3,927. The sequence similarity and identity of human LANCL2 are 74.7% and 57.9% compared with the human LANCL1 homologue, respectively (4). In contrast to LANCL1, the human LANCL2 N-terminal region is extended by 41 additional amino acids while 6 additional amino acids extend at the C-terminal end. In addition, LANCL2 contains a Walker A box at position 230, indicating a potential function dependent on ATP/GTP binding (17). Multiple sequence alignment of human LANCL2, human and mouse LANCL1 and other eukaryotic LANCL proteins showed 7 conserved repetitive hydrophobic regions, which are also highly conserved in the prokaryotic LanC/LanM families of peptide-modifying enzymes (1, 4, 5). LANCLs might represent an evolutionary adaptation of a prokaryotic enzyme responsible for intramolecular thioether formation, into a regulatory protein that controls mammalian signal transduction in immune and endocrine cells (in the case of LANCL2) and other neural regulatory processes (in the case of LANCL1).

### 1.4 Pattern of expression in tissues and cellular distribution of LANCLs

LANCL1 was shown to be highly expressed in neurons, various epithelial cells, thymocytes, alveolar macrophages, and megakaryocytes (4). Compared with LANCL1, LANCL2 is widely expressed in specialized organs of the immune system, such as blood, lymph node, spleen, and thymus. At the cellular level, it is also expressed by endothelial cells, macrophages, dendritic cells, and T cells (18). LANCL1 and LANCL2 have distinct

patterns of expression and sub-cellular localization. LANCL1 is mainly a cytosolic and nuclear protein. Although, a minor part of LANCL2 is also present in the nucleus, the major part of LANCL2 is associated with the plasma membrane through the LANCL2-specific N-terminal region. This region contains a myristoylation site and a polybasic stretch. The myristoylation of human LANCL2 has been shown essential for interaction with the plasma membrane (7).

### 1.5 Structure prediction of LANCL2

In order to further understand the function of LANCL2 through its structure and to investigate whether ABA activates LANCL2 via direct binding to its extracellular domain, we performed homology modeling of human LANCL2 using the crystal structure of human LANCL1 as a template (19), assessed the model quality and refined the model through energy minimization procedures (20). Homology modeling predicts the 3D structure of a protein of interest via identifying its homologous proteins from other members of the protein family whose structures have been solved experimentally. In most cases, two proteins with more than 35% sequence identity are likely to be homologous (21). The crystal structure of human LANCL1 (3E6U) shares 54% sequence identity with LANCL2 (14).

LANCL1 and LANCL2 are not only conserved in terms of sequence but are also functionally similar. Multiple sequence alignment was performed between five LANCL1 and five LANCL2 sequences from human, monkey, rat, mouse, cattle, and zebrafish (14). The alignment showed all LANCL2 sequences also had seven conserved GxxG motifs similar to LANCL1. These seven conserved GxxG-containing motifs are considered to be a signature feature of the LANCL family of proteins because they are absent in other double helix barrel proteins (19). GxxG motif has been previously identified to play roles in ligand-protein binding, such RNA binding (22) and folate binding (23). Furthermore, canonical SH3-binding motifs and GSH-binding residues of LANCL1 also appeared to be highly conserved in the five LANCL2 sequences. Thus, homology modeling of LANCL2 using the LANCL1 structure as a template is appropriate (14).

The homology model of LANCL2 was created by using SWISS-MODEL Workspace, according to the crystal structure of LANCL1 (24). As expected, the predicted structure of LANCL2 consists of two layers of α-helical barrels consisting of 14 α-helices. Both outer and inner barrels are formed by seven helices that are parallel to one another. The seven conserved GxxG-containing bulges are at the N-termini of the inner helices (Fig. 1.2). These bulged loops reduce the entry size of the central cavity formed by the inner helix barrel (14). Therefore, LANCL2 is unlikely to use the central cavity as a ligand-binding site and other biding pockets represent the most likely binding regions.

### 1.6 LANCL2 is required for abscisic acid binding and signaling

The plant hormone ABA regulates response to abiotic stress, seed dormancy and germination in plants (9, 25). Notably, ABA might also act as a hormone in mammals, where it modulates the activity of immune cells and the release of insulin from beta-pancreatic cells (26, 27). In human and murine ABA-responsive cells, ABA upregulates the functional activities specific for each cell type in autocrine fashion through a receptor-operated signal transduction pathway, sequentially involving a pertussis toxin-sensitive receptor/G-protein complex, cyclic adenosine monophosphate (cAMP), cyclic adenosine diphosphate (cADP)-ribose and intracellular calcium (10) and other downstream signaling networks yet unidentified.

LANCL2 is necessary for ABA binding and signaling in human granulocytes and in rat insulinoma cells. Overexpression of LANCL2 potentiates the ABA-induced signaling cascade via cAMP/$Ca^{2+}$ and stimulates the cell-specific functional responses in human granulocytes and in murine insulinoma cells. Conversely, LANCL2 silencing has the opposite effect, abrogating the ABA-induced biochemical and functional responses in human granulocytes, and in murine and rat insulinoma cell lines (8). In addition, our data show that LANCL2 is expressed in RAW 264.7 cells and *lancl2* knockdown studies provide evidence that ABA-mediated signaling is dependent on *lancl2* expression (13).

### 1.7 Binding of abscisic acid to LANCL2

Molecular modeling plays an important role in early drug discovery, including predicting macromolecule 3D structures, protein–ligand interactions, and biological activities (14, 16). Based on predicted structure of LANCL2, an *in silico* docking approach was used to elucidate the location of the potential binding site of LANCL2 for ABA. Docking results were evaluated by investigating the interaction of multiple ABA conformations with LANCL2. ABA binds inside a pocket in LANCL2. The binding pocket is surrounded by TYR279, LYS284, PHE285, PRO291, ASN296 and SER295. LYS 283 is located in the bottom of the pocket. Two hydrogen bonds formed between the nitrogen atom in the side chain of LYS283 and two hydroxyl groups of ABA that positioned ABA deep in the pocket and increased the affinity of ABA for LANCL2 (14) (Fig. 1.2). It is possible that LANCL2 might have several binding sites and that different classes of ligands might bind to distinct site of the LANCL2 molecule.

Direct evidence for ABA binding to human recombinant LANCL2 was provided *in vitro*. Two different LANCL2 recombinant proteins were used in that study: a glutathione-S-transferase (GST) tagged fusion protein and LANCL2 cleaved from its GST tag. Different methods were used to verify ABA binding to these proteins, including saturation binding with (R,S)-[$^{3}$H] ABA, scintillation proximity assays on immobilized LANCL2, dot blot experiments with biotinylated ABA and affinity chromatography of LANCL2 on immobilized ABA. LANCL2 recombinant proteins featured ABA-binding capacity with each of the methods employed. In addition, the ABA-LANCL2 interaction was confirmed by our studies via kinetic surface plasmon resonance (SPR) studies (unpublished observation). All these results indicate that human LANCL2 binds ABA and that both ABA enantiomers are recognized by the protein (15). The direct binding indicates that LANCL2 may have extracellular domain since previous studies suggest that the ABA-binding sites on LANCL2$^{+}$ HeLa cells are exposed to the extracellular side of the plasmamembrane while ABA-binding sites are not detectable on LANCL2$^{-}$ HeLa cells (8). The reported N-myristoylation of LANCL2 would not contrast with a transmembrane localization of the protein, as modifications of G protein-coupled receptors have been observed (7, 28).

### 1.8 LANCL2 increases cellular sensitivity to anticancer drug

A significant impediment to the success of cancer chemotherapy is multidrug resistance. MDR is partially attributable to the over-expression of membrane transport proteins, such as P-gp encoded by *MDR1* gene, which results in an increased drug efflux (29). The relationship between LANCL2 and the expression of MDR1, as well as P-gp, has been investigated using human sarcoma cells MES-SA. The level of endogenous P-gp decreases with overexpressed LANCL2 and cells with reduced P-gp are more sensitive to adriamycin, one chemotherapeutic agent against cancer. Results from reverse transcription-PCR and MDR1 promoter activity analyses suggest that LANCL2 transcriptionally suppresses MDR1 (6). LANCL2 overexpression enhanced the cellular sensitivity to adriamycin in human amniotic cells UAC and this sensitivity is dependent on the myristoylation and membrane association of LANCL2 (7). The potential for LANCL2 ligands in cancer treatment remains completely unexplored.

### 1.9 LANCL2 as modulator in inflammation and immunity

ABA has shown pre-clinical efficacy in the treatment of diabetes and inflammatory diseases such as IBD, influenza-related lung immunopathology and atherosclerosis (11, 12, 30-32); however, its molecular targets and the mechanisms of action underlying its immunomodulatory and insulin-sensitizing effects were unclear until its LANCL2-dependent properties were studied. Our group investigated the role of LANCL2 as a molecular target for immune modulatory and anti-diabetic efficacy of ABA. LANCL2 knockdown studies provide evidence that ABA mediated activation of immune modulatory activities in macrophages is dependent on *lancl2* expression. LANCL2 siRNA significantly disrupted PPAR γ activation stimulated by ABA and rosiglitazone (13). Consistent with the association between LANCL2 and G proteins (8), we demonstrated that ABA increases cAMP accumulation in immune cells. Because LANCL2 is coupled to a pertussis toxin-sensitive G-protein that regulates the cAMP synthesizing activity of adenylate cyclase, the cAMP signaling pathway represents a likely mechanism underlying some of the immune modulatory actions of ABA (13). Furthermore, there is some evidence demonstrating that cAMP/protein kinase A (PKA) activation increases basal and ligand-induced PPAR γ activity, providing a basis for

either cross-talk between the cAMP and PPAR γ pathways or the existence of a common cAMP/PKA/PPAR γ signaling axis (33). We also showed that oral ABA administration decreases lipopolysaccharide-mediated systemic inflammation and regulates innate immune responses through a bifurcating pathway involving LANCL2 and an alternative, ligand-binding domain-independent mechanism of PPAR γ activation (13). PKA-mediated phosphorylation of cAMP response element-binding (CREB) protein has been reported to suppress TNF-α production and promote IL-10 induction (34). CREB is a cellular transcription factor that binds to certain DNA sequences (CREs) to regulate the transcription of the downstream genes (35). LANCL2/cAMP/PKA/CREB axis represents one potential novel anti-inflammatory pathway independent of PPAR γ.

Interestingly, ABA has also been reported to exert some pro-inflammatory actions such as increased NF-κB activation and MCP-1 secretion in cultured human monocytes (27). As a key component in ABA signaling pathway, LANCL2 was revealed to mediate cell functions involved in inflammation stimulated by autocrine ABA. Silencing of LANCL2 in human keratinocytes by siRNA was accompanied by abrogation of the UV-B triggered release of $PGE_2$, TNF-α, and NO and ROS production (36). In addition, LANCL2 is also proposed to be involved in quartz-induced inflammation, since silencing LANCL2 in quartz-stimulated RAW 264.7 cells completely inhibited NF-κB nuclear translocation and $PGE_2$ and TNF-α release (37).

To more broadly investigate LANCL2 expression in cells of the immune system, we have examined microarray datasets deposited in the publicly available Gene Expression Omnibus (GEO) repository and have been able to infer unreported roles for LANCL2 in stimulated immune cells. Our data-mining efforts suggest that LANCL2 is consistently down-regulated or suppressed in immune cells early after introduction to an inflammatory stimulus. Reduced LANCL2 expression directly correlates to high expression of inflammatory genes. Moreover, down-regulated LANCL2 is linked to low expression of anti-inflammatory mediators including transforming growth factor (TGF) β1, interleukin (IL)-10, and PPARγ in many microarray datasets (Fig. 1.3A-C). We have also found time course data demonstrating LANCL2 expression increasing

simultaneously with IL-10 and TGF-β1 from 30 minutes to 2 hours following LPS stimulation (Fig. 1.3C). Interestingly, exhausted CD8+ T cells upregulate expression of LANCL2 during the chronic phase of lymphocytic choriomeningitis virus (LCMV) infection (Fig. 1.3D) (18) suggesting a potential role in regulating immune responses to sustained inflammation and intracellular pathogens and value as a therapeutic target for infectious diseases. Microarray profiles are limited to characterization of cellular changes that regulate mRNA levels and do not expose functional roles of proteins nor post-translational modification, synthesis and degradation mechanisms. High-throughput proteomic data and additional functional studies would be invaluable for enhancing the limited understanding of LANCL2 and future research should focus on demonstrating how LANCL2 influences the immune system at the protein level. Nevertheless, current transcriptomic profiling lends an enormous amount of insight toward the molecular regulation of LANCL2 in immune cells and prompts further mechanistic investigation of this enigmatic protein and therapeutic target.

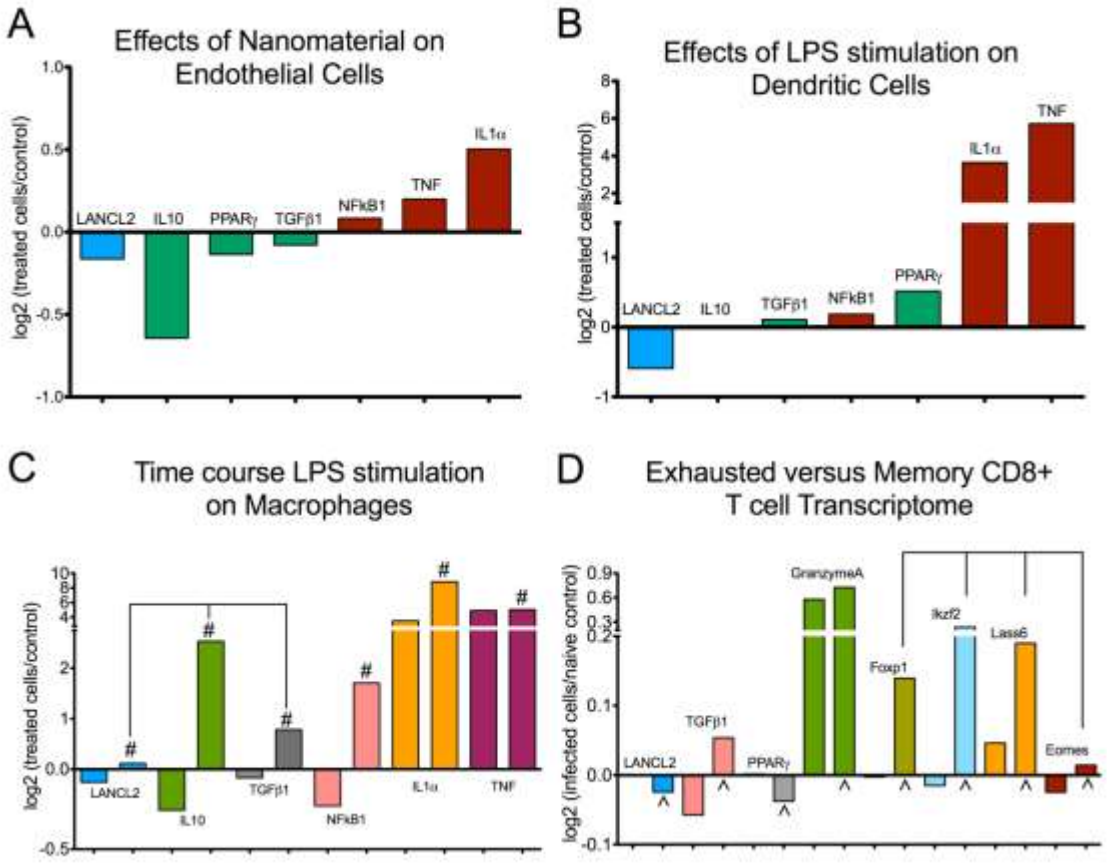

**Figure 1.3.** Lanthionine synthetase C-like protein 2 (LANCL2) acts as an immune modulatory mediator in immune cells. Microarray gene expression data was obtained from the Gene Expression Omnibus (GEO) repository. Data are presented as the log2 fold-change of expression between treated cells versus untreated controls. Gene IDs are labeled for each column. The effects of fullerene, a carbon-based nanomaterial, on human vascular endothelial cells were analyzed from GenBank accession no. GSE3364 (data represent the average fold change of treated (n=2) versus untreated (n=2) cells) (A). Gene expression in primary murine bone marrow derived dendritic cells (mBMDC) following 1-hour LPS stimulation were obtained from GenBank accession no. GSE17721 (data represent the average fold change of treated (n=2) versus untreated (n=2) cells) (B). Time course data for LPS stimulation in murine RAW 264.7 cells was obtained from GenBack accession no. GSE1906 (for each time point, n=1) (C). For time course data (C), the first unlabeled column represents gene expression for 30 minutes post stimulation while the #-labeled columns represent gene expression for 2 hours post stimulation. The bar highlights anti-inflammatory genes simultaneously up-regulated at 2 hours post LPS stimulation. Microarray data exposing the transcriptomic signature of exhausted CD8+ T cells was obtained from GenBank accession no. GSE41867 (data represent the average fold change of acute (n=4) or chronic (n=4) versus untreated (n=4) cells) (D). Results display responses in CD8+ T cells obtained from mice 30 days post acute (first unlabeled column) or chronic (^-labeled columns) infection. Bars (D) represent genes upregulated in exhausted CD8+ T cells.

These divergent reports regarding the role of LANCL2 in inflammation suggest the existence of complex regulatory feedback and feed-forward pathways controlling LANCL2-mediated signaling in immune modulation. Stimuli such as injury or infection trigger autocrine ligands binding to LANCL2 and activate the adenylate cyclase (AC)-cAMP-PKA pathway that is maintaining and enhancing inflammation by NF-κB. In turn, binding of natural or synthetic ligands to LANCL2 followed by activation of PPAR γ results in antagonism of NF-κB activity and promotes anti-inflammatory genes expression. In addition, PKA-mediated phosphorylation of CREB protein promotes TNF-α suppression and IL-10 induction. LANCL2-cAMP–PKA–CREB anti-inflammatory pathway is independent of PPAR γ, all of which further validates the important role of LANCL2 as a therapeutic target for immune modulation (Fig. 1.4).

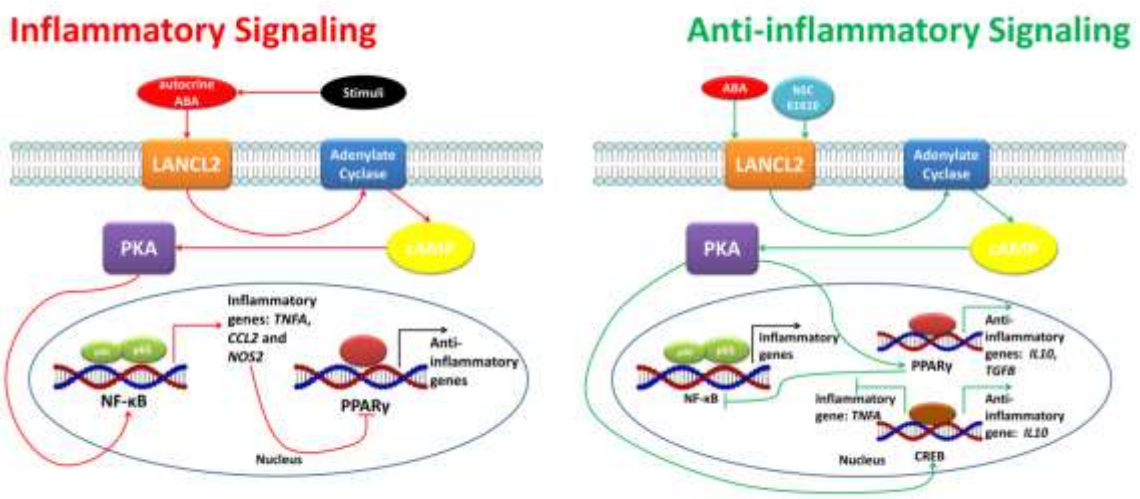


**Figure 1.4.** Molecular mechanism underlying regulation of inflammation by lanthionine synthetase C-like protein 2 (LANCL2). Stimuli such as injury or infection trigger autocrine ligands bind to LANCL2 and activate the adenylate cyclase (AC)-cAMP-protein kinase A (PKA) pathway that is maintaining and enhancing inflammation by nuclear factor kappa-light-chain-enhancer of activated B cells (NF-κB). In turn, binding of natural or synthetic ligands to LANCL2 followed by activation of peroxisome proliferator-activated receptor (PPAR) γ results in antagonism of NF-κB activity and promotes anti-inflammatory genes expression. In addition, PKA-mediated phosphorylation of cAMP response element-binding (CREB) protein promotes TNF-α suppression and IL-10 induction. LANCL2-cAMP–PKA–CREB anti-inflammatory pathway is independent of PPAR γ.

### 1.10 LANCL2 exerts antidiabetic effects

Our findings demonstrate that dietary ABA-supplementation decreases fasting blood glucose concentrations and ameliorated glucose tolerance. ABA also plays roles in attenuating adipocyte hypertrophy, tumor necrosis factor-a (TNF-a) expression, and macrophage infiltration in white adipose tissue (WAT) in db/db mice fed high-fat diets (11). In addition, ABA decreased plasma insulin levels and increased the percentages of blood regulatory T cells in mice with pre-existing obesity/diabetes through a membrane-initiated mechanism dependent on cAMP/PKA signaling (31). Thus, LANCL2 may play anti-diabetic roles in initiating anti-diabetic signaling by binding with ABA other small signaling molecules with efficacy in improving insulin sensitivity. Another potential antidiabetic mechanism of LANCL2 is to regulate the network of cytokine signals

exchanged between inflammatory cells and pancreatic β cells by binding to diabetic-related hormones (8).

### 1.11 LANCL2-based virtual screening of anti-inflammatory drugs

Structure-based virtual screening (SBVS) followed by targeted experimental validation is a more cost effective and efficient approach in drug discovery, when compared with the physical large scale, high-throughput screening of thematic compound libraries against a biological target. The basic procedure of SBVS is to sample binding geometry for compounds from large libraries into the structure of receptor targets by using molecular modeling approaches. Each compound is sampled in thousands to millions of possible poses and scored on the basis of its complementarity to the receptor. Of the hundreds of thousands of molecules in the library, tens of top-scoring predicted ligands are subsequently validated for activity in experimental assays (38).

LANCL2-based virtual screening was performed by using a LANCL2 structure-based approach to discover new LANCL2 agonists (16). The compound databases we employed include NCI Diversity Set II, ChemBridge, ZINC natural products and U.S. Food and Drug Administration (FDA)-approved drug databases. After docking into the LANCL2, all the compounds would be ranked by the calculated binding affinity (39). Utilizing surface plasmon resonance we demonstrate LANCL2 micromolar affinity to NSC61610, which validate the prediction from virtual screening (Fig. 1.2).

Our molecular modeling results suggested that NSC61610 might activate the LANCL2 pathway. To investigate the importance of LANCL2 in NSC61610-mediated anti-inflammatory effects, we determined whether knocking down LANCL2 in raw macrophages by using siRNA impaired or abrogated the effect of NSC61610 signaling. Our findings indicate that knocking down LANCL2 significantly attenuates the effect of NSC61610 signaling, including cAMP production, and PKA phosphorylation. These findings are consistent with the prediction of our previous studies that ABA exerts immune modulatory actions in a LANCL2-dependent manner (16).

Our group previously demonstrated that oral ABA administration ameliorates experimental IBD by downregulating cellular adhesion molecule expression and suppressing immune cell infiltration (30). Also, we identified for the first time that oral NSC61610 treatment significantly ameliorates colonic inflammation and clinical activity in mice with experimental IBD. We found that NSC61610 significantly down-regulated inflammatory mediators (MCP-1 and IL-6) in the colonic mucosa (16). At the cellular level, the percentages of regulatory T cells (Treg) cells in the colon, spleen, and blood of mice were significantly increased by oral NSC61610 treatment. In addition, the percentages of $CD4^{+}IL10^{+}$ T cells in colon, spleen, mesenteric lymph node, and blood were also significantly increased. Furthermore, NSC61610 reduced the percentage of infiltrating $F4/80^{+}CD11b^{+}$ macrophages in the colonic lamina propria, a possible source of inflammatory mediators. These results confirm that LANCL2 is a novel therapeutic target for inflammatory, chronic and immune-mediated diseases.

### 1.12 Conclusion

Based on this review, we propose that LANCL2 is a novel and promising target for the discovery and development of orally active, broad-based drugs against cancer, inflammatory, immune-mediated, and chronic metabolic diseases. LANCL1, a homolog of LANCL2, has been identified as a prominent Glutathione binding protein expressed in the mammalian central nervous system (40), which has been confirmed by protein crystallization and structural determination (19). Additionally, lanthionine ketimine, a downstream metabolite of lanthionime has also been showed to bind to LANCL1, which possess neuroprotective, neuritigenic and anti-inflammatory activities (41). Recent studies reveal that LANCL1 is a negative regulator of cystathionine-β-synthase and a sensor of oxidative stress (42). All of these findings indicate potential therapeutic value of in targeting the LANCL1 to treat neurological disorders. Due to high sequence similarity between LANCL2 and LANCL1, LANCL2 may also have similar structure features like LANCL1, thus playing potential roles in regulating neurological disorders by binding to glutathione or lanthionine metabolites.

### 1.13 Acknowledgements

This research was supported by funds of the Nutritional Immunology and Molecular Medicine Laboratory (NIMML).

### 1.14 References

1. Bauer H, Mayer H, Marchler-Bauer A, Salzer U, Prohaska R. Characterization of p40/GPR69A as a peripheral membrane protein related to the lantibiotic synthetase component C. Biochem Biophys Res Commun. 2000;275(1):69-74.
2. Chatterjee C, Paul M, Xie L, van der Donk WA. Biosynthesis and mode of action of lantibiotics. Chemical reviews. 2005;105(2):633-84.
3. Chen JG, Ellis BE. GCR2 is a new member of the eukaryotic lanthionine synthetase component C-like protein family. Plant Signal Behav. 2008;3(5):307-10.
4. Mayer H, Breuss J, Ziegler S, Prohaska R. Molecular characterization and tissue-specific expression of a murine putative G-protein-coupled receptor. Biochim Biophys Acta. 1998;1399(1):51-6.
5. Mayer H, Pongratz M, Prohaska R. Molecular cloning, characterization, and tissue-specific expression of human LANCL2, a novel member of the LanC-like protein family. DNA Seq. 2001;12(3):161-6.
6. Park S, James CD. Lanthionine synthetase components C-like 2 increases cellular sensitivity to adriamycin by decreasing the expression of P-glycoprotein through a transcription-mediated mechanism. Cancer Res. 2003;63(3):723-7.
7. Landlinger C, Salzer U, Prohaska R. Myristoylation of human LanC-like protein 2 (LANCL2) is essential for the interaction with the plasma membrane and the increase in cellular sensitivity to adriamycin. Biochim Biophys Acta. 2006;1758(11):1759-67.
8. Sturla L, Fresia C, Guida L, Bruzzone S, Scarfi S, Usai C, et al. LANCL2 is necessary for abscisic acid binding and signaling in human granulocytes and in rat insulinoma cells. J Biol Chem. 2009;284(41):28045-57.
9. Bassaganya-Riera J, Skoneczka J, Kingston DG, Krishnan A, Misyak SA, Guri AJ, et al. Mechanisms of action and medicinal applications of abscisic Acid. Curr Med Chem. 2010;17(5):467-78.
10. Bruzzone S, Moreschi I, Usai C, Guida L, Damonte G, Salis A, et al. Abscisic acid is an endogenous cytokine in human granulocytes with cyclic ADP-ribose as second messenger. Proceedings of the National Academy of Sciences of the United States of America. 2007;104(14):5759-64.
11. Guri AJ, Hontecillas R, Si H, Liu D, Bassaganya-Riera J. Dietary abscisic acid ameliorates glucose tolerance and obesity-related inflammation in db/db mice fed high-fat diets. Clin Nutr. 2007;26(1):107-16.
12. Guri AJ, Hontecillas R, Ferrer G, Casagran O, Wankhade U, Noble AM, et al. Loss of PPAR gamma in immune cells impairs the ability of abscisic acid to improve insulin sensitivity by suppressing monocyte chemoattractant protein-1 expression and macrophage infiltration into white adipose tissue. J Nutr Biochem. 2008;19(4):216-28.
13. Bassaganya-Riera J, Guri AJ, Lu P, Climent M, Carbo A, Sobral BW, et al. Abscisic acid regulates inflammation via ligand-binding domain-independent activation of peroxisome proliferator-activated receptor gamma. The Journal of biological chemistry. 2011;286(4):2504-16.

14. Lu P, Bevan DR, Lewis SN, Hontecillas R, Bassaganya-Riera J. Molecular modeling of lanthionine synthetase component C-like protein 2: a potential target for the discovery of novel type 2 diabetes prophylactics and therapeutics. J Mol Model. 2011;17(3):543-53.
15. Sturla L, Fresia C, Guida L, Grozio A, Vigliarolo T, Mannino E, et al. Binding of abscisic acid to human LANCL2. Biochemical and biophysical research communications. 2011;415(2):390-5.
16. Lu P, Hontecillas R, Horne WT, Carbo A, Viladomiu M, Pedragosa M, et al. Computational modeling-based discovery of novel classes of anti-inflammatory drugs that target lanthionine synthetase C-like protein 2. PLoS One. 2012;7(4):e34643.
17. Walker JE, Saraste M, Runswick MJ, Gay NJ. Distantly related sequences in the alpha- and beta-subunits of ATP synthase, myosin, kinases and other ATP-requiring enzymes and a common nucleotide binding fold. The EMBO journal. 1982;1(8):945-51.
18. Doering TA, Crawford A, Angelosanto JM, Paley MA, Ziegler CG, Wherry EJ. Network analysis reveals centrally connected genes and pathways involved in CD8+ T cell exhaustion versus memory. Immunity. 2012;37(6):1130-44.
19. Zhang W, Wang L, Liu Y, Xu J, Zhu G, Cang H, et al. Structure of human lanthionine synthetase C-like protein 1 and its interaction with Eps8 and glutathione. Genes Dev. 2009;23(12):1387-92.
20. Melo F, Feytmans E. Assessing protein structures with a non-local atomic interaction energy. Journal of molecular biology. 1998;277(5):1141-52.
21. Rost B. Twilight zone of protein sequence alignments. Protein Eng. 1999;12(2):85-94.
22. Keren I, Klipcan L, Bezawork-Geleta A, Kolton M, Shaya F, Ostersetzer-Biran O. Characterization of the molecular basis of group II intron RNA recognition by CRS1-CRM domains. The Journal of biological chemistry. 2008;283(34):23333-42.
23. Zhao R, Shin DS, Fiser A, Goldman ID. Identification of a functionally critical GXXG motif and its relationship to the folate binding site of the proton-coupled folate transporter (PCFT-SLC46A1). American journal of physiology Cell physiology. 2012;303(6):C673-81.
24. Arnold K, Bordoli L, Kopp J, Schwede T. The SWISS-MODEL workspace: a web-based environment for protein structure homology modelling. Bioinformatics. 2006;22(2):195-201.
25. Nambara E, Marion-Poll A. Abscisic acid biosynthesis and catabolism. Annual review of plant biology. 2005;56:165-85.
26. Bruzzone S, Bodrato N, Usai C, Guida L, Moreschi I, Nano R, et al. Abscisic acid is an endogenous stimulator of insulin release from human pancreatic islets with cyclic ADP ribose as second messenger. The Journal of biological chemistry. 2008;283(47):32188-97.
27. Magnone M, Bruzzone S, Guida L, Damonte G, Millo E, Scarfi S, et al. Abscisic acid released by human monocytes activates monocytes and vascular smooth muscle cell responses involved in atherogenesis. The Journal of biological chemistry. 2009;284(26):17808-18.
28. Utsumi T, Ohta H, Kayano Y, Sakurai N, Ozoe Y. The N-terminus of B96Bom, a Bombyx mori G-protein-coupled receptor, is N-myristoylated and translocated across the membrane. The FEBS journal. 2005;272(2):472-81.

29. Zhou J, Liu M, Aneja R, Chandra R, Lage H, Joshi HC. Reversal of P-glycoprotein-mediated multidrug resistance in cancer cells by the c-Jun NH2-terminal kinase. Cancer research. 2006;66(1):445-52.
30. Guri AJ, Hontecillas R, Bassaganya-Riera J. Abscisic acid ameliorates experimental IBD by downregulating cellular adhesion molecule expression and suppressing immune cell infiltration. Clin Nutr. 2010;29(6):824-31.
31. Guri AJ, Hontecillas R, Bassaganya-Riera J. Abscisic acid synergizes with rosiglitazone to improve glucose tolerance and down-modulate macrophage accumulation in adipose tissue: possible action of the cAMP/PKA/PPAR gamma axis. Clin Nutr. 2010;29(5):646-53.
32. Guri AJ, Misyak SA, Hontecillas R, Hasty A, Liu D, Si H, et al. Abscisic acid ameliorates atherosclerosis by suppressing macrophage and CD4+ T cell recruitment into the aortic wall. J Nutr Biochem. 2010;21(12):1178-85.
33. Lazennec G, Canaple L, Saugy D, Wahli W. Activation of peroxisome proliferator-activated receptors (PPARs) by their ligands and protein kinase A activators. Molecular endocrinology. 2000;14(12):1962-75.
34. Avni D, Ernst O, Philosoph A, Zor T. Role of CREB in modulation of TNFalpha and IL-10 expression in LPS-stimulated RAW264.7 macrophages. Molecular immunology. 2010;47(7-8):1396-403.
35. Bourtchuladze R, Frenguelli B, Blendy J, Cioffi D, Schutz G, Silva AJ. Deficient long-term memory in mice with a targeted mutation of the cAMP-responsive element-binding protein. Cell. 1994;79(1):59-68.
36. Bruzzone S, Basile G, Mannino E, Sturla L, Magnone M, Grozio A, et al. Autocrine abscisic acid mediates the UV-B-induced inflammatory response in human granulocytes and keratinocytes. J Cell Physiol. 2012;227(6):2502-10.
37. Magnone M, Sturla L, Jacchetti E, Scarfi S, Bruzzone S, Usai C, et al. Autocrine abscisic acid plays a key role in quartz-induced macrophage activation. FASEB journal : official publication of the Federation of American Societies for Experimental Biology. 2012;26(3):1261-71.
38. Shoichet BK. Virtual screening of chemical libraries. Nature. 2004;432(7019):862-5.
39. Irwin JJ, Shoichet BK. ZINC--a free database of commercially available compounds for virtual screening. J Chem Inf Model. 2005;45(1):177-82.
40. Chung CH, Kurien BT, Mehta P, Mhatre M, Mou S, Pye QN, et al. Identification of lanthionine synthase C-like protein-1 as a prominent glutathione binding protein expressed in the mammalian central nervous system. Biochemistry. 2007;46(11):3262-9.
41. Hensley K, Venkova K, Christov A. Emerging biological importance of central nervous system lanthionines. Molecules. 2010;15(8):5581-94.
42. Zhong WX, Wang YB, Peng L, Ge XZ, Zhang J, Liu SS, et al. Lanthionine synthetase C-like protein 1 interacts with and inhibits cystathionine beta-synthase: a target for neuronal antioxidant defense. The Journal of biological chemistry. 2012;287(41):34189-201.

# Chapter 2. Molecular modeling of lanthionine synthetase component C-like protein 2: a potential target for the discovery of novel type 2 diabetes prophylactics and therapeutics

**Pinyi Lu[1,2], David R. Bevan[3], Stephanie N. Lewis[1,3], Raquel Hontecillas[1,2], Josep Bassaganya-Riera[1, 2]**

Lu P, Bevan DR, Lewis SN, Hontecillas R, Bassaganya-Riera J. Molecular modeling of lanthionine synthetase component C-like protein 2: a potential target for the discovery of novel type 2 diabetes prophylactics and therapeutics. Journal of molecular modeling. 2011;17(3):543-53. Used with permission of Springer, 2015.

[1]Genetics, Bioinformatics, and Computational Biology Program, Virginia Polytechnic Institute and State University, Blacksburg, VA 24061, USA, [2]Nutritional Immunology and Molecular Nutrition Laboratory, Virginia Bioinformatics Institute, Virginia Polytechnic Institute and State University, Washington Street 0477, Blacksburg, VA 24061, USA, [3]Department of Biochemistry, Virginia Polytechnic Institute and State University, 201 Engel Hall 0308, Blacksburg, VA 24061, USA

CORRESPONDENCE: *To whom correspondence should be addressed at: Josep Bassaganya-Riera, Laboratory of Nutritional Immunology and Molecular Medicine Laboratory (www.nimml.org), Virginia Bioinformatics Institute, Virginia Tech, Blacksburg, VA 24061. Phone: (540) 231-7421, FAX: (540) 231-2606, and e-mail: jbassaga@vt.edu.

## 2.1 Abstract

The rates of type 2 diabetes (T2D) are rising to epidemic proportions in the US and worldwide. While current T2D medications are efficacious, significant side effects have limited their use and availability. Our laboratory has discovered that abscisic acid (ABA) exerts anti-diabetic effects, in part, by activating peroxisome proliferator-activated receptor γ (PPAR γ). However, since ABA does not bind to the ligand-binding domain (LBD) of PPAR γ, the mechanism of activation of PPAR γ by ABA remains unknown. Lanthionine synthetase component C-like protein 2 (LANCL2) was predicted to be a novel target for the binding and signaling of ABA in human granulocytes and rat insulinoma cells. The goal of this study was to determine whether LANCL2 is a molecular target of ABA and other PPAR γ agonists. To this end we performed homology modeling to construct a three-dimensional structure of LANCL2 using the crystal structure of LANCL1 as a template. Our molecular docking studies predicted that ABA and other PPAR γ agonists (e.g., rosiglitazone and pioglitazone) share a binding site on the surface of LANCL2. The identification of a binding site for PPAR γ agonists will facilitate the high-throughput virtual screening of large compound libraries and may shed new light on alternative mechanisms of PPAR γ activation.

## 2.2 Introduction

According to recent estimates from the Centers for Disease Control and Prevention (CDC), about 30% of the United States population is obese and 65% is overweight. One of the major consequences of these high rates is manifested by the increased prevalence of type 2 diabetes mellitus (T2D), a disorder that is characterized by high blood glucose in the context of insulin resistance that progresses towards pancreatic β-cell dysfunction leading to insulin deficiency (1). There are an estimated 23.6 million people in the US (7.8% of the population) with diabetes, 90% of whom are type 2 diabetics (2). With prevalence rates doubling between 1990 and 2005, CDC has characterized this increase as an epidemic.

Current antidiabetic drugs used in the management of T2D elicit important insulin-sensitizing and anti-inflammatory effects. However, side effects associated with using

these medications are serious, any of which may limit their use (3). For example, sulfonylureas, the first widely used oral hypoglycemic medications, cause hypoglycemia (4); biguanides are typically reserved for patients experiencing gastrointestinal side effects (5) and thiazolidinediones (TZDs) could lead to an increase in the incidence of liver damage and potential liver failure, fluid retention, weight gain and congestive heart failure (6). Thus, it is critical to discover novel, naturally occurring drugs and nutraceuticals against T2D.

Our laboratory is actively screening and discovering novel, naturally occurring, orally active nutraceuticals against diabetes, cardiovascular disease, gut inflammation and inflammation-driven cancer that activate nuclear receptors. Of note is the discovery of a peroxisome proliferator-activated receptor (PPAR) γ-activating and anti-inflammatory phytohormone, abscisic acid (ABA), which is also a potent insulin-sensitizing agent. PPAR γ is one of three PPAR isoforms (α, δ, and γ) that is a component of an extensive group of transcription factors controlling adipogenesis and glucose homeostasis, and both of these processes directly affect obesity and T2D (7). ABA is a phytochemical regulating fundamental physiological functions in plants but it can also be endogenously synthesized in mammalian cells, including granulocytes, pancreatic β-cells and monocytes (8).

PPAR γ is required for ABA to induce its full spectrum of effects (9), but our unpublished data indicate that ABA does not bind directly to the ligand-binding domain (LBD) of PPAR γ. Therefore, the complete mechanism of activation of PPAR γ by ABA is unknown. Recently, Sturla and his colleagues provided in vitro results suggesting that the lanthionine synthetase component C-like protein 2 (LANCL2) is the membrane receptor required for ABA binding on the membrane of human granulocytes, and that LANCL2 is necessary for transduction of the ABA signal into cell-specific functional responses in granulocytes (10). LANCL2 is a member of the eukaryotic lanthionine synthetase component C-like (LANCL) protein family, which is related to the bacterial lanthionine synthetase component C (11) and is a putative novel target for the discovery and development of drugs and nutraceuticals.

In order to further understand the function of LANCL2 through its structure and to investigate whether ABA activates LANCL2 via direct binding to its extracellular domain, we performed homology modeling of human LANCL2 using the crystal structure of human lanthionine synthetase component C-like protein 1 (LANCL1) as a template (12), assessed the model quality and refined the model through energy minimization procedures. We then used a blind docking approach to elucidate the location of the potential LBD of LANCL2 for ABA. Docking results were evaluated by investigating the interaction of multiple ABA conformations with LANCL2. We also tested whether other synthetic and naturally occurring agonists of PPAR γ could bind to LANCL2 by blind docking. Interestingly, we found that these PPAR γ agonists could bind to the binding region of LANCL2 we propose is occupied by ABA. Among the tested ligands, thiazolidinediones (TZDs) and ABA showed the most favorable binding energy, thereby indicating the highest probability of binding to LANCL2.

## 2.3 Materials and methods

### Template selection and model building

Template selection is a critical step in homology modeling. The amino acid sequence of LANCL2 (*Homo sapiens*) was obtained from the protein database at the National Center for Biotechnology Information (NCBI, http://www.ncbi.nlm.nih.gov/). LANCL2 includes 450 amino acid residues and its accession number is NP_061167. To determine if structural templates in addition to LANCL1 (12) were available, sequence searching was done. BLASTp (protein–protein BLAST) and the BLOSUM62 scoring matrix were applied to search for potential templates for LANCL2 in the non-redundant protein sequence database (13). Gap existence was penalized 11 from an overall score and each gap extension was deducted 1. Based on this analysis, LANCL1 (*H. sapiens*) was identified as the only template for modeling LANCL2 (*H. sapiens*).

To further verify whether LANCL1 is an appropriate template, multiple sequence alignment (MSA) was used to analyze conserved residues and potential sequence motifs of LANCL2. Five target sequences (LANCL2) and five template sequences (LANCL1)

from different organisms were selected from the protein database in NCBI. MSA was performed using the CLUSTALW package in Biology Workbench applying the default parameters to insure proper alignment between the template and target (14, 15). The high sequence identity (54%) and sequence similarity (71%) indicate the suitability of LANCL1 as a template for LANCL2 in homology modeling (Fig. 2.1).

```
 Score =  487 bits (1253),  Expect = 1e-135, Method: Compositional matrix adjust.
 Identities = 231/426 (54%), Positives = 304/426 (71%), Gaps = 27/426 (6%)

Query  19   MEERAFVNPFPDYEAAAGALLASGAAEETGCVRPPATTDEPGLPFHQDGKIIHNFIRRIQ  78
            M +RAF NP+ DY  +    LA G                     F   G++   F +R+
Sbjct  13   MAQRAFPNPYADYNKS----LAEGY------------------FDAAGRLTPEFSQRLT  49

Query  79   TKIKDLLQQMEEGLKTADPHDCSAYTGWTGIALLYLQLYRVTCDQTYLLRSLDYVKRTLR  138
             KI++LLQQME GLK+ADP D + YTGW GIA+LYL LY V  D  YL  +  YVK++L
Sbjct  50   NKIRELLQQMERGLKSADPRDGTGYTGWAGIAVLYLHLYDVFGDPAYLQLAHGYVKQSLN  109

Query  139  NLNGRRVTFLCGDAGPLAVGAVIYHKLRSDCESQECVTKLLQLQRSVVCQESDLPDELLY  198
             L  R +TFLCGDAGPLAV AV+YHK+ ++ ++++C+T+L+ L +     +   P+E+LY
Sbjct  110  CLTKRSITFLCGDAGPLAVAAVLYHKMNNEKQAEDCITRLIHLNKI----DPHAPNEMLY  165

Query  199  GRAGYLYALLYLNTEIGPGTVCESAIKEVVNAIIESGKTLSREERKTERCPLLYQWHRKQ  258
            GR GY+YALL++N   G   + +S I+++   I+ SG+ L+R+   T + PL+Y+W+++
Sbjct  166  GRIGYIYALLFVNKNFGVEKIPQSHIQQICETILTSGENLARKRNFTAKSPLMYEWYQEY  225

Query  259  YVGAAHGMAGIYYMLMQPAAKVDQETLTEMVKPSIDYVRHKKFRSGNYPSSLSNETDRLV  318
            YVGAAHG+AGIYY LMQP+ +V Q  L  +VKPS+DYV   KF SGNYP  + +  D LV
Sbjct  226  YVGAAHGLAGIYYYLMQPSLQVSQGKLHSLVKPSVDYVCQLKFPSGNYPPCIGDNRDLLV  285

Query  319  HWCHGAPGVIHMLMQAYKVFKEEKYLKEAMECSDVIWQRGLLRKGYGICHGTAGNGYSFL  378
            HWCHGAPGVI+ML+QAYKVF+EEKYL +A +C+DVIWQ GLL+KGYG+CHG+AGN Y+FL
Sbjct  286  HWCHGAPGVIYMLIQAYKVFREEKYLCDAYQCADVIWQYGLLKKGYGLCHGSAGNAYAFL  345

Query  379  SLYRLTQDKKYLYRACKFAEWCLDYGAHGCRIPDRPYSLFEGMAGAIHFLSDVLGPETSR  438
            +LY LTQD KYLYRACKFAEWCL+YG HGCR PD P+SLFEGMAG I+FL+D+L P  +R
Sbjct  346  TLYNLTQDMKYLYRACKFAEWCLEYGEHGCRTPDTPFSLFEGMAGTIYFLADLLVPTKAR  405

Query  439  FPAFEL  444
            FPAFEL
Sbjct  406  FPAFEL  411
```

**Figure 2.1.** Sequence alignment of LANCL2 (*Homo sapiens*) with LANCL1 (*H. sapiens*) using the BLASTp algorithm. The Query is the LANCL2 amino acid sequence, while the Sbjct is the LANCL1 sequence. Identical residues are showed in the line between Query and Sbjct. A plus (+) indicates a conserved substitution. The three-dimensional structure of LANCL2 was constructed by using the SWISS-MODEL Workspace (16). The template used was the X-ray structure of LANCL1 (2.6 Å resolution, PDB entry code 3E6UC) (17).

### Model assessment and refinement

Model quality was assessed employing two types of assessment tools, ANOLEA (18) and PROCHECK (19). Local quality model estimation (ANOLEA) describes the quality of different fragments of the same model. Energies of each residue were calculated based on

an atomic empirical mean force potential. The stereochemical check (PROCHECK) was applied to determine if the φ and ψ dihedral angles were in available zones of the Ramachandran plot.

After initial model assessment, an energy minimization (EM) procedure was carried out with the GROMACS 4.0.5 software suite using an all-atom force field (OPLS-AA) (20, 21). The purpose of an EM procedure is to reduce steric clashes in the input structure and to obtain lower potential energy in the system and therefore a more stable structure. The EM algorithm used was steepest descent minimization (22). The maximum force to stop minimization, energy step size and maximum number of minimization steps to perform were set to 1,000 KJ $mol^{-1}$ $nm^{-1}$, 0.01 and 50,000, respectively. The final LANCL2 model was superimposed on the crystal structure of LANCL1 to check the structural differences between the homology model and template by using the RAPIDO program (23).

**Ligand structure**

The three-dimensional structure of ABA was downloaded from PubChem, a database of chemical molecules maintained by the NCBI (24). The compound ID of ABA is 5280896 and its molecular formula is $C_{15}H_{20}O_4$.

**Molecular docking**

The docking of ABA into the LANCL2 model was performed with AutoDock (version 4.2) (25). AutoDockTools, the graphical front-end for AutoDock and AutoGrid, was used to set up, run and analyze AutoDock dockings. The Lamarckian genetic algorithm (LGA) was used in AutoDock as the search method to perform automated molecular dockings (26). Default parameters were applied, except for the number of GA runs, population size and maximum number of evaluations, which were set to 100, 250 and 25,000,000, respectively.

In order to identify potential binding sites of ABA on LANCL2, the docking procedure was performed in two steps. At first, the docking was applied to the whole protein target,

with a grid covering the whole surface of the protein. AutoDock can be used when the location of the binding site is unknown. This is often referred to as “blind docking”, when all that is known is the structure of the ligand and the macromolecule (27-32). To search the entire surface of the protein of interest, very large grid maps were created using AutoGrid, with the maximum number of points in each dimension. The grid was a 126 Å cube with grid points separated by 0.59 Å and centered at the middle of the protein. This grid was big enough to cover the entire surface of LANCL2. Then the preliminary dockings with AutoDock were performed to search for particular regions of LANCL2 that were preferred by ABA. In the second round of docking, smaller grids were built around potential binding sites. The X, Y, Z dimensions of grid were set to 70 Å with grid points separated by 0.375 Å.

**Analyzing results of docking**

The search for the best ways to fit ABA into LANCL2 using AutoDock resulted in docking log files that contained detailed records of docking. These log files were read into ADT to analyze the results of docking. The similarity of docked structures was measured by computing the root-mean-square-deviation (RMSD) between the coordinates of the atoms and creating clustering of the conformations based on these RMSD values. In most cases the first cluster was also the largest cluster found. The lowest binding energy conformation in the first cluster was considered as the most favorable docking pose. Binding energies that are reported represent the sum of the total intermolecular energy, total internal energy and torsional free energy minus the energy of the unbound system.

## 2.4 Results and discussion

**Template search**

Homology modeling relies on establishing an evolutionary relationship between the sequence of a protein of interest and other members of the protein family whose structures have been solved experimentally by X-ray crystallography or NMR. For this reason, the major limitation of this technique is the availability of homologous templates. In most cases, two proteins with more than 35% sequence identity are likely to be

homologous (33). The crystal structure of human LANCL1 (3E6U), which shares 54% sequence identity with LANCL2, has been reported by Zhang and colleagues (12).

To further verify whether functionally important residues and motifs are conserved, multiple sequence alignment was performed between five LANCL1 and five LANCL2 sequences from different organisms (Fig. 2.2). The alignment showed all LANCL2 sequences also had seven conserved GxxG motifs similar to LANCL1. These seven conserved GxxG-containing motifs are considered to be a signature feature of the LANCL family of proteins because they are absent in other double helix barrel proteins (12). Furthermore, canonical SH3-binding motifs and GSH-binding residues of LANCL1 also appeared to be highly conserved in the five LANCL2 sequences. All of these findings suggest that LANCL1 and LANCL2 are not only conserved in terms of sequence but are also functionally similar, thus homology modeling of LANCL2 using the LANCL1 structure as template is appropriate.

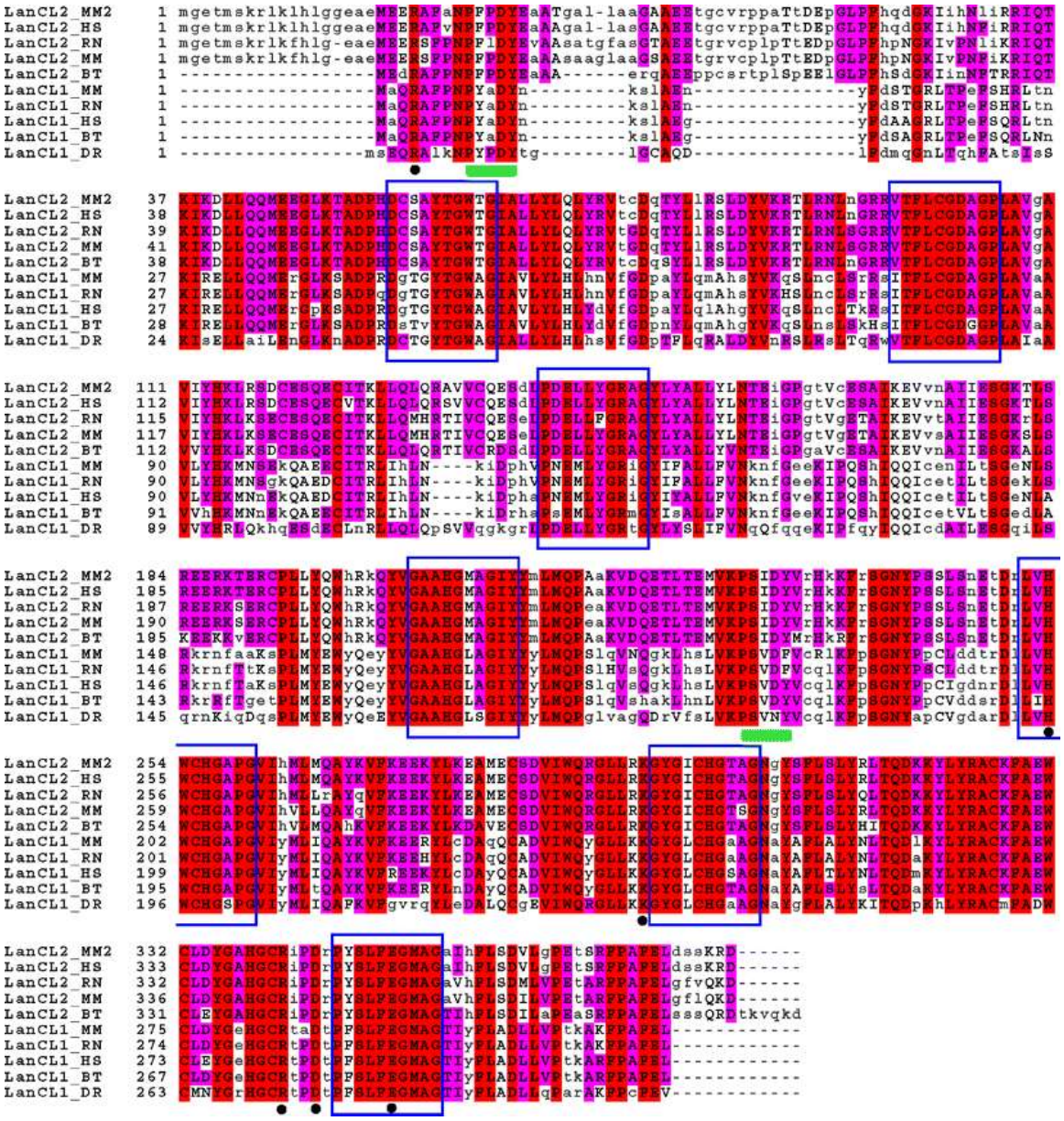


**Figure 2.2.** Multiple sequence alignment of selected LanC proteins. LANCL2_MM2: *Macaca mulatta*; LANCL2_HS: *Homo sapiens*; LANCL2_RN: *Rattus norvegicus*; LANCL2_MM: *Mus musculus*; LANCL2_BT: *Bos taurus*; LANCL1_MM: *Mus musculus*; LANCL1_RN: *R. norvegicus*; LANCL1_HS: *H. sapiens*; LANCL1_BT: *B. taurus*; LANCL1_DR: *Danio rerio*. Completely conserved residues in the listed sequences are highlighted with a *red*background. Identical residues are highlighted with a *magenta* background. Different residues are shown in lower-case letters. Seven conserved GxxG motifs and corresponding loop bulges are outlined by *blue boxes*. Canonical SH3-binding motifs are underlined with *green lines*. Positions of GSH-binding residues in LANCL1 are denoted by *black dots*

**Model building**

SWISS-MODEL Workspace was used to generate the homology model of LANCL2 according to the crystal structure of LANCL1 (16). As expected, the predicted structure of LANCL2 consists of two layers of α-helical barrels consisting of 14 α-helices. The outer barrel is formed by seven helices that are parallel to one another, while the inner barrel is formed by seven helices that are also parallel to one another. The orientation of the two layer barrel helices is opposite, but both inner and outer barrels have a left-handed twist. The seven conserved GxxG-containing bulges are at the N-termini of the inner helices. These bulged loops reduce the entry size of the central cavity formed by the inner helix barrel. Therefore, LANCL2 is unlikely to use the central cavity as a ligand binding site. The structure of LANCL2 is shown in Fig. 2.3 (34).

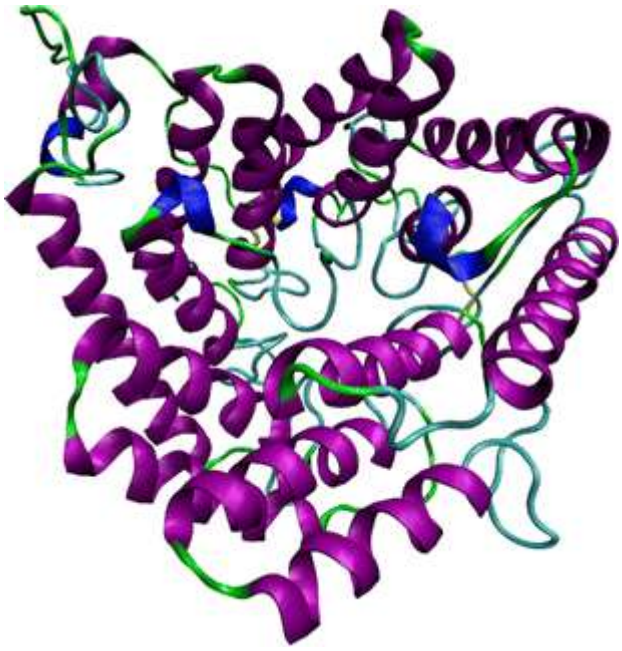

**Figure 2.3.** Overall structure of LANCL2. The homology model of human LANCL2 is shown in *New Cartoon* representation with coloring according to secondary structure. *Purple* Alpha helix, *blue* other helix, *yellow* bridge_beta, *cyan* turn, *green* coil. The image was rendered in VMD

### Model assessment and refinement

Two levels of assessment were performed to determine the quality of the model generated. The atomic empirical mean force potential ANOLEA was used to assess packing quality of the models (18). ANOLEA performs energy calculations on a protein

chain, evaluating the "non-local environment" (NLE) of each heavy atom in the molecule. In the ANOLEA plot, the y-axis of the plot represents the energy for each amino acid of the protein chain. Negative energy values (in green) represent a favorable energy environment whereas positive values (in red), an unfavorable energy environment for a given amino acid. Most amino acid residues in the LANCL2 model appeared in a favorable environment (Fig. 2.4). The PROCHECK suite of programs assesses the stereochemical quality of a given protein structure (19). The Ramachandran plot from PROCHECK also indicated the good quality of the model, with 85.3% of φ,ψ angles in the favored core region, 13.7% in allowed regions, and only 0.5% of residues in generously allowed regions and 0.5% in disallowed regions (Fig. 2.4).

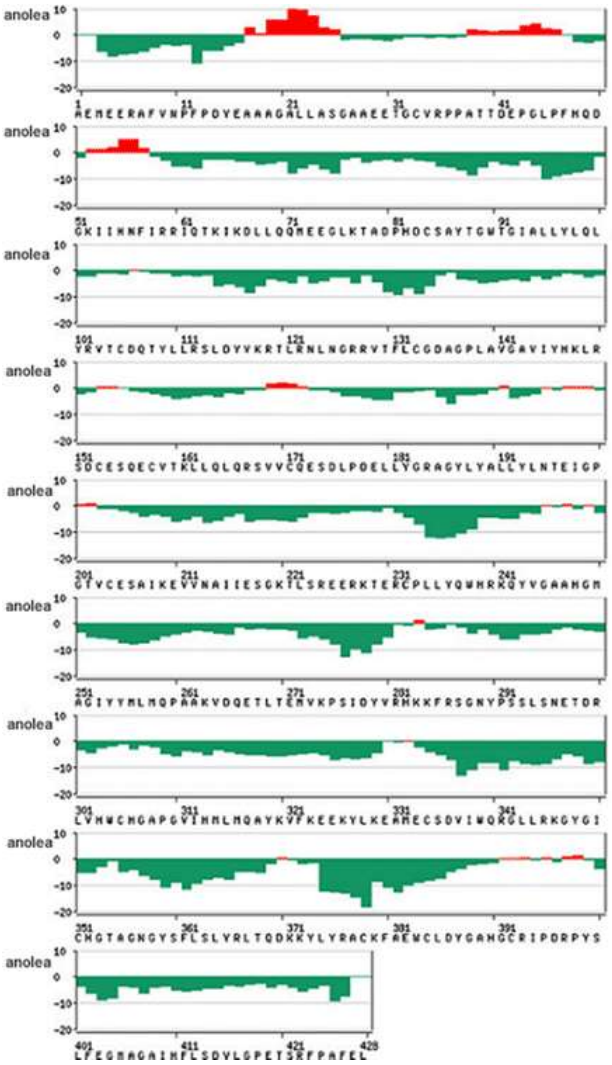


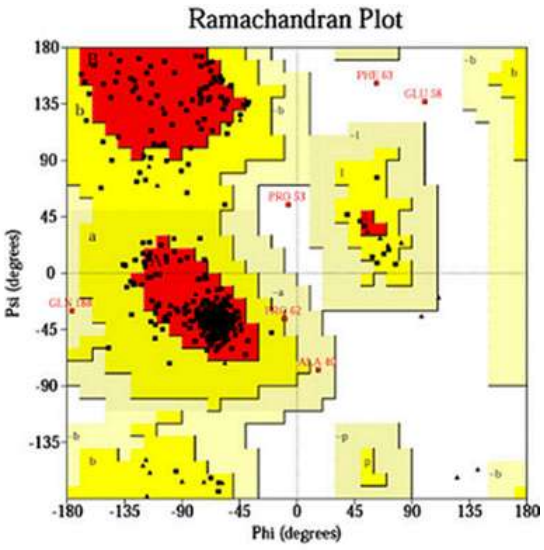


Plot statistics

| | | |
|---|---|---|
| Residues in most favoured regions [A,B,L] | 318 | 85.3% |
| Residues in additional allowed regions [a,b,l,p] | 51 | 13.7% |
| Residues in generously allowed regions [~a,~b,~l,~p] | 2 | 0.5% |
| Residues in disallowed regions | 2 | 0.5% |
| Number of non-glycine and non-proline residues | 373 | 100.0% |
| Number of end-residues (excl. Gly and Pro) | 2 | |
| Number of glycine residues (shown as triangles) | 34 | |
| Number of proline residues | 19 | |
| Total number of residues | 428 | |

**Figure 2.4.** ANOLEA plot (*left*) and Ramachandran plot (*right*) of modeled LANCL2. In the ANOLEA plot, negative values (*green*) indicate residues in a favorable environment and positive values (*red*) indicate residues in an unfavorable environment. In the Ramachandran plot, the favored and most favored region is *yellow* and *red* respectively; *pale yellow* is the generously allowed and disallowed regions are *white*

To improve and verify the stability of the initial structure, an energy minimization procedure was applied to the LANCL2 model (22). The energy minimization procedure was set to stop when the maximum force reached 1,000 KJ $mol^{-1}$ $nm^{-1}$. The potential energy in the system decreased in the energy minimization procedure. At the same time, the RMSD of LANCL2 structure relative to the starting structures increased only 0.03 nm. These results show that after the energy minimization procedure, the LANCL2 structure became more stable. Finally, the homology model of LANCL2 improved by the EM procedure and crystal structure of template (LANCL1) were compared using RAPIDO, a superposition webserver (23). Figure 2.5 shows that the LANCL2 model is very similar to the LANCL1 structure, including two layers of α-helical barrels and seven GxxG-containing bulges. The RMSD between the LANCL2 model and LANCL1 structure is 0.47 Å. On the basis of the above analysis, the homology model of LANCL2 improved by the EM procedure was employed for the following docking study.

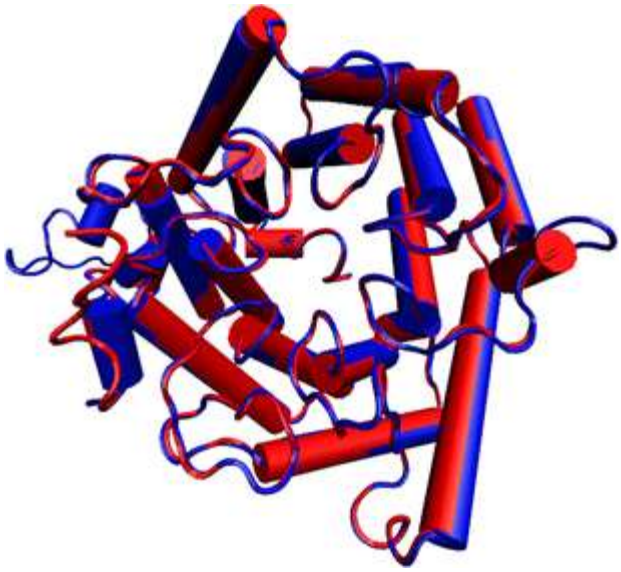

**Figure. 2.5** Superposition of the LANCL2 model and the LANCL1 template structures. *Blue* LANCL2, *red* LANCL1, *cylinders* helices, *tube* random coil

**Molecular docking and result analysis**

The AutoDock program is one of the most widely cited docking programs in the research community, owing its efficiency to the use of the LGA and a grid-based scoring function comprising several terms, including dispersion/repulsion energy, directional hydrogen bonding, screened Coulomb potential electrostatics, a volume-based solvation term, and a weighted sum of torsional degrees of freedom to estimate the entropic cost of binding [32]. Furthermore, it can identify potential binding sites of a ligand on a protein using blind docking, without the information about binding sites. In addition, full consideration of flexibility of ligands during the docking procedure makes AutoDock an appropriate tool for binding site identification. The docking of ABA with LANCL2 was performed in two steps.

In the first step, the blind docking approach was used in order to identify the potential binding sites of LANCL2. The grid generated by AutoGrid was big enough to cover the entire surface of LANCL2. The 100 resulting conformations of ligands were clustered with an RMSD cluster tolerance of 2.0 Å. The clustering plot revealed that 58% of the poses of ABA are located in the first cluster with a mean binding energy of −6.70 kcal mol−1 (Fig. 2.6). Examination of the distribution of the binding site on the LANCL2 implies that ABA shows preferential binding to the loop regions of LANCL2, which is consistent with our prediction about the substrate-binding site of LANCL2 (Fig. 2.7). This region on the LANCL2 with the high population of clusters was considered as the potential binding site for ABA. Figure 2.8 shows ABA bound inside a pocket in LANCL2. The binding pocket was surrounded by TYR279, LYS284, PHE285, PRO291, ASN296 and SER295. LYS 283 was located in the bottom of the pocket. Two hydrogen bonds formed between the nitrogen atom in the side chain of LYS283 and two hydroxyl groups of ABA that positioned ABA deep in the pocket and increased the affinity of ABA for LANCL2 (Fig. 2.8).

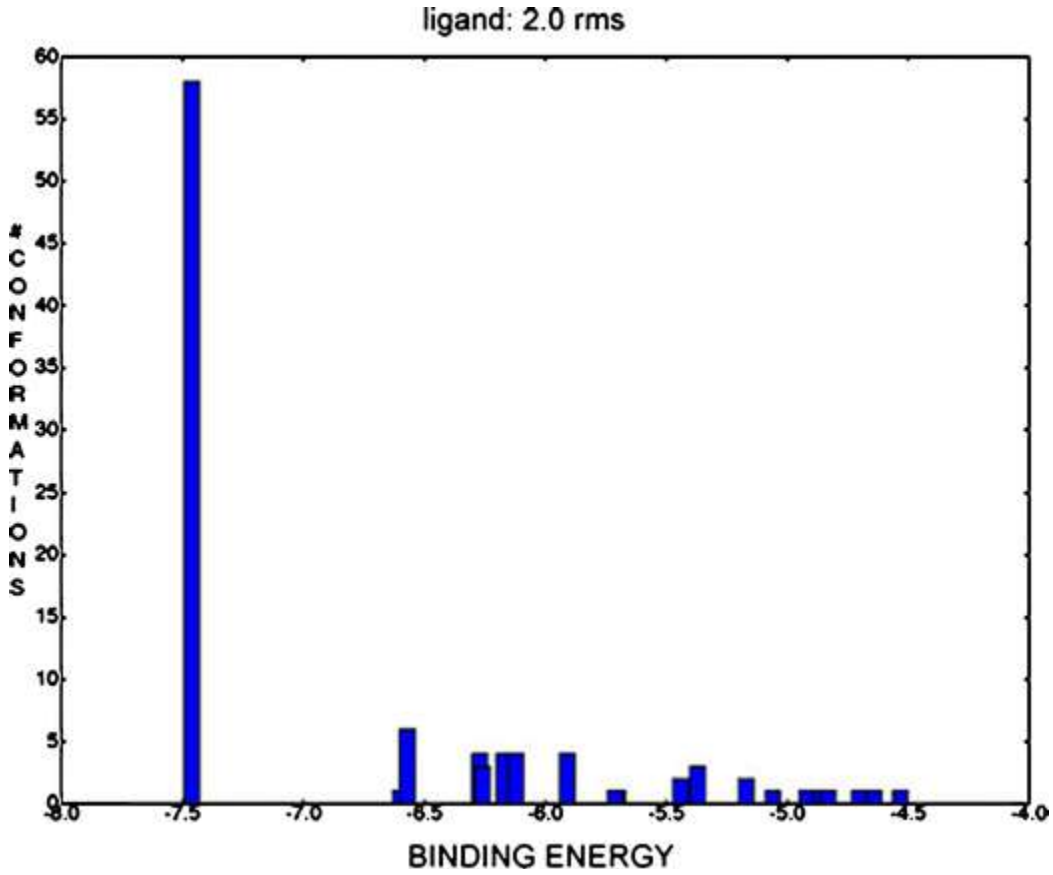


**Figure 2.6.** Representations of docked results by clustering histogram. The 100 resulting conformations of ligands were clustered with root-mean-square-deviation (RMSD) cluster tolerance of 2.0 Å. *Abscissa* represents the lowest binding energy in each cluster

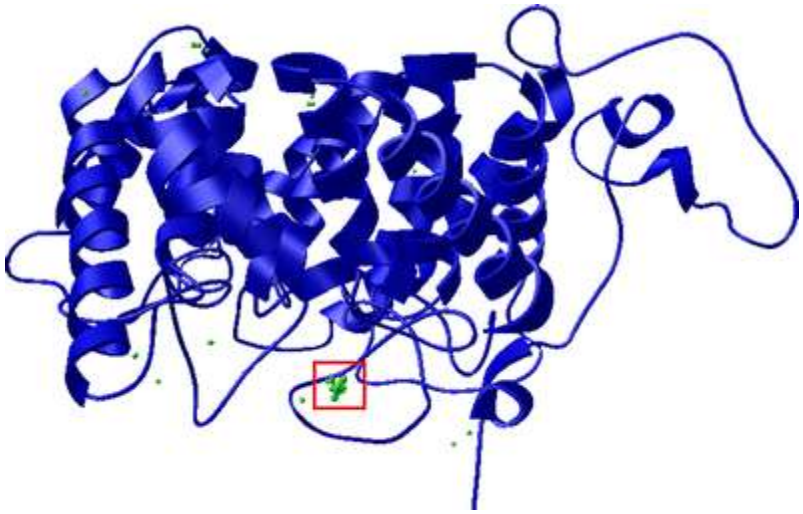

**Figure 2.7.** Overview of the distribution of conformations. Each docked conformation is represented by a *green* sphere placed at the average position of the coordinates of all the atoms in that conformation. The binding site with the most poses of ABA is outlined by the *red box*

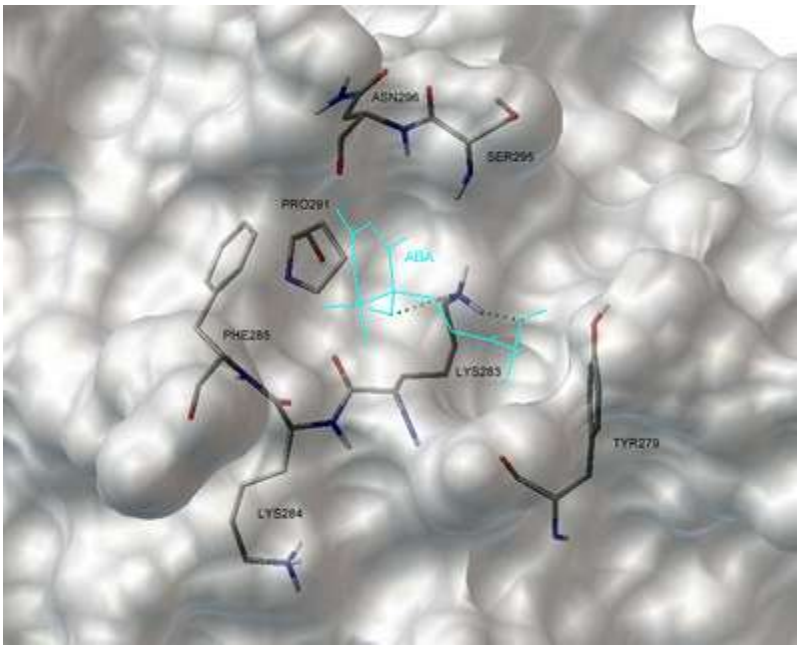


**Figure 2.8.** Representative binding modes of the most stable docked orientation of abscisic acid (ABA) with LANCL2. LANCL2 is shown in a *molecular surface model*. ABA is shown by a *cyan stick model*, and selected residues of LANCL2 are depicted by *gray stick models*. Hydrogen bonds are shown as *dashed green lines*. Amino acid residues surrounding ABA are labeled

In the second step (focused docking), ABA was docked into the binding site previously found. The use of an increased grid resolution focusing on the predicted binding site allows more focused searching and better evaluation of the protein-ligand interactions, and consequently lower binding energies are obtained with respect to the blind docking (Fig. 2.9). Comparisons of docking results were performed between blind docking and focused docking (Table 2.1).

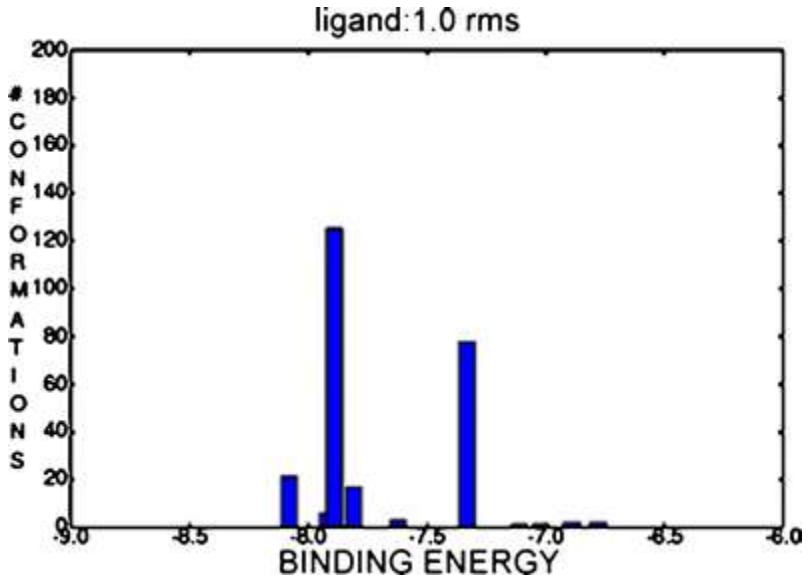


**Figure 2.9.** Clustering histogram (left). The 256 resulting conformations of ligands were clustered with RMS cluster tolerance of 1.0 Å. *Abscissa* represents the lowest binding energy in each cluster

**Table 2.1** Comparison docking results between blind docking and focused docking

| | **Cluster number** | **Lowest binding energy** | **Mean binding energy in the first cluster** |
|---|---|---|---|
| Blind docking | 20 | -7.46 kcal/mol | -6.70 kcal/mol |
| Focused docking | 10 | -8.08 kcal/mol | -7.92 kcal/mol |

**Docking test of other PPAR γ agonists on LANCL2**

In order to determine whether other PPAR γ agonists might also bind to LANCL2, we docked several small molecules, including rumenic acid, punicic acid, catalpic acid, eleostearic acid, calendic acid, jacaric acid, pioglitazone and rosiglitazone, to LANCL2 using the blind docking method. Docking results are displayed in Table 2.2 according to the lowest binding energy of these chemicals. Compared to the other molecules, pioglitazone and rosiglitazone showed better binding ability to LANCL2 with lower binding energy. These compounds belong to the TZD class of T2D drugs and, in contrast to ABA, are known to bind to the LBD of PPAR γ. Docking results showed that pioglitazone and rosiglitazone could bind to the same binding site as ABA on LANCL2

(Fig. 2.10). On the basis of this result, we propose that LANCL2 is not just necessary for transduction of the ABA signal into cell-specific functional responses, but it may also be one important membrane receptor for a series of antidiabetic drugs that act by activating PPAR γ. Further studies are in process to verify our prediction.

**Table 2.2** Docking results of small molecules to LANCL2, ranked by the lowest binding energy

| Common Name | Chemical Name | Chemical Structure | Lowest Binding Energy (kcal/mol) |
|---|---|---|---|
| abscisic acid | [*S*-(*Z*,*E*)]-5-(1-Hydroxy-2,6,6 -trimethyl-4-oxo-2-cyclohexen-1-yl)-3-methyl-2,4-pentanedienoic acid | 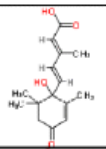 | -7.46 |
| rosiglitazone | (RS)-5-[4-(2-[methyl(pyridin-2-yl)amino]ethoxy)benzyl]thiazolidine-2,4-dione | 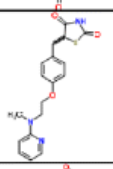 | -7.95 |
| pioglitazone | (RS)-5-(4-[2-(5-ethylpyridin-2-yl)ethoxy]benzyl) thiazolidine-2,4-dione | 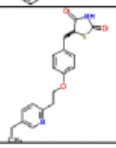 | -7.08 |
| α-Calendic acid | (8E,10E,12Z)-octadeca-8,10,12-trienoic acid | 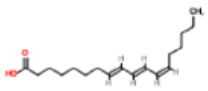 | -5.79 |
| catalpic acid | (9Z,11Z,13E)-octadeca-9,11,13-trienoic acid | 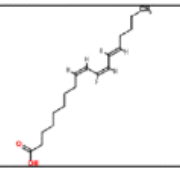 | -5.72 |
| β-Calendic acid | (8E,10E,12E)-octadeca-8,10,12-trienoic acid | 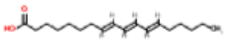 | -5.65 |
| t10,c12 conjugated linoleic acid | (10E,12Z)-octadeca-9,11-dienoic acid | 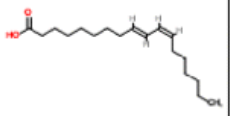 | -5.40 |
| β -eleostearic acid | (9E,11E,13E)-octadeca-9,11,13-trienoic acid | 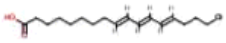 | -5.28 |
| α -eleostearic acid | (9Z,11E,13E)-octadeca-9,11,13-trienoic acid | 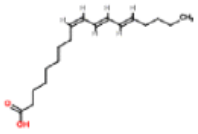 | -5.21 |
| punicic acid | (9Z,11E,13Z)-octadeca-9,11,13-trienoic acid | 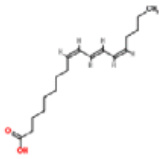 | -5.18 |
| jacaric acid | (8E,10Z,12E)-octadeca-8,10,12-trienoic acid | 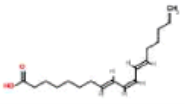 | -5.09 |
| c9, t11 conjugated linoleic acid | (9Z,11E)-octadeca-9,11-dienoic acid | 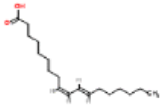 | -4.98 |

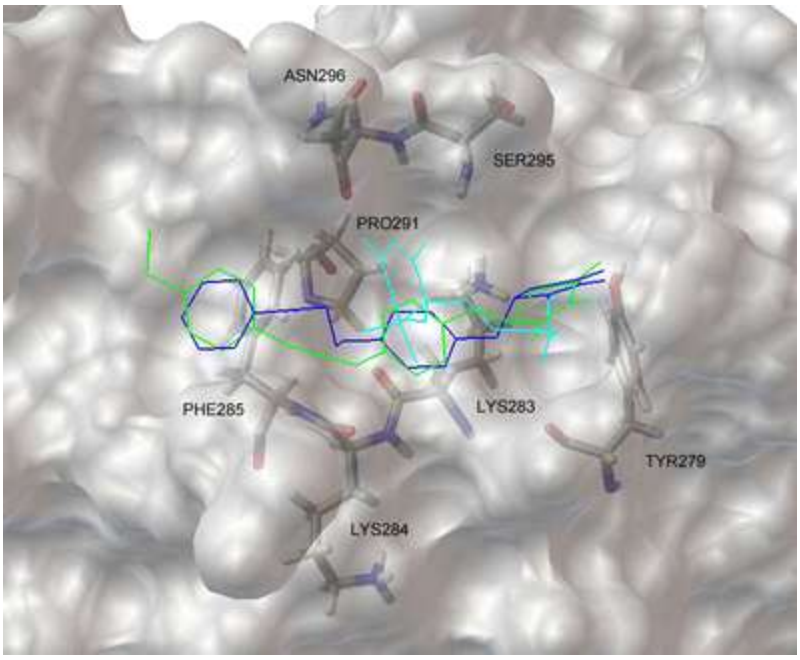


**Figure 2.10.** Representation of the binding modes of ABA and thiazolidinedione (TZD) on LANCL2. *Cyan* ABA, *green* pioglitazone, *blue* rosiglitazone. LANCL2 is shown in a *molecular surface model*. Selected residues of LANCL2 are depicted by *stick-and-ball models* and colored by atom types (*red* oxygen, *blue* nitrogen, *white* hydrogen). This figure illustrates that ABA and TZDs may bind to the same site on LANCL2

## 2.5 Conclusions

The aim of this study was to build a three-dimensional structural model of LANCL2 and to identify the binding site of ABA in LANCL2. In the present work, we generated the model of LANCL2 by homology modeling, to which ABA was docked using the blind docking method. By focused docking, the best binding site of ABA with low binding energy was identified, which indicates that LANCL2 may serve as the membrane receptor for ABA. Additionally, pioglitazone and rosiglitazone bound to the same site as ABA on LANCL2. On the basis of these findings, we propose a novel mechanism by which PPAR γ agonists can elicit their biological effects. Our LANCL2 model will be applicable for virtual screening of novel compounds for the treatment of T2D and other inflammatory diseases.

## 2.6 Acknowledgments

Supported by award number 5R01AT4308 of the National Center for Complementary and Alternative Medicine at the National Institutes of Health awarded to J.B.-R.,

European Commission grant number 224836, the Ramon y Cajal Program and funds from the Nutritional Immunology and Molecular Nutrition Laboratory.

## 2.7 References

1. Kumar V, Abbas A, Fausto N. Robbins and Cotran pathologic basis of disease. Elsevier Saunders. Philadelphia, Pa. 2005:10-1.
2. Inzucchi SE, Sherwin RS. The prevention of type 2 diabetes mellitus. Endocrinology and metabolism clinics of North America. 2005;34(1):199-219.
3. DeFronzo RA. Pharmacologic therapy for type 2 diabetes mellitus. Annals of internal medicine. 2000;133:73-4.
4. DeFronzo R, Ratner R, Han J, Kim D, Fineman M, Baron A. Effects of exenatide (exendin-4) on glycemic control and weight over 30 weeks in metformin-treated patients with type 2 diabetes. Diabetes care. 2005;28:1092-100.
5. Rang H, Dale MM, Ritter J, Moore P. Pharmacology Churchill Livingstone. New York. 2003.
6. Nesto RW, Bell D, Bonow RO, Fonseca V, Grundy SM, Horton ES, et al. Thiazolidinedione use, fluid retention, and congestive heart failure: a consensus statement from the American Heart Association and American Diabetes Association. October 7, 2003. Circulation. 2003;108:2941-8.
7. Lewis SN, Bassaganya-Riera J, Bevan DR. Virtual Screening as a Technique for PPAR Modulator Discovery. PPAR research. 2010;2010:861238.
8. Bassaganya-Riera J, Skoneczka J, Kingston DGJ, Krishnan A, Misyak SA, Guri AJ, et al. Mechanisms of Action and Medicinal Applications of Abscisic Acid. Current medicinal chemistry. 2010.
9. Guri AJ, Hontecillas R, Ferrer G, Casagran O, Wankhade U, Noble AM, et al. Loss of PPARγ in immune cells impairs the ability of abscisic acid to improve insulin sensitivity by suppressing monocyte chemoattractant protein-1 expression and macrophage infiltration into white adipose tissue. The Journal of nutritional biochemistry. 2008;19(4):216-28.
10. Sturla L, Fresia C, Guida L, Bruzzone S, Scarfì S, Usai C, et al. LANCL2 is necessary for abscisic acid binding and signaling in human granulocytes and in rat insulinoma cells. The Journal of biological chemistry. 2009;284:28045-57.
11. Landlinger C, Salzer U, Prohaska R. Myristoylation of human LanC-like protein 2 (LANCL2) is essential for the interaction with the plasma membrane and the increase in cellular sensitivity to adriamycin. Biochimica et biophysica acta. 2006;1758:1759-67.
12. Zhang W, Wang L, Liu Y, Xu J, Zhu G, Cang H, et al. Structure of human lanthionine synthetase C-like protein 1 and its interaction with Eps8 and glutathione. Genes & development. 2009;23:1387-92.
13. Altschul SF, Gish W, Miller W, Myers EW, Lipman DJ. Basic local alignment search tool. Journal of molecular biology. 1990;215:403–10.
14. Subramaniam S. The Biology Workbench-a seamless database and analysis environment for the biologist. Proteins. 1998;32:1-2.
15. Thompson JD, Higgins DG, Gibson TJ. CLUSTAL W: improving the sensitivity of progressive multiple sequence alignment through sequence weighting, position-

specific gap penalties and weight matrix choice. Nucleic acids research. 1994;22:4673-80.
16. Arnold K, Bordoli L, Kopp J, Schwede T. The SWISS-MODEL workspace: a web-based environment for protein structure homology modelling. Bioinformatics (Oxford, England). 2006;22:195-201.
17. Berman HM, Westbrook J, Feng Z. The protein data bank. Nucleic acids research. 2000;28:235-42.
18. Melo F, Feytmans E. Assessing protein structures with a non-local atomic interaction energy. J Mol Biol. 1998;277:1141-52.
19. Laskowski R, MacArthur M, Moss D, Thornton J. PROCHECK: a program to check the stereochemical quality of protein structures. Journal of Applied Crystallography. 1993;26:283-91.
20. Hess B, Kutzner C, van der Spoel D, Lindahl E. GROMACS 4: Algorithms for Highly Efficient, Load-Balanced, and Scalable Molecular Simulation. Journal of Chemical Theory and Computation. 2008;4:435-47.
21. Jorgensen WL, Tirado-rives J. The OPLS Force Field for Proteins. Energy Minimizations for Crystals of Cyclic Peptides and Crambin. J Am Chem Soc. 1988;110:1657-66.
22. Wiberg KB. A Scheme for Strain Energy Minimization. Journal of the American Chemical Society. 1965;87:1070-8.
23. Mosca R, Schneider TR. RAPIDO: a web server for the alignment of protein structures in the presence of conformational changes. Nucleic acids research. 2008;36:W42-6.
24. Wang Y, Xiao J, Suzek TO, Zhang J, Wang J, Bryant SH. PubChem: a public information system for analyzing bioactivities of small molecules. Nucleic acids research. 2009;37:W623-33.
25. Morris GM, Huey R, Lindstrom W, Sanner MF, Belew RK, Goodsell DS, et al. Software News and Updates AutoDock4 and AutoDockTools4 : Automated Docking with Selective Receptor Flexibility. J Comput Chem. 2009;30:2785-91.
26. Morris GM, Goodsell DS, Halliday RS, Huey R, Hart WE, Belew RK, et al. Automated docking using a Lamarckian genetic algorithm and an empirical binding free energy function. Journal of computational chemistry. 1998;19:1639-62.
27. Bikádi Z, Hazai E, Zsila F, Lockwood SF. Molecular modeling of non-covalent binding of homochiral (3S,3'S)-astaxanthin to matrix metalloproteinase-13 (MMP-13). Bioorganic & medicinal chemistry. 2006;14:5451-8.
28. Hazai E, Bikádi Z, Zsila F, Lockwood SF. Molecular modeling of the non-covalent binding of the dietary tomato carotenoids lycopene and lycophyll, and selected oxidative metabolites with 5-lipoxygenase. Bioorganic & medicinal chemistry. 2006;14:6859-67.
29. Hetenyi C, van Der Spoel D. Efficient docking of peptides to proteins without prior knowledge of the binding site. Protein Science: A Publication of the Protein Society. 2002;11:1729.
30. Hetényi C, van der Spoel D. Blind docking of drug-sized compounds to proteins with up to a thousand residues. FEBS letters. 2006;580:1447-50.

31. Iorga B, Herlem D, Barré E, Guillou C. Acetylcholine nicotinic receptors: finding the putative binding site of allosteric modulators using the "blind docking" approach. Journal of molecular modeling. 2006;12:366-72.
32. Kovács M, Tóth J, Hetényi C, Málnási-Csizmadia A, Sellers JR. Mechanism of blebbistatin inhibition of myosin II. The Journal of biological chemistry. 2004;279:35557-63.
33. Rost B. Twilight zone of protein sequence alignments. Protein Eng. 1999;12:85-94.
34. Humphrey W, Dalke A, Schulten K. VMD: visual molecular dynamics. Journal of molecular graphics. 1996;14(1):33-8.

# Chapter 3. Computational modeling-based discovery of novel classes of anti-inflammatory drugs that target lanthionine synthetase C-like protein 2

**Pinyi Lu[1,2,*], Raquel Hontecillas[1,2], William T. Horne[1,2], Adria Carbo[1,2], Monica Viladomiu[1,2], Mireia Pedragosa[1,2], David R. Bevan[1,3], Stephanie N. Lewis[1,2,3], and Josep Bassaganya-Riera[1,2,*]**

Lu P, Hontecillas R, Horne WT, Carbo A, Viladomiu M, Pedragosa M, et al. Computational modeling-based discovery of novel classes of anti-inflammatory drugs that target lanthionine synthetase C-like protein 2. PloS one. 2012;7(4):e34643. Used with permission of PLOS, 2015.

[1]Center for Modeling Immunity to Enteric Pathogens, Virginia Tech, Blacksburg, VA 24061, USA, [2]Nutritional Immunology and Molecular Medicine Laboratory, Virginia Bioinformatics Institute, Virginia Tech, Washington Street 0477, Blacksburg, VA 24061, USA, [3]Department of Biochemistry, Virginia Tech, 201 Engel Hall 0308, Blacksburg, VA 24061, USA

[*]E-mail: jbassaga@vbi.vt.edu (JBR); lpy0526@vbi.vt.edu (PL)

## 3.1 Abstract

***Background:*** Lanthionine synthetase component C-like protein 2 (LANCL2) is a member of the eukaryotic lanthionine synthetase component C-like protein family involved in signal transduction and insulin sensitization. Recently, LANCL2 is a target for the binding and signaling of abscisic acid (ABA), a plant hormone with anti-diabetic and anti-inflammatory effects.

***Methodology/Principal Findings:*** The goal of this study was to determine the role of LANCL2 as a potential therapeutic target for developing novel drugs and nutraceuticals against inflammatory diseases. Previously, we performed homology modeling to construct a three-dimensional structure of LANCL2 using the crystal structure of lanthionine synthetase component C-like protein 1 (LANCL1) as a template. Using this model, structure-based virtual screening was performed using compounds from NCI (National Cancer Institute) Diversity Set II, ChemBridge, ZINC natural products, and FDA-approved drugs databases. Several potential ligands were identified using molecular docking. In order to validate the anti-inflammatory efficacy of the top ranked compound (NSC61610) in the NCI Diversity Set II, a series of *in vitro* and pre-clinical efficacy studies were performed using a mouse model of dextran sodium sulfate (DSS)-induced colitis. Our findings showed that the lead compound, NSC61610, activated peroxisome proliferator-activated receptor gamma in a LANCL2- and adenylate cyclase/cAMP dependent manner *in vitro* and ameliorated experimental colitis by down-modulating colonic inflammatory gene expression and favoring regulatory T cell responses.

***Conclusions/Significance:*** LANCL2 is a novel therapeutic target for inflammatory diseases. High-throughput, structure-based virtual screening is an effective computational-based drug design method for discovering anti-inflammatory LANCL2-based drug candidates.


## 3.2 Introduction

Prokaryotic LanC is a part of a multimeric membrane-associated lanthionine synthetase complex involved in the modification and transport of peptides. LanC itself is a zinc-

containing enzyme that acts in concert with specific dehydratases to facilitate intramolecular conjugation of cysteine to serine or threonine residues, yielding macrocyclic thioether analogs of cysteine known as lanthionines. These products display potent antimicrobial activity, and are also known as lantibiotics (1). The first member of the eukaryotic lanthionine synthetase component C-like (LANCL) protein family, LANCL1, was isolated from human erythrocyte membranes (2). A related protein, LANCL2, was subsequently identified in human brain and testis (3). LANCL1 and 2 have similar expression patterns, with strong expression in brain and testis, and weak but ubiquitous expression in other tissues (2, 3). LANCL2 is most highly expressed in testis, and its exogenous introduction has been shown to cause increased cellular sensitivity to the anticancer drug, adriamycin, by suppressing the expression of MultiDrug-Resistance 1 and its cognate protein, P-glycoprotein (4). On the other hand, overexpressed LANCL2 interacted with the actin cytoskeleton, implying that LANCL2 may also have a role in cytoskeletal reorganization and cellular movement (5).

Sturla and colleagues provided *in vitro* results suggesting that LANCL2 is required for abscisic acid (ABA) binding to the membrane of human granulocytes and for transduction of the ABA signal into cell-specific functional responses in granulocytes (6). ABA is an isoprenoid phytohormone that plays important roles in plant responses to environmental stresses and host responses (7). In addition, ABA has received recent attention due its peroxisome proliferator-activated receptor (PPAR) γ-activating and anti-inflammatory properties, which make it a target for development of potent anti-inflammatory and insulin-sensitizing therapeutics (7). We demonstrated that PPAR γ is required for ABA to induce its full spectrum of effects, but ABA does not bind directly to the ligand-binding domain (LBD) of PPAR γ (8). The mechanism of activation of PPAR γ by ABA is not completely understood, but there is evidence supporting the observation that ABA-mediated PPAR γ activation requires expression of LANCL2 in immune cells (8). Indeed, we demonstrated that ABA binds to LANCL2 *in silico* (8). Moreover, by using molecular modeling approaches, we elucidated the location of the potential LBD of LANCL2 for ABA. Recently, a series of *in vitro* binding studies on human LANCL2 recombinant protein confirmed direct binding of ABA to LANCL2, including saturation

binding, scintillation proximity assays, dot blot experiments, and affinity chromatography (9). Identification of ABA binding to LANCL2 paves the way for the discovery and development novel anti-inflammatory drugs that target LANCL2. Based on previous findings, we proposed that LANCL2 might be a putative novel target for the discovery and development of orally active, broad-based drugs against inflammatory, infectious and chronic metabolic diseases (10).

The predominant technique employed in the identification of new drugs is the physical large scale, high-throughput screening of thematic compound libraries against a biological target, which is very costly and yields mixed results. Recent successes in predicting new ligands and their receptor-bound structures make use of structure-based virtual screening (SBVS), which is a more cost-effective approach in drug and nutraceutical discovery. The basic procedure of SBVS is to sample binding geometry for compounds from large libraries into the structure of receptor targets by using molecular modeling approaches. Each compound is sampled in thousands to millions of possible poses and scored on the basis of its complementarity to the receptor. Of the hundreds of thousands of molecules in the library, tens of top-scoring predicted ligands are subsequently tested for activity in experimental assays (11). One of the main requirements for SBVS is availability of the three-dimensional structure of a validated protein target (12). In some cases, when the crystal structure of the receptor target is unknown, computer-modeled structures have been verified to suffice for successful virtual screening (13-16). In a previous study from our group, homology modeling of human LANCL2 was performed using the crystal structure of human LANCL1 as a template (17) and the model quality was assessed (10).

We performed LANCL2-based virtual screening using the structure of LANCL2 obtained through homology modeling to discover new LANCL2 agonists. Thousands of compounds from NCI Diversity Set II, ChemBridge, ZINC natural products and U.S. Food and Drug Administration (FDA)-approved drug databases were docked into the LANCL2 model and ranked by the calculated affinity. The effect of the top ranked compound in the NCI Diversity Set II, the benzimidazophenyl compound denoted

NSC61610, on the activity of PPAR γ was tested *in vitro* using a dual luciferase reporter activity assay. Its *in vivo* efficacy and cell-specific PPAR γ dependency were then examined using a mouse model of experimental IBD.

### 3.3 Materials and methods

#### Expression of LANCL2 in Mouse Tissues

Proteins were extracted from different mouse tissue, including thymus, lung, spleen, stomach, ileum, colon, Peyer's patches (PP), mesenteric lymph node (MLN), gastric lymph node (GLN), blood, white adipose tissue (WAT), and bone marrow (BM) as previously described (8). The protein extracts were analyzed using a 10% SDS-PAGE gel in a Bio-Rad mini-gel box running condition (75 V × 3 hrs). Afterward, proteins were electrotransferred to nitrocellulose by standard methods along with the Precision Plus Kaleidoscope Standard (BIO-RAD). Filters were blocked by 5% BSA in TBS-Tween for 1 hour, followed by incubation with rabbit anti-LANCL2 primary antibody (SIGMA-ALDRICH) in TBS-Tween for 6 hours at room temperature. Goat anti-rabbit horseradish peroxidase-conjugated secondary antibody (Santa Cruz Biotechnology) was used at a dilution of 1:2000 in TBS-Tween, and protein bands were detected with Immun-StarTM chemiluminescent substrate (BIO-RAD). Re-probing western blot was applied by incubating nitrocellulose in stripping buffer (Thermo scientific) for 15 minutes.

#### Compound Database Management and Ligand Structure

The structure files of compounds were obtained from the ZINC database in mol2 format (18), and the individual mol2 files were converted into pdbqt files using the python script prepare_ligand4.py available in the Autodock Tools package (19). The NCI diversity set II is a reduced set of 1,364 compounds selected from the almost 140,000 compounds available for distribution from the DTP (Developmental Therapeutics Program) repository. The selection process is outlined in more detail at the NCI DTP website (http://www.dtp.nci.nih.gov/branches/dscb/div2_explanation.html). The ChemBridge Corporation maintains a stock of more than 800,000 drug-like and lead-like screening compounds. Structures for these compounds are available for download from the ZINC database (http://zinc.docking.org/vendor0/chbr/index.html). The ZINC natural products

database has a structure collection of 89,425 natural products available for download from the ZINC database (http://zinc.docking.org/vendor0/npd/index.html). The FDA-approved drugs database includes 3,180 FDA-approved drug structures, which also are available for download from the ZINC database (http://zinc.docking.org/vendor0/fda/index.html).

**Virtual Screening**

The docking of compounds available in the NCI Diversity Set II, ChemBridge, ZINC natural products and FDA-approved drugs databases into the LANCL2 computational model was performed with AutoDock Vina (version 1.0) (20). AutoDockTools, the graphical front-end for AutoDock and AutoGrid, was used to define the search space, including grid box center and x,y,z-dimensions (19). A variety of stochastic global optimization approaches were used in AutoDock Vina, including genetic algorithms, particle swarm optimization, simulated annealing and others. Five bound conformations were generated by AutoDock Vina for each compound. The docking was applied to the whole protein target, with a grid covering the whole surface of the protein. To search the entire surface of LANCL2, grid maps were set with the maximum spacing between grid points. The grid was a rectangular cuboid (70Å ×70Å × 60Å) with grid points separated by 1.000 Å and centered at the middle of the protein. This grid was big enough to cover the entire surface of LANCL2.

**Analyzing the Virtual Screening Results**

The search for the best way to fit each compound into LANCL2 using AutoDock Vina resulted in docking log files that contained records of docking, including binding energy of each predicted binding mode for all the compounds. Binding energies represent the sum of the total intermolecular energy, total internal energy and torsional free energy minus the energy of the unbound system. For each database, compounds were ranked by the most negative energy value. All predicted binding poses were placed into one multimodel PDBQT file.

**PPAR γ Reporter Activity Assays on Raw Macrophages**

To determine PPAR γ activity, pCMX.PPAR γ expression plasmid and a pTK.PPRE3x luciferase reporter plasmid driven by the peroxisome proliferator responsive element-containing Acyl-CoA oxidase promoter were purified using maxi kit from Qiagen (Valencia, CA). RAW 264.7 macrophages were cultured with DMEM (Mediatech, Manassas, VA) containing 10% fetal bovine serum (FBS) and grown until 60–70% confluence. Cells were cotransfected in two 25 cm2 flasks with 1.5 μg plasmid of DNA and 0.15 μg of pRL reporter control with or without 100pmol LANCL2 siRNA using Lipofectamine 2000 transfection reagent (Invitrogen) according to the manufacturer's protocol. After 24 h, transfected cells were seeded into white, opaque 96-well plates (BD Biosciences) at a concentration of 25,000 cells/well. Transfected cells were then treated in replicates with rosiglitazone (Ros 1 μM; Cayman Chemical, Ann Arbor, MI), NSC61610 (2.5 μM) with and without 2'5'-dideoxyadenosine (10 μM; Sigma) or vehicle (DMSO) and placed in a 37 ℃ incubator with 5% CO2. After 20 h, cells were harvested in reporter lysis reagent. Luciferase activity, normalized to pRL activity in the cell extracts, was determined by using the Dual-Luciferase II reporter assay system (Promega, Madison, WI) using a Modulus 96-well luminometer (Turner Biosystems, Sunnyvale, CA). All values were normalized to control wells to calculate relative luciferase activity.

**Ethics Statement**

All experimental procedures were approved by the Institutional Animal Care and Use Committee (IACUC) of Virginia Tech and met or exceeded requirements of the Public Health Service/National Institutes of Health and the Animal Welfare Act. The IACUC approval ID for the study was 11-057-VBI.

**Animal Procedures to Test the Anti-inflammatory Efficacy of Lead Compound NSC61610 in IBD**

Eight week old C57BL/6J mice were housed at the animal facilities at Virginia Tech in a room maintained at 75 ℉, with a 12:12 hr light-dark cycle starting from 6:00 AM. Mice were randomly assigned into four groups: a control group including 8 mice and the other three NSC61610 treatment groups containing 10 mice each. The three treatment groups received 0.5, 10 or 20 mg NSC61610/kg body weight by orogastric gavage for 7 days.

All the mice were challenged with 2.5% DSS, 36,000-44,000 molecular weight (ICN Biomedicals, Aurora, OH) in the drinking water for 7 days. Mice were weighed on a daily basis and examined for clinical signs of disease associated with colitis (i.e., perianal soiling, rectal bleeding, diarrhea, and piloerection). For the DSS challenge, the disease activity indices (DAIs) and rectal bleeding scores were calculated using a modification of a previously published compounded clinical score (21). Briefly, DAI consisted of a scoring for diarrhea and lethargy (0-3), whereas rectal bleeding consisted of a visual observation of blood in feces and the perianal area (0-4). On day 7 of the challenge, mice in the DSS study were euthanized.by $CO_2$ narcosis followed by secondary thoracotomy and blood was drawn from the heart. Colon, spleen, and MLN were scored based on size and macroscopic inflammatory lesions (0-3), excised, and single-cell suspensions were prepared for flow cytometric analyses.

**Histopathology**

Colonic sections were fixed in 10% buffered neutral formalin, later embedded in paraffin, and then sectioned (5 mm) and stained with H&E stain for histologic examination. Colons were blindly graded with a compounded histologic score including the extent of (1) leukocyte infiltration, (2) mucosal thickening, and (3) epithelial cell erosion. The sections were graded with a score of 0-4 for each of the previous categories and data were analyzed as a normalized compounded score as previously described (21).

**Quantitative Real-time RT-PCR**

Total RNA was isolated from colons using the RNA isolation Minikit (Qiagen) according to the manufacturer's instructions. Total RNA (1 mg) was used to generate complementary DNA (cDNA) template using the iScript cDNA Synthesis Kit (Bio-Rad, Hercules, CA). The total reaction volume was 20 μL with the reaction incubated as follows in an MJ MiniCycler: 5 min at 25 ℃, 30 min at 52 ℃, 5 min at 85 ℃, and hold at 4 ℃. PCR was performed on the cDNA using Taq DNA polymerase (Invitrogen, Carlsbad, CA) and using previously described conditions. Each gene amplicon was purified with the MiniElute PCR Purification Kit (Qiagen) and quantitated on an agarose gel by using a DNA mass ladder (Promega). These purified amplicons were used to

optimize quantitative real-time RT-PCR conditions and to generate standard curves. Primer concentrations and annealing temperatures were optimized for the iCycler iQ system (Bio-Rad) for each set of primers using the system's gradient protocol. PCR efficiencies were maintained between 92 and 105% and correlation coefficients above 0.98 for each primer set during optimization and also during the real-time PCR of sample DNA.

cDNA concentrations for genes of interest were examined by RT-PCR using an iCycler IQ System and the iQ SYBR green supermix (Bio-Rad). A standard curve was generated for each gene using 10-fold dilutions of purified amplicons starting at 5 pg of cDNA and used later to calculate the starting amount of target cDNA in the unknown samples. SYBR green I is a general double-stranded DNA intercalating dye and may therefore detect non-specific products and primer/dimers in addition to the amplicon of interest. In order to determine the number of products synthesized during the real-time PCR, a melting curve analysis was performed on each product. RT- PCR was used to measure the starting amount of nucleic acid of each unknown sample of cDNA on the same 96-well plate. Results are presented as starting quantity of target cDNA (picograms) per microgram of total RNA as previously described (21). Primer sequences and Genebank accession numbers are outlined in Supplementary Table S3.1.

**Immunophenotyping of tissues of mice with IBD**

Colonic lamina proprial lymphocytes (LPL) were isolated from digested colons. Spleens and MLNs were excised and single cell suspensions were prepared. Splenocytes were freed of red blood cells with erythrocyte lysis buffer, and spleen and MLN were resuspended in PBS and enumerated by using a Coulter Counter (Beckman Coulter, Fullerton, CA). LPL, spleen and MLN-derived cells ($2 \times 10^5$ cells/well) or whole blood (10 µL/well) were seeded onto 96-well plates, centrifuged at 4 ℃ at 3000 rpm for 4 min, and washed with PBS containing 5% serum and 0.09% sodium azide (FACS buffer). To assess differential monocyte/macrophage infiltration, the cells were then incubated in the dark at 4 ℃ for 20 min in FcBlock (20 µg/ml, BD Pharmingen) for macrophage assessment, and then for an additional 20 min with fluorochrome-conjugated primary

antibodies anti-F4/80-PE-Cy5 (0.2 mg/mL, ebioscience) and anti-CD11b-Alexa Fluor 700 (0.2 mg/mL, BD Pharmingen). For lymphocyte subset assessment, cells were incubated with anti-CD45-APC-Cy7 (for LPL only) (0.2 mg/mL, BD Pharmingen), anti-CD4-PE-Cy7 (0.2 mg/mL, BD Pharmingen), anti-CD8-PerCp-Cy5.5 (0.2 mg/mL, eBioscience), anti-CD3-PE-Cy5 (0.2 mg/mL, ebioscience), anti-FoxP3-APC (0.2 mg/mL, eBioscience), and anti-IL10-FITC (0.5 mg/mL, BD Pharmingen). Flow results were computed with a BD LSR II flow cytometer and data analyses were performed with FACS Diva software (BD).

**Characterization of the Immunoregulatory Mechanisms of NSC61610 in Mice with Experimental IBD**

PPAR γ fl/fl Cre- (n=20), tissue-specific PPAR γ fl/fl CD4-Cre+ (T cell-deficient) PPAR γ null mice (n=20) and tissue-specific PPAR γ fl/fl Lysozyme M-Cre+ (myeloid-deficient) PPAR γ null mice (n=20) in a C57BL/6J background were generated by using the Cre-lox recombination system as previously described (21). In each group, 20 mice were randomly divided into two groups: a control group including 10 mice and a NSC61610 treatment group containing 10 mice. The three treatment groups received 20 mg/kg NSC61610 by orogastric gavage for 6 days. We selected 20 mg/kg for subsequent testing in this study because this dose had shown the greatest anti-inflammatory activity in the dose-response study (described above). All the mice (n=60) were challenged with drinking water containing 2.5% DSS, 36,000-44,000 molecular weight (ICN Biomedicals, Aurora, OH) for 6 days. Mice were weighed on a daily basis and examined for clinical signs of disease associated with colitis. For the DSS challenge, the disease activity indices and rectal bleeding scores were calculated using a modification of a previously published compounded clinical score (21). Mice in the DSS study were euthanized on day 6 of the DSS challenge. On day 6, colon, spleen, and MLN were scored based on size and macroscopic inflammatory lesions (0-3), excised, and then crushed to produce single-cell suspensions for flow cytometry.

**Statistics**

Data were analyzed as a completely randomized design. To determine the statistical significance of the model, analysis of variance (ANOVA) was performed using the general linear model procedure of Statistical Analysis Software (SAS), and probability value ($P$) <0.05 was considered to be significant. When the model was significant, ANOVA was followed by multiple comparison method to identify pairwise treatments with significant difference.

**Reverse docking NSC61610 to Novel Potential Drug Targets**

The potential drug target database (PDTD) is a dual function database that associates an informatics database to a structural database of known and potential drug targets. PDTD is a comprehensive, web-accessible database of drug targets, and focuses on those drug targets with known 3D-structures. The target proteins collected in PDTD were selected from the literature, and from several online databases, such as DrugBank and Therapeutic Targets Database (TTD). PDTD contains 1,207 entries covering 841 known and potential drug targets with structures from the PDB. Drug targets of PDTD were categorized into 15 and 13 types, respectively, according to two criteria: therapeutic areas and biochemical criteria (22). Target Fishing Dock (TarFisDock) is a web-based tool for seeking potential binding proteins for a given ligand. It applies a ligand-protein reverse docking strategy to search out all possible binding proteins for a small molecule from the PDTD (23). TarFisDock was developed on the basis of DOCK (version 4.0) program (24). The reverse docking procedure is as follows: 1) The NSC61610 structure file in sdf format was downloaded from PubChem (SID 109036). The NSC61610 structure file was transformed to the standard mol2 format using the Chimera program (25). 2) TarFisDock docked NSC61610 into the possible binding sites of proteins in the target list. Putative binding proteins are selected by ranking the values of the interaction energy, which is composed of van der Waals and electrostatic interaction terms.

## 3.4 Results

**Virtual Screening and Result Analysis**

In a previous study, we constructed the homology model of LANCL2 according to the crystal structure of LANCL1 using SWISS-MODEL Workspace (26). The structure of

LANCL2 is shown in Figure 3.1A (27). Two levels of assessment, ANOLEA (28) and PROCHECK (29), both indicated the good quality of the model (10).

To discover novel naturally occurring compounds, new drugs and repurposed drugs that target the LANCL2 and potentially exert insulin-sensitizing and anti-inflammatory actions, virtual screening was applied to identify potential ligands of LANCL2. The compound databases used for screening contain NCI Diversity Set II, ChemBridge and ZINC natural product, existing drug databases and FDA-approved drugs databases.

During the *in silico* screening process, compounds were ranked according to their estimated free energy of binding. The best ten docking solutions based on the energy scores were selected for each database (Supplementary Tables S3.2-3.5) using AutoDock Vina. A lower binding free energy indicates a more stable protein-ligand system and a higher affinity between protein and ligand. In our integrated discovery pipeline, lead compounds in each category are further validated by *in vitro* testing and pre-clinical studies using mouse models of human diseases. NSC61610, the structure of which is given in Figure 3.1B, had the lowest free energy of binding (-11.1 kcal/mol) compared to other compounds in NCI Diversity Set II. To further verify the binding between NSC61610 and LANCL2 *in silico*, we docked NSC61610 to LANCL2 using AutoDock (version 4.2) (19). The detailed approach is the same as the one we applied in docking experiments of ABA (10). The 100 resulting poses of NSC61610 were clustered with an RMSD cluster tolerance of 2.0 Å. The lowest binding energy pose in the first cluster was considered as the most favorable docking pose. The region on the LANCL2 with the first cluster was considered as the potential binding site for NSC61610. By comparing the amino acid residues involved in binding sites, we found the binding sites predicted by the two different docking programs were identical to each other in most regions. The shared amino acid residues included ARG102, VAL103, TYR189, THR196, ASP414, LEU416, GLY417, ARG422, and LEU428 (Fig. 3.1C). Thus, the identical region on the LANCL2 identified by the two docking programs was considered as the potential binding site for NSC61610. In addition to this binding site, AutoDock also identified a binding site for NSC61610 on LANCL2 that is similar to the binding site for ABA (Fig. 3.1D) (10).

Since the binding energy is only one of many possible criteria for identifying potential binding sites, further experimentation was needed to verify the binding site of NSC61610 or determine whether NSC61610 has multiple binding sites on LANCL2.

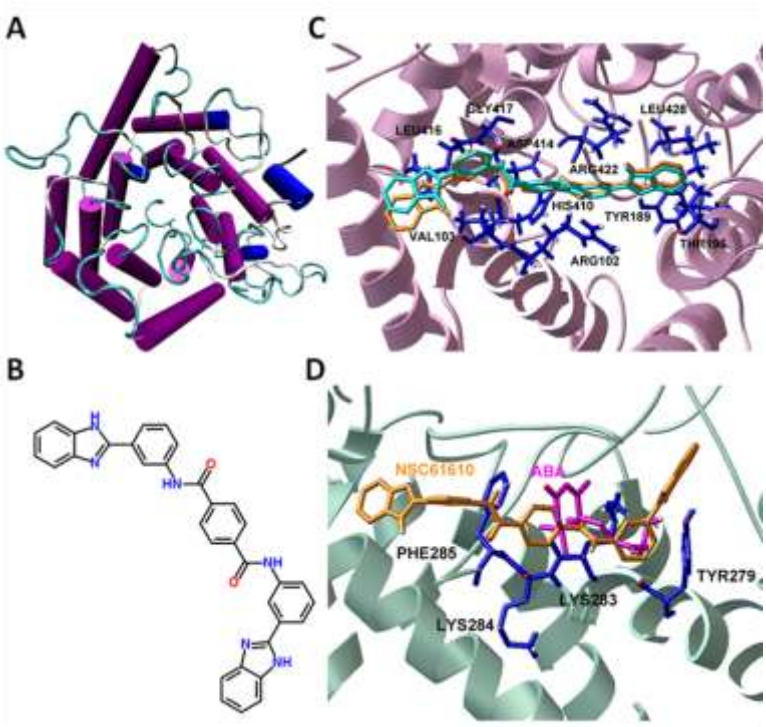


**Figure 3.1.** Lanthionine synthetase C-like 2 (LANCL2) and NSC61610 *in silico*. (A) The homology model of human LANCL2 is shown in Cartoon representation with coloring according to secondary structure. Purple: alpha helix; Blue: other helix; Yellow: bridge_beta; Cyan: turn; Green: coil. (B) 2-D structure of NSC61610. (C) Representative binding mode of the most stable docked orientation of NSC61610 with LANCL2. The LANCL2 model is shown in ribbon mode. NSC61610 pose generated by AutoDock Vina is colored in cyan and the one generated by AutoDock is colored in orange. Selected residues of LANCL2 (blue) are depicted by stick-and-ball models and colored by atom types. Amino acid residues surrounding NSC61610 are labeled. (D) Representative binding modes of the docked orientation of abscisic acid (ABA) and NSC61610 with LANCL2. LANCL2 is shown in a ribbon mode. NSC61610 (orange) and ABA (magenta) are shown in stick-and-ball model. Selected residues of LANCL2 surrounding both NSC61610 and ABA are depicted by stick-and-ball model and labeled. The images were rendered in Visual Molecular Dynamics (VMD).

### Knockdown of LANCL2 Disrupts NSC61610-induced PPAR γ Activation

To determine PPAR γ activity, pCMX.PPAR γ expression plasmid and a pTK.PPRE3x luciferase reporter plasmid driven by the peroxisome proliferator responsive element-containing Acyl-CoA oxidase promoter were purified using maxi kit from Qiagen

(Valencia, CA). RAW 264.7 macrophages were cultured with DMEM (Mediatech, Manassas, VA) containing 10% fetal bovine serum (FBS) and grown until 60–70% confluence. Cells were cotransfected in two 25 cm2 flasks with 1.5 μg plasmid of DNA and 0.15 μg of pRL reporter control with or without 100 pmol LANCL2 siRNA using Lipofectamine 2000 transfection reagent (Invitrogen) according to the manufacturer's protocol. After 24 h, transfected cells were seeded into white, opaque 96-well plates (BD Biosciences) at a concentration of 25,000 cells/well. Transfected cells were then treated in replicates with rosiglitazone (Ros 1 μM; Cayman Chemical, Ann Arbor, MI), NSC61610 (2.5 μM) with and without 2'5'-dideoxyadenosine (10 μM; Sigma) or vehicle (DMSO) and placed in a 37 ℃ incubator with 5% CO2. After 20 h, cells were harvested in reporter lysis reagent. Luciferase activity, normalized to pRL activity in the cell extracts, was determined by using the Dual-Luciferase II reporter assay system (Promega, Madison, WI) using a Modulus 96-well luminometer (Turner Biosystems, Sunnyvale, CA). All values were normalized to control wells to calculate relative luciferase activity. In the same project, we assessed whether introduction of LANCL2 siRNA affects NSC61610-induced PPAR γ activation. To measure the effect of LANCL2 knockdown on NSC61610-induced PPAR γ activation, raw macrophages were transfected with a PPAR γ expression and dual luciferase plasmids with or without l LANCL2 siRNA, and treated with NSC61610 (2.5 μM). Our data indicate that the addition of LANCL2 siRNA disrupted PPAR γ activation by NSC61610 (Fig. 3.2).

**NSC61610 activates PPAR γ by AC-cAMP Signaling Pathway**

To determine whether NSC61610-induced activation of PPAR γ is dependent on adenylate cyclase (AC)-cyclic adenosine monophosphate (cAMP) signaling, raw macrophage were treated with NSC61610 (2.5 μM) with or without 2'5'-dideoxyadenosine (10 μM). NSC61610 increased PPAR γ activity and addition of the AC-specific inhibitor prevented NSC61610-induced PPAR γ activation (Fig. 3.2). We also examined whether the inhibitor influenced PPAR γ activity in raw macrophage with knockdown of LANCL2. The PPAR γ activity was not further reduced by addition of AC-specific inhibitor (Fig. 3.2).

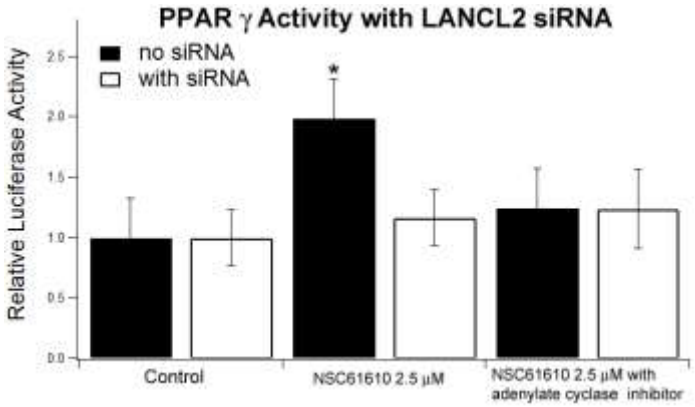


**Figure 3.2.** Effect of LANCL2 disruption and cAMP inhibition on PPAR γ activation in RAW 264.7 macrophages. Cells were cotransfected with a pTK.PPRE3x luciferase reporter plasmid driven by the PPRE-containing Acyl-CoA oxidase promoter with or without LANCL2 siRNA. Then, cells were treated with vehicle (DMSO) or NSC61610 (2.5 μM), the adenylate cyclase-specific inhibitor 2'5'-dideoxyadenosine (10 μM). Luciferase activity was normalized to pRL activity in the cell extracts and relative luciferase activity was calculated a ratio of the activity in the treatment wells to control wells. Data are represented as mean ± standard error. Points with an asterisk indicate that a treatment is significantly different from its control (*P<0.05*).

**NSC61610 Ameliorates Disease Activity and Inflammatory Lesions in Mice with IBD**

To determine the effect of NSC61610 on colonic inflammation we performed a dose-response study. Specifically, mice received placebo or were treated orally with increasing concentrations of NSC61610 (0.5, 10 and 20 mg/kg body weight) for 7 days during a DSS challenge. After 7 days, mice treated with NSC61610 had a significantly reduced disease activity index (DAI) compared to untreated control mice (Fig. 3.3A). Based on the gross pathological observation from Figure 3.3B, 3C, and 3D, NSC61610 treatment significantly decreased inflammation caused by DSS in colon, spleen and MLN. To more closely examine the effect of NSC61610, colonic specimens were examined histologically for the presence of inflammatory lesions. Our data indicate that NSC61610 significantly reduced epithelial erosion, mucosal thickening and leukocyte infiltration in mice with DSS colitis (Fig. 3.4).

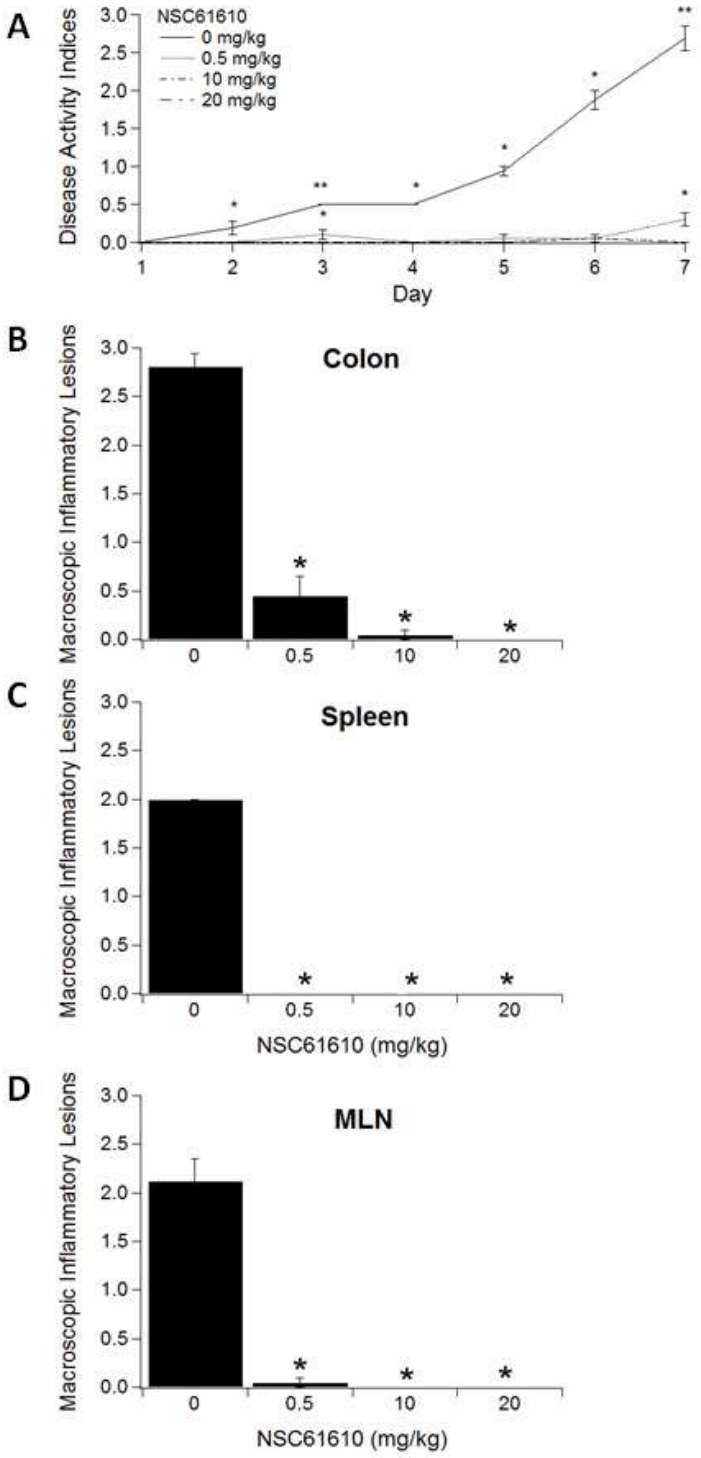


**Figure 3.3.** Oral treatment with NSC61610 ameliorates experimental inflammatory bowel disease. Mice were challenged with 2.5% dextran sodium sulfate in the drinking water for 7 days. Disease activity index (DAI), a composite score reflecting clinical signs of the disease (i.e. perianal soiling, rectal bleeding, diarrhea and piloerection), was

assessed daily. Panel A illustrates the effect of NSC61610 on disease severity in mice with colitis. Panels B-D illustrate the effect of NSC61610 on macroscopic inflammatory lesions in the colon (B), spleen (C), and mesenteric lymph nodes (MLN) (D). Data are represented as mean ± standard error (n=10). In figure A, data points with asterisks are significantly different from control and data points with two asterisks are significantly different from those with one asterisk (*P<0.05*). In figure B-D, bars with an asterisk indicate that a treatment is significantly different from its control (*P<0.05*).

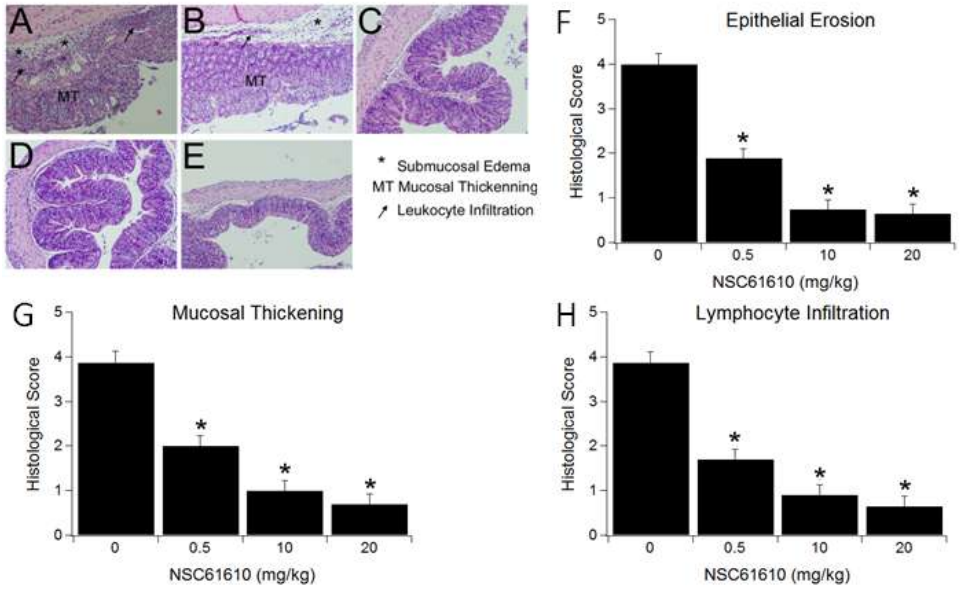


**Figure 3.4.** Oral treatment with NSC61610 ameliorates inflammatory lesions in mice with inflammatory bowel disease. Mice were challenged with 2.5% dextran sodium sulfate in the drinking water for 7 days. Representative photomicrographs from the control (A-B) and NSC61610 treatment (C-E) groups are illustrated. Colonic specimens underwent blinded histological examination and were scored based on epithelial erosion (F), mucosal wall thickening (G), and leukocyte infiltration (H). Data are represented as mean ± standard error (n=10). Bars with an asterisk indicate that a treatment is significantly different from its control (*P<0.05*).

**NSC61610 Modulates Colonic Gene Expression**

Our previous research suggested that ABA activates PPAR γ, and PPAR γ agonists have been successfully used in the treatment of IBD (30). Thus, we sought to determine whether NSC61610 modulates gene expression in a manner that resembled established agonists of PPAR γ such as rosiglitazone or conjugated linoleic acid. Here, we found evidence of PPAR γ-mediated effects in colons of NSC61610-treated mice. For instance, NSC61610 increased the PPAR γ gene expression in colon compared with control mice

(Fig. 3.5A). In addition, NSC61610 significantly lowered expression of inflammatory mediators including monocyte chemoattractant protein-1 (MCP-1) (Fig. 3.5B) and interleukin-6 (IL-6) (Fig. 3.5C) in colons of DSS-challenged mice.

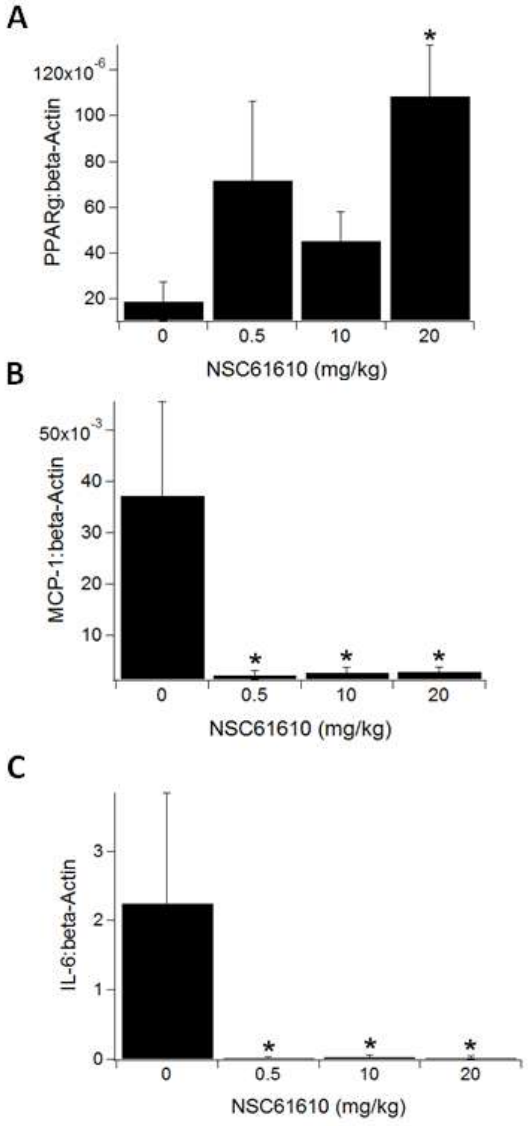


**Figure 3.5.** Modulation of colonic gene expression by oral treatment with NSC61610. Mice were challenged with 2.5% dextran sodium sulfate in the drinking water for 7 days. Colonic mRNA expression of peroxisome proliferator-activated receptor γ (PPAR γ) (A), monocyte chemoattractant protein-1 (MCP-1) (B), and interleukin-6 (IL-6) (C) were assessed by quantitative real-time RT-PCR. Data are represented as mean ± standard error (n=10). Bars with an asterisk indicate that a treatment is significantly different from its control ($P<0.05$).

**NSC61610 Influences the Phenotype and Distribution of Immune Cells in Mice with IBD**

To determine the effect of NSC61610 on immune cell subsets, we performed flow cytometric analysis on cells isolated from the colon, spleen, MLN, and blood. Our analyses indicated that NSC61610 significantly increased the percentage of Treg cells in colon, spleen, and blood (Fig. 3.6). The highest concentration NSC61610 (20 mg/kg) also significantly increased the percentages of CD4+ IL10+ T cells in colon, spleen, MLN, and blood. In addition, NSC61610 numerically reduced the percentage of F4/80+CD11b+ macrophages infiltrating the colonic lamina propria (Fig. 3.7).

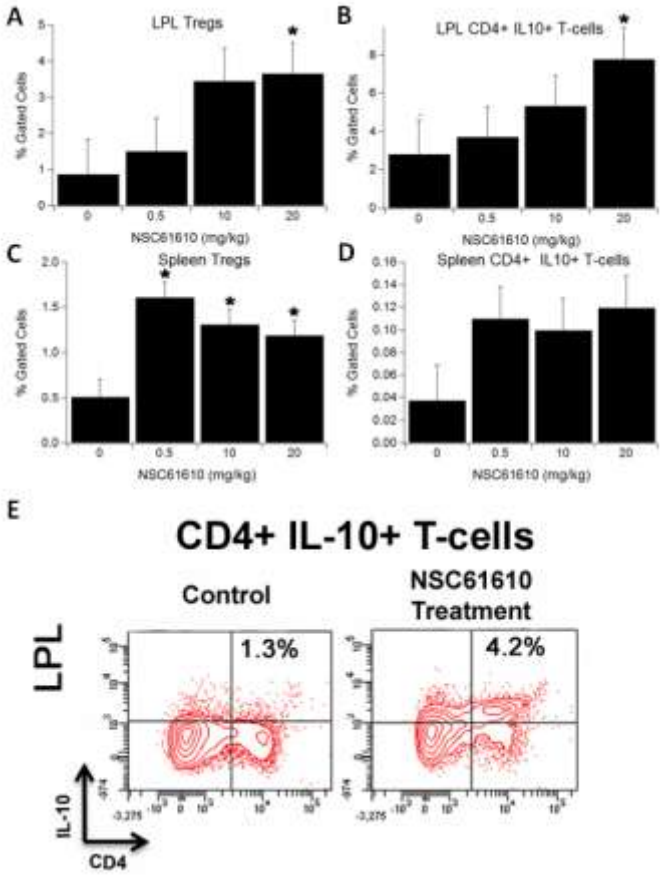


**Figure 3.6.** Oral treatment with NSC61610 on the distribution of immune cell subsets in colonic lamina propria and spleen. Colonic lamina propria lymphocytes (LPL, A, B, and E) and spleen (C and D), were immunophenotyped to identify regulatory T cells (Treg) and CD4+IL-10+ T cell subsets through flow cytometry. Data are represented as mean ± standard error (n=10). Bars with an asterisk indicate that a treatment is significantly different from its control ($P<0.05$).

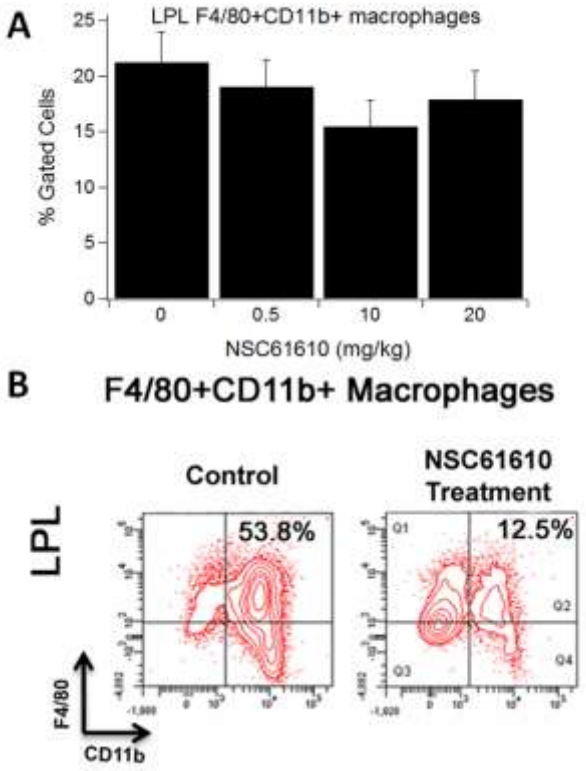


**Figure 3.7.** Oral treatment with NSC61610 on the distribution of macrophages in colonic lamina propria. Colonic lamina propria lymphocytes (LPL) were immunophenotyped to identify F4/80+CD11b+ macrophage subsets through flow cytometry. Data are represented as mean ± standard error (n=10). Bars with an asterisk indicate that a treatment is significantly different from its control (*P<0.05*).

**NSC61610 Reduces Disease Activity and Inflammatory Lesions via a PPAR γ-dependent Mechanism**

To investigate whether the beneficial effects of NSC61610 in IBD required expression of PPAR γ in T cells or macrophages, wild-type (PPAR γ fl/fl, Cre-) mice, macrophage-specific PPAR γ null mice (PPAR γ fl/fl; lysozyme M-Cre+) and T cell-specific PPAR γ null mice (PPAR γ fl/fl; CD4-Cre+) were challenged with 2.5% DSS in the drinking water for 6 days, and disease activity was monitored daily. Macrophage-specific PPAR γ null mice had worsened disease activity throughout the challenge period. From day 4, macrophage-specific PPAR γ null mice had a significantly higher disease activity compared with PPAR γ fl/fl Cre- and PPAR γ fl/fl; CD4-Cre+ mice in both control and

treatment groups (Fig. 3.8A). In line with the DAI scores, both the colons and spleens were significantly more inflamed in PPAR γ fl/fl; Lysozyme M-Cre+ mice than PPAR γ fl/fl Cre- and PPAR γ fl/fl; CD4-Cre+ mice. (Fig. 3.8B and 3.8C).

Based on the results of the dose response study showing maximum anti-inflammatory efficacy at the highest dose tested, we used an oral dose of 20 mg NSC61610/kg body weight via gastric gavage in this study. NSC61610 treatment significantly reduced DAI compared to untreated control mice following the DSS challenge (Fig. 3.8A). To more closely examine the effect of NSC61610 on immunopathology caused by DSS, colons, spleens and MLNs were examined macroscopically for the presence of inflammatory lesions. Our data indicate that NSC61610 significantly reduced macroscopic inflammatory lesions in PPAR γ-expressing and T cell-specific PPAR γ null mice with DSS colitis (Fig. 3.8B, 3.8C and 3.8D). However, the therapeutic effect of NSC61610 on IBD was abrogated in spleens and MLNs of macrophage-specific PPAR γ null mice (Fig. 3.8C and 3.8D). Thus, we posit that the anti-inflammatory efficacy of NSC61610 is dependent on PPAR γ expression in macrophages.

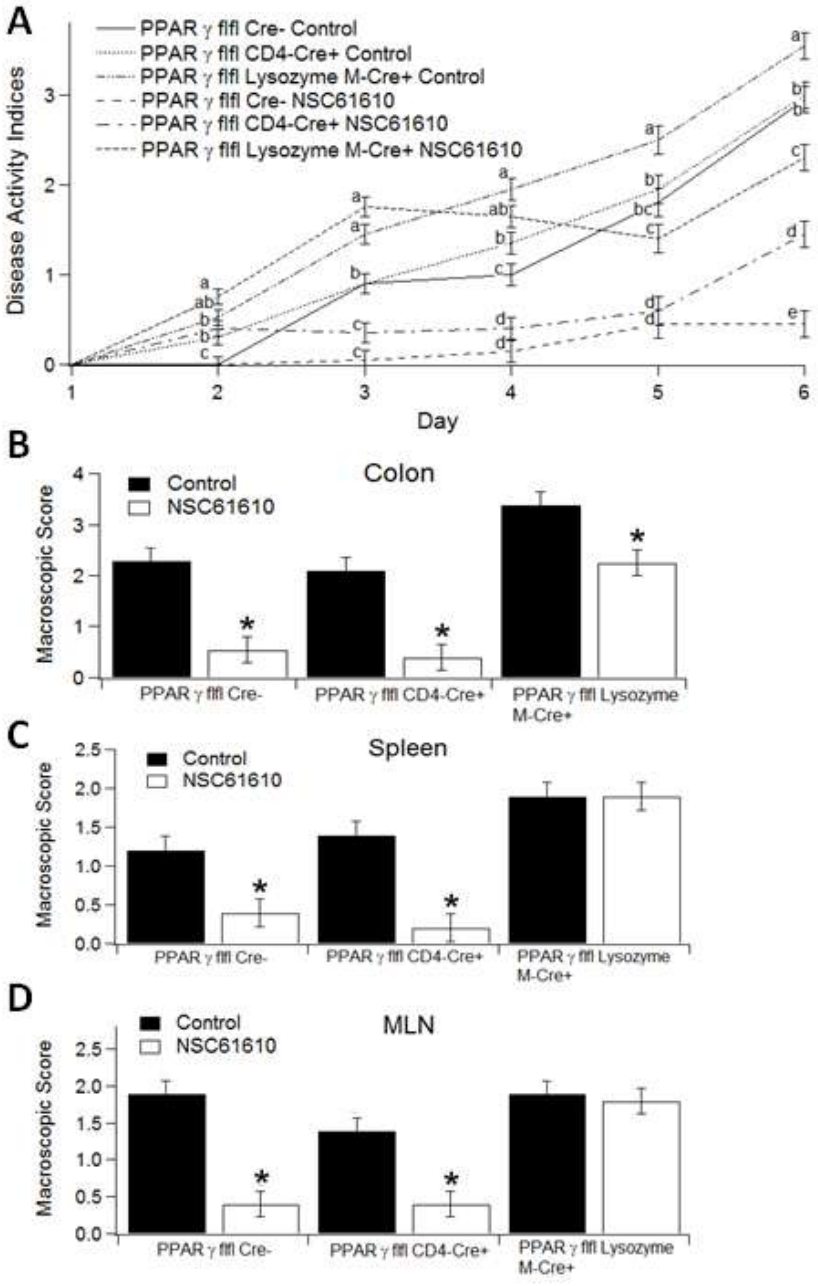


**Figure 3.8.** Effect of tissue-specific PPAR γ deletion and oral NSC61610 treatment in experimental inflammatory bowel disease. Mice were challenged with 2.5% dextran sodium sulfate in the drinking water. Panel A illustrates the effect of oral NSC61610 treatment on disease severity. Means within time points with different letterssuperscripts are significant different ($P<0.05$). Panels B-D illustrate the effect of oral NSC61610 on macroscopic lesions in the colon (B), spleen (C), and mesenteric lymph nodes (MLN) (D). Data are represented as mean ± standard error (n=10). Bars with an asterisk indicate that a treatment is significantly different from its control ($P<0.05$).

### 3.5 Discussion

LANCL2 has received some recent attention as a potential therapeutic target due to its function related to ABA binding and signaling (6) and the recent discovery of an alternative membrane-based mechanism of PPAR γ activation (8). Furthermore, we determined the LANCL2 expression in a series of mouse tissues, which showed that beside brain and testis, LANCL2 is also expressed in other tissues, such as thymus, spleen, colon, and PP, which indicates the possible relationship between LANCL2 and immune responses and suggest the broader potential of LANCL2 as a therapeutic target.

ABA has been shown to play an important role in regulating immune and inflammatory processes (8) via PPAR γ-mediated responses in mouse models of obesity-related inflammation, diabetes, atherosclerosis, and IBD (30-34). We discovered that ABA activates PPAR γ and the loss of PPAR γ in immune cells impairs its ability to normalize blood glucose concentrations and ameliorate macrophage infiltration in the white adipose tissues of obese mice (32). PPAR γ suppresses the expression of pro-inflammatory cytokines and chemokines by antagonizing the activities of transcription factors, enhancing nucleocytoplasmic shuttling of the activated p65 subunit of NF- B, and targeting co-repressor complexes onto inflammatory gene promoters (8). These molecular changes induced by PPAR γ agonists are linked to anti-inflammatory efficacy in mouse models of systemic and mucosal inflammation (8, 31, 35).

At the molecular level, the mechanism underlying ABA-mediated activation of PPAR γ is independent of direct binding to PPAR γ's LBD (8). The inability of ABA to bind directly to the LBD was further validated by competitive ligand-binding assays demonstrating the inability of ABA to displace the trace for binding to the PPAR γ LBD. These results suggested existence of a potential molecular target for ABA upstream of PPAR γ. ABA was shown to increase cAMP accumulation in insulin-secreting pancreatic β-cell lines, splenocytes, and macrophages (34, 36). LANCL2 represents a possible membrane-associated target for ABA involved in the initiation of the cAMP signal. In a previous study on LANCL2 *in silico*, we used homology modeling approaches to construct a three dimensional structure of LANCL2 and identified a putative ABA-

binding site on the surface of LANCL2 (10). A series of *in vitro* experiments further demonstrated that LANCL2 is a putative novel target for the discovery and development of orally active, broad-based drugs against inflammatory, infectious and chronic metabolic diseases. In this study, we used LANCL2 docking studies for the large-scale, high-throughput screening of thematic compound databases for novel drugs for treating inflammatory, infectious and chronic diseases. These molecular modeling studies facilitated that discovery of numerous potential ligands of LANCL2 from NCI Diversity Set II, ChemBridge, ZINC natural products, FDA-approved drugs database and ABA analogs. Furthermore, in order to validate these predictions and determine the anti-inflammatory efficacy of the top ranked compound, denoted as NSC61610 in NCI Diversity Set II, a series of *in vitro* and pre-clinical efficacy studies using a mouse model of DSS-induced colitis were performed.

Previously, we have reported that ABA transactivates PPAR γ *in vitro* and suppresses systemic inflammation similar to other PPAR γ agonists. Since both ABA and NSC61610 target LANCL2, NSC61610 might also act via PPAR γ activation. Experimental results show that NSC61610 treatment activates PPAR γ in raw macrophages, thereby providing evidence of a potential signaling relationship between LANCL2 and PPAR γ and indicating that NSC61610 might target the LANCL2-PPAR γ axis *in vitro*. To investigate the importance of LANCL2 in NSC61610-mediated activation of PPAR γ, we determined whether knocking down LANCL2 in raw macrophages by using siRNA impaired or abrogated the effect of NSC61610 on PPAR γ reporter activity. Our findings indicate that knocking down LANCL2 significantly attenuates the effect of NSC61610 on PPAR γ activity. These findings are consistent with the prediction of our previous studies that ABA activates PPAR γ reporter activity in an LANCL2-dependent manner (8). In addition, to determine whether NSC61610-induced activation of PPAR γ is dependent on adenylate cyclase-cAMP signaling, we measured the NSC61610-induced PPAR gamma activity with or without 2’5’-dideoxyadenosine, AC-specific inhibitor. AC transmits signals by converting adenosine triphosphate to cAMP, a second messenger. The results show addition of the AC-specific inhibitor prevented NSC61610-induced PPAR gamma activation, which indicates NSC61610-induced PPAR gamma activation is AC/cAMP

dependent. We also examined whether the AC-specific inhibitor influenced PPAR γ activity in cells with knockdown of LANCL2. The PPAR γ activity was not further inhibited with addition of AC-specific inhibitor that indicates that LANCL2 is one receptor upstream of AC-cAMP signaling pathway, which is in line with our previous findings that LACNCL2 stimulation is followed by cAMP accumulation (8).

Herein, we demonstrate for the first time that oral NSC61610 treatment significantly ameliorates colonic inflammation and clinical activity in mice with experimental IBD. Consistent with *in vitro* results in raw macrophages showing increased PPAR γ reporter activity, we found that NSC61610 treatment upregulated colonic PPAR γ gene expression in mice with IBD. In addition, NSC61610 significantly decreased inflammatory mediators in the colonic mucosa, including MCP-1 and IL-6. MCP-1 plays an important role in the pathogenesis of colitis in relation to the recruitment of immune cells, and the absence of this chemokine is associated with a significant reduction in inflammation (37). CD4+ T cells at the site of inflammation are critically dependent on anti-apoptotic IL-6 signaling. This circle of T cell accumulation, mediated by apoptosis resistance, which leads to chronic inflammation, can be blocked by anti-IL-6 receptor antibodies (38). In combination with transforming growth factor-β, IL-6 is also involved in differentiation of naïve CD4+ T cells into a pro-inflammatory T helper (Th) 17 phenotype that has been associated with autoimmunity (39).

At the cellular level, we observed that oral NSC61610 treatment significantly increased the percentages of Treg cells in the colon, spleen, and blood of mice. Tregs are important for the maintenance of intestinal self-tolerance and suppression of inflammation. Therapies that increase Treg numbers and function are under intense investigation and may prove to be promising treatments for patients with IBD (40, 41). In addition, treatment with NSC61610 at the highest concentration also significantly increased the percentages of CD4+IL10+ T cells in colon, spleen, MLN, and blood. IL-10 is a regulatory cytokine that inhibits both antigen presentation and subsequent pro-inflammatory cytokine release, and it is proposed as a potent anti-inflammatory biological therapy in chronic IBD (42, 43). Furthermore, NSC61610 reduced the

percentage of infiltrating F4/80+CD11b+ macrophages in the colonic lamina propria, a possible source of inflammatory mediators. Our previous research indicated that ABA ameliorates experimental IBD by suppressing immune cell infiltration (31, 35), which meshes with the immunosuppressive responses seen with NSC61610. This commonality may indicate that ABA and NSC61610 do indeed share similar anti-inflammatory mechanisms that are possibly initiated via LANCL2 binding. In previous study on ABA, we found T cell PPAR γ is a crucial mediator of ABA's anti-inflammatory responses. The absence of PPAR γ in T cells essentially abolished the ability of ABA to decrease experimental IBD, including the anti-inflammatory action of ABA in the colon. T cell PPAR γ was required for the regulation of Treg cell number in the mucosal inductive (MLNs) and effector (colonic lamina propria) sites (30). To investigate the cell specificity and molecular targets underlying the anti-inflammatory mechanism of NSC61610 *in vivo*, we tested whether the beneficial effect of NSC61610 in IBD required expression of PPAR γ in T cells or macrophages. Since the beneficial effect of NSC61610 treatment on IBD was abrogated in macrophage-specific PPAR γ null mice, we posit that the anti-inflammatory efficacy of NSC61610 is dependent on PPAR γ expression in macrophages. Although the anti-inflammatory mechanisms of ABA and NSC61610 are involve LANCL2, their differences in cell specificity indicate that activation of LANCL2 possibly can trigger multiple signal pathways in different cells which would finally promote PPAR γ expression and exert anti-inflammatory efficacy. Based on this finding, synergistic effect of ABA and NSC61610 will be tested in our future studies.

In an attempt to identify additional targets to shed new light on potential alternative mechanisms of action for NSC61610 we used TarFisDock to analyze the reverse docking results of this compound. Putative targets were selected by ranking the values of the interaction energy, which consist of van der Waals and electrostatic interaction terms. The top 10 reverse docking results of NSC61610 are shown in Supplementary Table S3.6. Of note, we show novel data indicating that NSC61610 may decrease inflammation by alternatively targeting the leukotriene A4 hydrolase, which is an enzyme linked to the production of inflammatory lipid mediators such as leukotrienes, suggesting a possible

role of NSC61610 in modulating the synthesis of lipid mediators such as prostaglandins and leukotrienes that worsen the pathogenesis of IBD. It is obvious that the docking energy scores obtained in TarFisDock are more negative than those in AutoDock and AutoDock Vina, which is generated by the differences between scoring functions. TarFisDock was developed on the basis of the DOCK (version 4.0) program with a force-field-based scoring function, while AutoDock and AutoDock Vina use an empirical scoring function. Different scoring functions have been compared and assessed in previous studies (44). In terms of the TarFisDock energy score, this value represented strength of ligand association where a more negative value translated to a stronger predicted protein-ligand complex.

In conclusion, this study employed an integrated drug discovery pipeline consisting of molecular modeling approaches followed by experimental validation. We performed large-scale screening of compound libraries based on predicted binding to an LANCL2 binding site and identified novel putative compounds for the treatment of inflammatory diseases. NSC61610, the top ranked lead compound based on binding free energy, significantly ameliorated experimental IBD in mice in a LANCL2- and PPAR γ-dependent manner. These results confirm that LANCL2 is a novel therapeutic target for inflammatory diseases and NSC61610 is a potential new drug.

### 3.6 Funding

Supported by award number 5R01AT004308 of the National Center for Complementary and Alternative Medicine at the National Institutes of Health awarded to J.B.-R. and NIAID Contract No. HHSN272201000056C to JBR and funds from the Nutritional Immunology and Molecular Medicine Laboratory.

### 3.7 References

1. Chatterjee C, Paul M, Xie L, van der Donk WA. Biosynthesis and mode of action of lantibiotics. Chemical reviews. 2005;105(2):633-84.
2. Mayer H, Salzer U, Breuss J, Ziegler S, Marchler-Bauer A, Prohaska R. Isolation, molecular characterization, and tissue-specific expression of a novel putative G protein-coupled receptor. Biochim Biophys Acta. 1998;1395(3):301-8.

3. Mayer H, Pongratz M, Prohaska R. Molecular cloning, characterization, and tissue-specific expression of human LANCL2, a novel member of the LanC-like protein family. DNA Seq. 2001;12(3):161-6.
4. Park S, James CD. Lanthionine synthetase components C-like 2 increases cellular sensitivity to adriamycin by decreasing the expression of P-glycoprotein through a transcription-mediated mechanism. Cancer Res. 2003;63(3):723-7.
5. Landlinger C, Salzer U, Prohaska R. Myristoylation of human LanC-like protein 2 (LANCL2) is essential for the interaction with the plasma membrane and the increase in cellular sensitivity to adriamycin. Biochim Biophys Acta. 2006;1758(11):1759-67.
6. Sturla L, Fresia C, Guida L, Bruzzone S, Scarfi S, Usai C, et al. LANCL2 is necessary for abscisic acid binding and signaling in human granulocytes and in rat insulinoma cells. J Biol Chem. 2009;284(41):28045-57.
7. Bassaganya-Riera J, Skoneczka J, Kingston DG, Krishnan A, Misyak SA, Guri AJ, et al. Mechanisms of action and medicinal applications of abscisic Acid. Curr Med Chem. 2010;17(5):467-78.
8. Bassaganya-Riera J, Guri AJ, Lu P, Climent M, Carbo A, Sobral BW, et al. Abscisic acid regulates inflammation via ligand-binding domain-independent activation of peroxisome proliferator-activated receptor gamma. J Biol Chem. 2011;286(4):2504-16.
9. Sturla L, Fresia C, Guida L, Grozio A, Vigliarolo T, Mannino E, et al. Binding of abscisic acid to human LANCL2. Biochem Biophys Res Commun. 2011;415(2):390-5.
10. Lu P, Bevan DR, Lewis SN, Hontecillas R, Bassaganya-Riera J. Molecular modeling of lanthionine synthetase component C-like protein 2: a potential target for the discovery of novel type 2 diabetes prophylactics and therapeutics. J Mol Model. 2011;17(3):543-53.
11. Shoichet BK. Virtual screening of chemical libraries. Nature. 2004;432(7019):862-5.
12. Canduri F, de Azevedo WF. Protein crystallography in drug discovery. Curr Drug Targets. 2008;9(12):1048-53.
13. Bissantz C, Bernard P, Hibert M, Rognan D. Protein-based virtual screening of chemical databases. II. Are homology models of G-Protein Coupled Receptors suitable targets? Proteins. 2003;50(1):5-25.
14. Costanzi S. On the applicability of GPCR homology models to computer-aided drug discovery: a comparison between in silico and crystal structures of the beta2-adrenergic receptor. J Med Chem. 2008;51(10):2907-14.
15. Evers A, Klebe G. Ligand-supported homology modeling of g-protein-coupled receptor sites: models sufficient for successful virtual screening. Angew Chem Int Ed Engl. 2004;43(2):248-51.
16. Schapira M, Raaka BM, Das S, Fan L, Totrov M, Zhou Z, et al. Discovery of diverse thyroid hormone receptor antagonists by high-throughput docking. Proc Natl Acad Sci U S A. 2003;100(12):7354-9.
17. Zhang W, Wang L, Liu Y, Xu J, Zhu G, Cang H, et al. Structure of human lanthionine synthetase C-like protein 1 and its interaction with Eps8 and glutathione. Genes Dev. 2009;23(12):1387-92.
18. Irwin JJ, Shoichet BK. ZINC--a free database of commercially available compounds for virtual screening. J Chem Inf Model. 2005;45(1):177-82.

19. Morris GM, Huey R, Lindstrom W, Sanner MF, Belew RK, Goodsell DS, et al. AutoDock4 and AutoDockTools4: Automated docking with selective receptor flexibility. J Comput Chem. 2009;30(16):2785-91.
20. Trott O, Olson AJ. AutoDock Vina: improving the speed and accuracy of docking with a new scoring function, efficient optimization, and multithreading. J Comput Chem. 2010;31(2):455-61.
21. Bassaganya-Riera J, Reynolds K, Martino-Catt S, Cui Y, Hennighausen L, Gonzalez F, et al. Activation of PPAR gamma and delta by conjugated linoleic acid mediates protection from experimental inflammatory bowel disease. Gastroenterology. 2004;127(3):777-91.
22. Gao Z, Li H, Zhang H, Liu X, Kang L, Luo X, et al. PDTD: a web-accessible protein database for drug target identification. BMC Bioinformatics. 2008;9:104.
23. Li H, Gao Z, Kang L, Zhang H, Yang K, Yu K, et al. TarFisDock: a web server for identifying drug targets with docking approach. Nucleic Acids Res. 2006;34(Web Server issue):W219-24.
24. Ewing TJ, Makino S, Skillman AG, Kuntz ID. DOCK 4.0: search strategies for automated molecular docking of flexible molecule databases. J Comput Aided Mol Des. 2001;15(5):411-28.
25. Pettersen EF, Goddard TD, Huang CC, Couch GS, Greenblatt DM, Meng EC, et al. UCSF Chimera--a visualization system for exploratory research and analysis. J Comput Chem. 2004;25(13):1605-12.
26. Arnold K, Bordoli L, Kopp J, Schwede T. The SWISS-MODEL workspace: a web-based environment for protein structure homology modelling. Bioinformatics. 2006;22(2):195-201.
27. Humphrey W, Dalke A, Schulten K. VMD: visual molecular dynamics. J Mol Graph. 1996;14(1):33-8, 27-8.
28. Melo F, Feytmans E. Assessing protein structures with a non-local atomic interaction energy. Journal of molecular biology. 1998;277(5):1141-52.
29. Laskowski R, MacArthur M, Moss D, Thornton J. PROCHECK: a program to check the stereochemical quality of protein structures. J Appl Cryst. 1993;26:283-91.
30. Guri AJ, Hontecillas R, Ferrer G, Casagran O, Wankhade U, Noble AM, et al. Loss of PPAR gamma in immune cells impairs the ability of abscisic acid to improve insulin sensitivity by suppressing monocyte chemoattractant protein-1 expression and macrophage infiltration into white adipose tissue. J Nutr Biochem. 2008;19(4):216-28.
31. Guri AJ, Hontecillas R, Bassaganya-Riera J. Abscisic acid ameliorates experimental IBD by downregulating cellular adhesion molecule expression and suppressing immune cell infiltration. Clin Nutr. 2010;29(6):824-31.
32. Guri AJ, Hontecillas R, Si H, Liu D, Bassaganya-Riera J. Dietary abscisic acid ameliorates glucose tolerance and obesity-related inflammation in db/db mice fed high-fat diets. Clin Nutr. 2007;26(1):107-16.
33. Guri AJ, Hontecillas R, Bassaganya-Riera J. Abscisic acid synergizes with rosiglitazone to improve glucose tolerance and down-modulate macrophage accumulation in adipose tissue: possible action of the cAMP/PKA/PPAR gamma axis. Clin Nutr. 2010;29(5):646-53.

34. Guri AJ, Misyak SA, Hontecillas R, Hasty A, Liu D, Si H, et al. Abscisic acid ameliorates atherosclerosis by suppressing macrophage and CD4+ T cell recruitment into the aortic wall. J Nutr Biochem. 2010;21(12):1178-85.
35. Guri AJ, Evans NP, Hontecillas R, Bassaganya-Riera J. T cell PPAR gamma is required for the anti-inflammatory efficacy of abscisic acid against experimental IBD. Journal of Nutritional Biochemistry. 2010;In press.
36. Bruzzone S, Bodrato N, Usai C, Guida L, Moreschi I, Nano R, et al. Abscisic acid is an endogenous stimulator of insulin release from human pancreatic islets with cyclic ADP ribose as second messenger. The Journal of biological chemistry. 2008;283(47):32188-97.
37. Khan WI, Motomura Y, Wang H, El-Sharkawy RT, Verdu EF, Verma-Gandhu M, et al. Critical role of MCP-1 in the pathogenesis of experimental colitis in the context of immune and enterochromaffin cells. Am J Physiol Gastrointest Liver Physiol. 2006;291(5):G803-11.
38. Mudter J, Neurath MF. Il-6 signaling in inflammatory bowel disease: pathophysiological role and clinical relevance. Inflamm Bowel Dis. 2007;13(8):1016-23.
39. Kimura A, Naka T, Kishimoto T. IL-6-dependent and -independent pathways in the development of interleukin 17-producing T helper cells. Proc Natl Acad Sci U S A. 2007;104(29):12099-104.
40. Groux H, Powrie F. Regulatory T cells and inflammatory bowel disease. Immunol Today. 1999;20(10):442-5.
41. Boden EK, Snapper SB. Regulatory T cells in inflammatory bowel disease. Curr Opin Gastroenterol. 2008;24(6):733-41.
42. Leach MW, Davidson NJ, Fort MM, Powrie F, Rennick DM. The role of IL-10 in inflammatory bowel disease: "of mice and men". Toxicol Pathol. 1999;27(1):123-33.
43. Li MC, He SH. IL-10 and its related cytokines for treatment of inflammatory bowel disease. World J Gastroenterol. 2004;10(5):620-5.
44. Ferrara P, Gohlke H, Price DJ, Klebe G, Brooks CL, 3rd. Assessing scoring functions for protein-ligand interactions. J Med Chem. 2004;47(12):3032-47.

### 3.8 Supplementary figures and tables

Supplementary Table S1. Oligonucleotide sequences for quantitative real-time PCR. [a,b]

| Primer | Sequence | Length | Accession Number |
|---|---|---|---|
| β-actin F | 5’ CCCAGGCATTGCTGACAGG3’ | 141 | X03672 |
| β-actin R | 5’ TGGAAGGTGGACAGTGAGGC3’ | | |
| PPAR γ F | 5’ AGAACCTGCATCTCCACCTT3’ | 117 | NM_011146 |
| PPAR γ R | 5’ ACAGACTCGGCACTCAATGG3’ | | |
| IL-6 F | 5’ TTTCCTCTGGTCTTCTGGAG3’ | 92 | NM_031168 |
| IL-6 R | 5’ CTGAAGGACTCTGGCTTTGT3’ | | |
| MCP-1 F | 5’ CTTTGAATGTGAAGTTGACCC3’ | 129 | NM_011333 |
| MCP-1 R | 5’ AGGCATCACAGTCCGAGTC3’ | | |
| TNF-α F | 5’ AGGCATCACAGTCCGAGTC3’ | 137 | NM_013693 |
| TNF-α R | 5’ AGGCATCACAGTCCGAGTC3’ | | |

[a] F, forward; R, reverse. PCR primer pairs were designed for an optimal annealing temperature of 57.2 ℃ and product lengths between 92 and 141 base pairs.

[b] When plotting threshold cycle versus log starting quantity (pg), standard curves had slopes between -1.932 and -2.989; PCR efficiencies between 105.3 and 229.3 and $R^2$ above 0.98 mostly.

Supplementary Table S3.2. Docking results of compounds in NCI Diversity Set II to lanthionine synthetase C-like 2, ranked by the lowest binding energy (N=1,364 compounds).

| ZINC Number | Name | Chemical Structure | Lowest Binding Energy (kcal/mol) |
|---|---|---|---|
| ZINC01690699 (NSC61610) | 1-N,4-N-bis[3-(1H-benzimidazol-2-yl)phenyl]benzene-1,4-dicarboxamide | 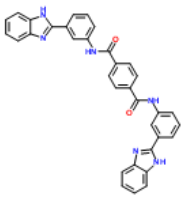 | -11.1 |
| ZINC29589888 | 2-[2-[(6-oxo-5H-phenanthridin-3-yl)carbamoyl]phenyl]benzoic acid | 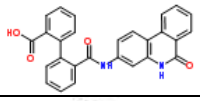 | -10.5 |
| ZINC13130018 | 6-(1,3-dihydrophenanthro[9,10-d]imidazol-2-ylidene)cyclohexa-2,4-dien-1-one | 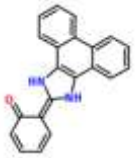 | -10.3 |
| ZINC01726776 | 3-(4-chloro-6-phenoxy-1,3,5-triazin-2-yl)-1-phenylindole | 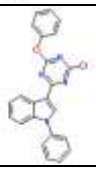 | -10.2 |
| ZINC01736228 | (2R)-5-phenyl-2-[(2R)-5-phenyl-2,3-dihydro-1,3-benzoxazol-2-yl]-2,3-dihydro-1,3-benzoxazole | 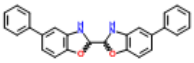 | -10.2 |
| ZINC04783229 | 1-N,4-N-bis(3-phenylphenyl)piperazine-1,4-dicarboxamide | 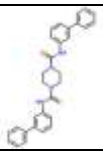 | -10.1 |
| ZINC00990239 | 3-(4,5-dimethylbenzo[h][1,6]naphthyridin-1-ium-2-yl)-2-methylquinolin-4-amine | 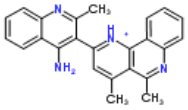 | -10 |
| ZINC18057104 | 4-[(1-methyl-6-nitroquinolin-1-ium-4-yl)amino]-N-[4-[(1-methylpyridin-1-ium-4-yl)amino]phenyl]benzamide | 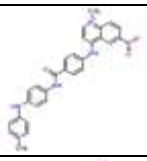 | -10 |
| ZINC04214344 | Genostrychnine | 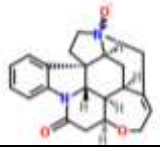 | -9.7 |
| ZINC04720972 | 2-hydroxy-N-(4-methoxyphenyl)-11H-benzo[a]carbazole-3-carboxamide | 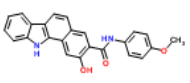 | -9.6 |

Supplementary Table S3.3. Docking results of compounds in ChemBridge to lanthionine synthetase C-like 2, ranked by the lowest binding energy (N=884,105 compounds).

| ZINC Number | Name | Chemical Structure | Lowest Binding Energy (kcal/mol) |
|---|---|---|---|
| ZINC22146248 | 3-[4-(5,5-dioxidodibenzo[b,d]thien-2-yl)-5-phenyl-1H-imidazol-2-yl]-3a,7a-dihydro-1H-indole | 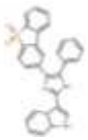 | -10.9 |
| ZINC02848490 | N-(6-chloro-1,3-dioxo-1H-benzo[de]isoquinolin-2(3H)-yl)-9-hydroxy-9H-fluorene-9-carboxamide | 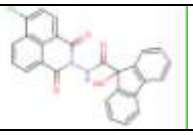 | -10.8 |
| ZINC13081141 | 2-[2-(4-hydroxyphenyl)-5-phenyl-1H-imidazol-4-yl]-7-nitro-9H-fluoren-9-one | 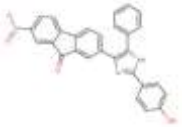 | -10.8 |
| ZINC05799242 | 2-(1,3-benzodioxol-5-yl)-4,4-dimethyl-6-phenyl-1,4,5,6-tetrahydroimidazo[4,5-e]indazole | 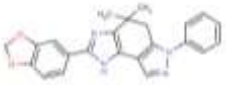 | -10.5 |
| ZINC04602469 | 2-[4-amino-6-(dimethylamino)-1,3,5-triazin-2-yl]-3-dibenzo[b,d]furan-2-ylacrylonitrile | 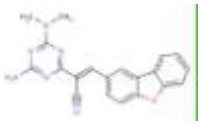 | -10.3 |
| ZINC02909739 | 1-phenyl-5-{[(5-phenyl-1,3,4-thiadiazol-2-yl)amino]methylene}-2,4,6(1H,3H,5H)-pyrimidinetrione | 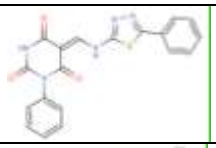 | -10.2 |
| ZINC14740873 | 7-[(6-chloro-2H-chromen-3-yl)methyl]-3-(3,4-dihydro-2H-chromen-3-yl)-1-methyl-5,6,7,8-tetrahydroimidazo[1,5-a]pyrazine | 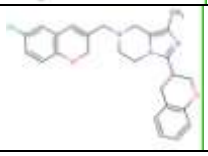 | -10.2 |
| ZINC05338533 | 1-phenyl-4,11-dihydroimidazo[4,5-e]naphtho[2,3-b][1,4]diazepin-2(1H)-one | 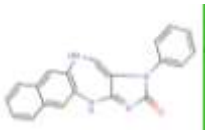 | -10.2 |
| ZINC08387449 | 1-phenyl-4,11-dihydroimidazo[4,5-e]naphtho[2,3-b][1,4]diazepin-2(1H)-one | 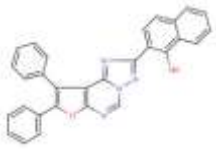 | -10.2 |
| ZINC05564677 | ethyl 4-[5-(4-fluorophenyl)-2-furyl]-2-oxo-6-phenyl-1,2-dihydro-5-pyrimidinecarboxylate | 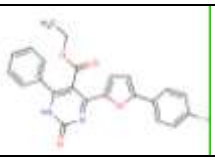 | -10.1 |

Supplementary Table S3.4. Docking results of compounds in ZINC Natural Products database to lanthionine synthetase C-like 2, ranked by the lowest binding energy (N=89,425 compounds).

| ZINC Number | Name | Chemical Structure | Lowest Binding Energy (kcal/mol) |
|---|---|---|---|
| ZINC03845566 | 3,7-bis(2-oxo-1H-indol-3-ylidene)-1,5-dihydropyrrolo[2,3-f]indole-2,6-dione | 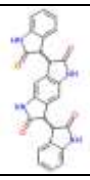 | -12.8 |
| ZINC03848528 | 1-amino-3-[(4-amino-9,10-dioxoanthracen-2-yl)amino]anthracene-9,10-dione | 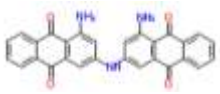 | -12.0 |
| ZINC05220992 | benzo[lmn]diquinazolino[2,1-b:2',3'-i][3,8]phenanthroline-5,9,11,19-tetrone | 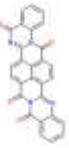 | -11.7 |
| ZINC08792261 | N-1,3-benzothiazol-2-yl-2-[(9-oxo-9H-benzo[c]indolo[3,2,1-ij][1,5]naphthyridin-5-yl)oxy]propanamide | 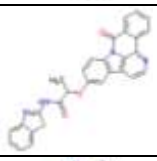 | -11.5 |
| ZINC09033168 | 1-(2-dibenzofuran-3-ylhydrazinyl)-[1]benzofuro[3,2-e]indol-2-one | 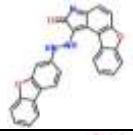 | -11.4 |
| ZINC02121309 | 2-(2-dibenzofuran-2-ylhydrazinyl)-[1]benzofuro[2,3-f]indol-1-one | 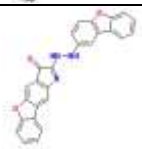 | -10.8 |
| ZINC12654409 | 3',11'-Dihydroxy-3H-spiro[2-benzofuran-1,7'-dibenzo[c,h]xanthen]-3-one | 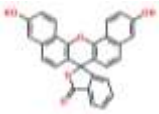 | -10.7 |
| ZINC03843486 | [1,4]benzodioxino[2,3-b][1,4]benzodioxino[2',3':5,6]pyrazino[2,3-g]quinoxaline |  | -10.6 |
| ZINC04701574 | 6-chloro-3-[(2E)-2-[1-(2-oxochromen-3-yl)ethylidene]hydrazinyl]indol-2-one | 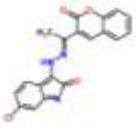 | -10.6 |
| ZINC04266071 | (2Z)-2-(3-oxo-1H-indol-2-ylidene)naphtho[3,2-e][1]benzothiole-1,6,11-trione | 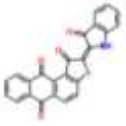 | -10.4 |

Supplementary Table S3.5. Docking results of compounds in Food and Drug Administration-approved drugs database to lanthionine synthetase C-like 2, ranked by the lowest binding energy (N=3,180 compounds).

| ZINC Number | Name | Chemical Structure | Function | Lowest Binding Energy (kcal/mol) |
|---|---|---|---|---|
| ZINC03830554 | 4-amino-3-[[4-[4-[(1-amino-4-sulfonatonaphthalen-2-yl)diazenyl]phenyl]phenyl]diazenyl]naphthalene-1-sulfonate | 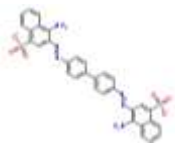 | inhibit amyloid polymerization | -10.5 |
| ZINC11678081 | Carminomycin | 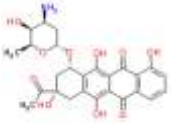 | antibiotics, antineoplastic | -9.9 |
| ZINC08552616 | Algestone Acetophenide | 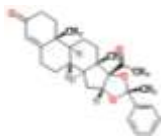 | progestins, contraceptives,anti-inflammatary agents | -9.7 |
| ZINC08101049 | Acetyldigitoxins | 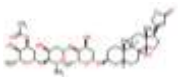 | anti-arrhythmia, cardiotonic agents | -9.5 |
| ZINC08101053 | Aclacur | 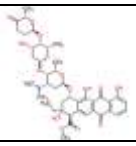 | antibiotics, antineoplastic | -9.4 |
| ZINC08101078 | Digitoxin | 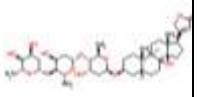 | anti-arrhythmia, cardiotonic agents | -9.4 |
| ZINC01529463 | Estrone hydrogen sulfate | 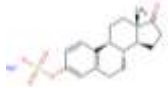 | female hormone | -9.4 |
| ZINC03830332 | 4,4'-((2,4-Dihydroxy-5-(hydroxymethyl)-1,3-phenylene)bis(azo))bis naphthalene-1-sulphonic acid | 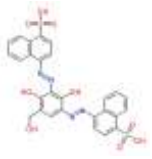 | | -9.4 |
| ZINC11592963 | Idarubicin | 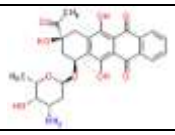 | antibiotics, antineoplastic | -9.4 |
| ZINC03830975 | Itraconazole | 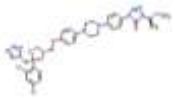 | antifungal agents | -9.3 |

Supplementary Table S3.6. Potential therapeutic targets of NSC61610.

| PDB_ID | Energy Score | Target Name | Processes and Diseases |
|---|---|---|---|
| 1Q0N | -63.44 | 6-Hydroxymethyl-7, 8-dihydropterin pyrophosphokinase (HPPK) | Infections; Microbial infections |
| 1HS6 | -61.89 | Leukotriene A4 hydrolase | Inflammation; leukotriene synthesis; Esophageal cancer |
| 1K6W | -61.24 | Cytosine deaminase | Epigenetic events; Cancer |
| 1HDT | -59.59 | Serine Proteinase alpha-thrombin | Haemostatic Disorders |
| 1FNO | -58.78 | Peptidase | |
| 1LGR | -57.52 | Glutamine Synthetase | Alzheimer's Disease, Huntington Disease |
| 1HDT | -57.5 | Serine Proteinase alpha-thrombin | Haemostatic Disorders |
| 1XID | -57.47 | D-Xylose Isomerase | Carbohydrate metabolism |
| 1ED5 | -56.78 | Nitric Oxide Synthase | Vasodilation; Inflammation |
| 1GPN | -55.86 | Acetylcholinesterase | Alzheimer's Disease, Cognitive Deficits, Hypoxic-ischemic Encephalopathy, Motor Neurone Disease, Parkinson's Disease |

# Chapter 4. Phase III placebo-controlled, randomized clinical trial with synthetic Crohn's disease patients to evaluate treatment response

**Vida Abedi[1,§], Pinyi Lu[1,§], Raquel Hontecillas[1], Meghna Verma[1], Gavin Vess[1], Casandra W. Philipson[2], Adria Carbo[2], Andrew Leber[1], Nuria Tubau-Juni[1], Stefan Hoops[1], Josep Bassaganya-Riera[1]**

Abedi V[§], Lu P[§], Hontecillas R, Verma M, Vess G, Philipson CW, et al. Phase III Placebo-Controlled, Randomized Clinical Trial with Synthetic Crohn's disease Patients to Evaluate Treatment Response. Emerging Trends in Computational Biology, Bioinformatics, and Systems Biology-–Systems & Applications: Elsevier. Under review.

[1]Nutritional Immunology and Molecular Medicine Laboratory (www.nimml.org), Virginia Bioinformatics Institute, Virginia Tech, Blacksburg, VA 24061 USA, [2]BioTherapeutics Inc, 1800 Kraft Drive, Suite 200, Blacksburg, VA 24060 USA.

[§]Both authors contributed equally to this work.

CORRESPONDENCE: *To whom correspondence should be addressed at: Prof. Josep Bassaganya-Riera, Laboratory of Nutritional Immunology and Molecular Medicine Laboratory (www.nimml.org), Virginia Bioinformatics Institute, Virginia Tech, Blacksburg, VA 24061. Phone: (540) 231-7421, FAX: (540) 231-2606, and e-mail: jbassaga@vt.edu.

## 4.1 Abstract

Crohn's disease (CD) is one of the two most prevailing clinical manifestations of inflammatory bowel disease (IBD), a disease that afflicts 1.4 million Americans and 4 million people worldwide. The current treatment paradigm for IBD includes medications with limited efficacy and significant side effects. Thus, there is an unmet clinical need for safer and more effective CD therapeutics. Drug discovery and development is a lengthy, and costly process, especially in clinical trial stages requiring billions of dollars to advance new products to market. To accelerate the path to cures, we have developed a novel integrated approach for creating a synthetic patient population and testing the efficacy of novel therapeutics for Crohn's disease in large clinical cohorts *in silico*. By using supervised machine learning methods, thousands of virtual patients were created based on clinical and immunological data of Crohn's disease patients. A nutritional intervention, conjugated linoleic acid (CLA), a Phase IIa therapeutic targeting Mothers against decapentaplegic homolog 7 (SMAD7), GED-0301, a novel pre-clinical stage lanthionine synthetase C-like 2 (LANCL2) therapeutic, and a placebo were administered to 10,000 virtual patients *in silico*. Efficacy of these treatments on Crohn's disease was evaluated by analyzing predicted changes of Crohn's disease activity index (CDAI) scores and correlations with immunological variables were evaluated. Our study shows that targeting LANCL2, a novel therapeutic target for inflammation and diabetes, significantly ameliorates disease activity of CD patients with an average drop of 126 points of CDAI for severe cases. This is the first study to design and implement an *in silico* Phase III clinical trial for CD to investigate response to treatment in terms of changes in pharmacodynamic immunological marker profile (i.e., TNF-a and IFN-γ) and health outcomes.

## 4.2 Introduction

Crohn's disease (CD) and ulcerative colitis are two clinical manifestations of inflammatory bowel disease (IBD). Current epidemiology data suggest that there are over 630,000 cases of CD in North America, with an increasing rate at 25% (1). CD is a chronic relapsing inflammatory condition that affects mainly the gastrointestinal tract with extraintestinal manifestations caused by a combination of genetic susceptibility

factors, environmental triggers and immune dysregulation (2-5). The current treatment for the most severe cases of this condition is the use of anti-tumor necrosis factor α (TNF-α) antibodies, with the attempt to stimulate mucosal healing. Despite significant adverse side effects of this treatment including cancer, infection and death, there are no effective substitutes in the market (6, 7). Thus, there is an unmet clinical need for safer and more effective CD therapeutics. In fact, over the past decade many studies have explored the use of new therapeutics for the treatment of CD; however, even with a strong mechanism of action and promising pre-clinical data, clinical studies have failed (8-10). The lack of success may be attributed to a number of factors, including inadequate dosing, population selection, drug inefficacy or even insufficient design optimization. Therefore, there is pressing need to re-invent the design of pre-clinical studies in order to achieve superior results during the Phase I, II, III clinical testing to accelerate either failure or New Drug Application (NDA) filing. In addition, data from marginally successful clinical studies can be used to identify key parameters and driver elements for the treatment. We have utilized data from a small scale phase IIa clinical trial with CD patients treated with a nutritional anti-inflammatory compound, conjugated linoleic acid (CLA) (11), in order to develop a synthetic CD population and a large scale clinical trial simulation. The *in silico* clinical trial is used to optimize the various parameters of the design and testing of new promising CD therapeutics with strong animal pharmacology packages and safety profiles acting on novel therapeutic targets (*LANCL2* and *SMAD7*).

Creating large sample size of virtual patients for *in silico* clinical experimentation has been implemented successfully only in a limited number of studies (12-14). For example, due to the high number of failed trials for Alzheimer's disease, a clinical trial simulator was recently developed and deemed reliable for future clinical trials by the US Food and Drug Administration (FDA) and European Medicines Agency (EMA) (12). The computational tool can be used to test disease-modifying effects by using randomized, parallel, placebo-controlled or other types of trials. This tool is a successful example of integration of patient-level and literature based data. However, due to the complex nature of the process and accessibility to comprehensive clinical data, these studies are only beginning to emerge for other diseases including inflammatory or immune mediated

diseases. For instance, in a recent work by Brown and colleagues (13), a computational model was constructed based on clinical data from 33 blunt trauma patients. The model was subsequently used to generate 10,000 virtual patients. Sensitivity analysis on the parameters in the model identified key elements that could provide a small survival benefit of IL-6 inhibition. Similarly, in more generalized frameworks, researchers have attempted to created synthetic electronic medical records (EMR) to bridge the gap between novel bio-surveillance algorithms operating on full EMRs and the lack of non-identifiable EMR data (14). In that case, the main concern includes privacy and confidentiality of medical information for monitoring large-scale outbreaks. In all these examples, accessibility to reliable clinical data linked to key cellular and molecular markers of disease is a key factor. In addition, for modeling purposes, levels of different biomarkers as well as patient's disease activity, such as Crohn's Disease Activity Index (CDAI) and patient reported outcomes (PRO), have to be measured before and after treatment. Furthermore, such data is prone to the missing value problem, and efficient methods have to be in place to address these inherent complications (see a review by Eekhout *et al.* (15)). Statistical methods may not always be suitable, especially when dealing with a very small sample size. Therefore, novel computational techniques are needed to address these recurring problems on the path of accelerating development of cures for widespread and debilitating human diseases.

Creating large populations of diverse virtual patients for Phase II and III testing requires a balanced representative patient-level data; such data can be used to build deterministic or non-deterministic models. For instance, researchers used the data and literature-based information to construct an ordinary differential equation (ODE) based model and used the model to generate instances of virtual patients (13). In 2010, we published the first ODE-based computational model of the key immunological changes occurring in the colonic mucosa during IBD (16), and more recently we built models of CD4+ T cells differentiation to determine the modulation of mucosal immune responses by CD4+ T cell subsets during gut inflammation (17, 18). For complex diseases with a large number of parameters and limited available clinical and biomarker data for calibration, it is also possible to use advanced machine learning methods. In fact, in a recent study in modeling

of CD4+ T cell heterogeneity, we have demonstrated the use of machine learning method as a reliable alternative to large complex ODE-based models (19, 20).

The predictive power of *in silico* simulations can provide additional insight for designing clinical trials (21) based on nutritional therapies such as CLA (11) or novel therapeutics such as those targeting SMAD7 (22) or LANCL2 (23). For instance, based on a series of *in silico*, biochemical and *in vivo* studies (23), LANCL2 has already been proposed as a novel and promising target for the discovery and development of orally active, broad-based drugs against inflammatory, immune-mediated and chronic metabolic diseases. LANCL2 is a key mediator in inflammation and reduces the levels of pro-inflammatory cytokines including *TNF-α* and *IFN-γ* while increasing the anti-inflammatory cytokine IL-10 (24, 25). Indeed, *TNF-α* and *IFN-γ* have been also reported as molecular markers of CD (26). These cytokines were also measured in the clinical study on CD (11) that is used for the development of a virtual patient population. Similarly, SMAD7-targeting therapies alter the expression of regulatory signaling molecules, specifically TGF-*β1*. *TGF-β1* mainly functions as a negative regulator of T cell immune responses and signals to downstream target cells via a family of *Smad* proteins. In patients with IBD, there is an overexpression of *Smad7* that further inhibits *TGF-β1* induced signaling (27). Thus, the inhibition of Smad7 has been proposed as an investigational therapeutic for CD that favors regulatory responses. In addition, principal component analyses detect and highlight the key molecular biomarkers of CD, namely *IFN-γ* and *TNF-α.* The latter solidifies the immunological features of the synthetic CD population.

In this study, advanced machine learning methods are used to generate virtual patients based on data from clinical studies on CD. In particular Artificial Neural Network and Random Forest Models are built from clinical data and used to generate population level features. Treatment regimens are also designed based on clinical data and applied to the large virtual population to quantify and compare different treatments in the context of a randomized, placebo-controlled Phase III *in silico* clinical trial.

### 4.3 Materials and methods

**Study design**

Developing a synthetic population of healthy individual or patients from clinical data and designing *in silico* treatment requires a series of steps including *Data Extraction*, *Data Generation*, and *Data Analytics* (Figure 4.1). During the first stage, *Data Extraction*, clinical data from trials on CD were extracted from publications, including clinical trials on CLA, GED-0301 and placebo. During the second stage, *Data Generation*, the missing values (including levels of biomarkers at different time points) in original clinical trial data were predicted using supervised machine learning approaches. Based on the complete dataset, a large patient population was generated synthetically. The latter was further utilized for *in silico* randomized, placebo-controlled Phase III clinical trial using virtual treatments. Finally, during the final stage, *Data Analytics*, statistical analyses were performed to determine 1) statistically significant differences between efficacy of virtual treatments and placebo, 2) statistically significant differences between different treatments, 3) personalized treatment options based on patient's characteristics and previous or concomitant medications.

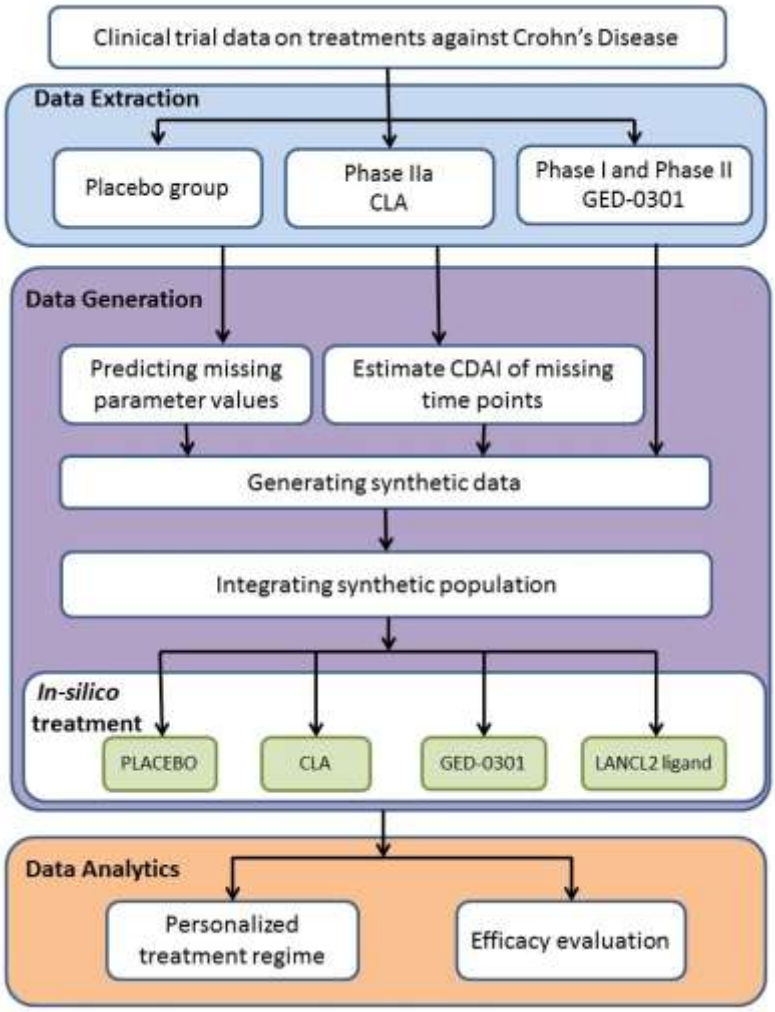


**Figure 4.1.** Study design overview. The study includes three steps. 1) Data Extraction. 2) Data Generation. 3) Data Analytics.

**Data Extraction**

Data from previously published phase IIa clinical trial (11) was used to develop a large virtual population for *in silico* experimentation. The clinical data incorporated de-identified patient information and CD biomarker measurements (i.e., cellular and molecular immunological readouts) prior to treatment, 6 weeks and 12 weeks after treatment as well as CDAI score at these three time points. There are 19 parameters measured during each time point. However, there are also missing value of parameters and a relatively small number of patients (11 patients) that underwent the treatment. In addition, this initial phase IIa clinical trial did not have a placebo group and all the patients received the treatment without discontinuation of their current treatment regime.

The second clinical dataset used in this study comprised patients that received a *Smad7* inhibitor – *Mongersen* (formerly GED-0301). The study by Monteleone *et al.* 2001 showed that a Smad7 inhibitor aided in restoring TGF-β1 signaling in chronic inflammatory bowel disease (IBD). TGF-β1 mainly functions as a negative regulator of T cell immune responses and signals to downstream target cells via a family of *Smad* proteins. In patients with IBD, there is an overexpression of Smad7 that further inhibits TGF-β1 induced signaling (27) thereby causing an increase in production of pro-inflammatory cytokines such as TNF-α, a main driver underlying inflammatory processes in IBD. Smad7 intracellular protein acts by binding to the TGF-β receptor, thereby preventing TGFβ signaling, making it an attractive therapeutic target for suppressing CD. The data used for *in silico* clinical study was extracted from the phase I clinical trial (28) that involved administration of *Mongersen* (GED0301) to 15 patients with active CD and phase 2 clinical trial (29) that was conducted in order to evaluate the efficacy of *Mongersen* in 166 patients for the treatment of active CD (30).

Additionally, clinical data for the placebo group were obtained from clinical trial studies on certolizumab pego (31) and GED-0301 (22). In the clinical trial study of certolizumab pego, CDAIs of patients receiving placebo were reported in terms of mean and standard deviation prior and after treatment. In the clinical trial study of *Mongersen*, CDAIs of patients receiving placebo were reported using median and range including minimum and maximum value; in that study, the distribution of patients receiving placebo treatment was biased toward lower initial CDAI scores. However, synthetic data generation was designed to create a balanced representative population by adjusting the sampling parameters.

**Data Generation**

There are four main steps for the Data Generation procedure; 1) estimating the missing values of parameters, 2) creating *in silico* population, 3) designing the clinical trial, and 4) providing treatment to the virtual patients.

**1. Estimating missing values**

The clinical dataset is high-dimensional because there are few patients (cases) and a larger parameter set (variables). Using an iterative process, an ANN model was optimized to predict the missing values for all patients. The iterative process (Figure 4.2) uses a subset of parameters randomly chosen to estimate the missing value. The process was repeated 100 times and average estimates were calculated. In addition, the entire process was repeated with different model parameters (the number of hidden nodes in the ANN model) and the values were averaged with the exclusion of extreme estimations. The estimation was performed in R using the neuralnet package (32). The method was optimized using a subset of the dataset. In the optimization process, a subset of dataset was selected with no missing values, 20 parameters were randomly removed and estimated using this iterative process. The mean and median differences between estimated values and expected values were 31% and 22% respectively. Different ANN models with varying number of hidden nodes were able to better estimate missing values depending on the range and variation of the parameters.

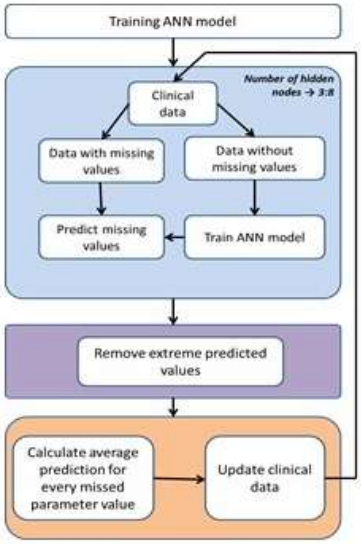


Algorithm:

PreditMissaingValue
For numberOfHiddenNodes = 3 : 8
NHN ← set number of hidden nodes
DF ← Full dataset
DF_ColNullWhole ← Subset of DF with missing values
DF_ColNonNull ← Subset of DF without missing values
For each column (Nullcol) in DF_ColNullWhole
For each missing value in Nullcol
For i = 1 : 100
RS ← Randomly select 5 columns from DF_ColNonNull
Merged ← Combine RS with Nullcol
TrainingSet ← rows in Merged without missing data
Build ANN model with selected number of hidden nodes
Predict the missing value using ANN model
Calculate the average value of 100 predictions
Update the missing value in the column Nullcol
Update the column Nullcol in DF
Update DF_ColNullWhole
For each missing value, calculate the average estimate by excluding the negative estimates (if any) and as well as the extreme scores.

**Figure 4.2.** Flow chart and algorithm used to estimate the missing values in clinical dataset.

**2. Creation of a synthetic CD patient population**

The dataset for a real patient population enrolled in the phase IIa clinical trial (11) was used to create the synthetic CD population. In particular, patients with mild to moderately

active CD (estimated CDAI > 150 - < 450) were screened for enrollment in the study. Patients were required to be on stable medications 2 months prior to entry and could not be on prednisone at the time of screening. Patients were allowed to continue their baseline CD medications with the exception of oral prednisone and oral dietary supplements. The virtual patients are created to represent family members of these real patients. Specifically, synthetic patients are to some extent similar to the real patients with slight differences in their features. This strategy ensures that synthetic patients have features that are supported by clinical cases. This is further explained by Figure 4.4. The complete dataset includes a range of cases: there are 30% of cases with a highest drop (>100) in the CDAI score, additional 30% have a lower drop in the CDAI score (>50), there are 30% of cases with no significant difference in their CDAI scores after 12 weeks of treatment; and finally, there are 10% of cases with a significant increase in CDAI score after treatment. Using each patient data as a seed entity, one parameter is randomly chosen and a random positive value (within a certain range) is added to that parameter. In addition, the remaining parameters are changed from their initial value using the relationship matrix (Figure 4.3). Positively relevant parameters are increased (by a random percentage), while negatively relevant parameters are decreased by a random percentage. This is further explained in Figure 4.4. The relationship matrix ensures that the random variations applied to generate the synthetic patient are biologically acceptable. For instance, a CD patient that is similar to a given real patient may more likely have a higher TNF-α and IFN-γ but lower TGFb1; in essence, TNF-α and IFN-γ are positively correlated, and both negatively correlated with TGFb1. Finally 1,100 virtual patients are created through this process (100 virtual patients for each real patient). The process is streamlined and number of virtual patients can expand without any technical impediment. Unlike the real population, the virtual population has no missing values; however, the disease activity scores have to be predicted since these are not randomly generated. This is possible, because clinical patient level data that includes biomarker levels as well as CDAI scores are available (11) and can be used to build models. In this study, the CDAI scores were predicted using Random Forest method (randomForest package in R (33)), similar to Algorithm 1. However, in this situation RF yields better results than ANN and therefore was selected as the preferred method. The

optimized parameters used for RF model are mtry=4 and ntree=250. In fact, we have previously shown that ANN and RF have comparable results for complex immunological systems; however, ANN can be faster for large networks (19). The RF model is trained using data of the 11 real patients from the CLA clinical trial (11).

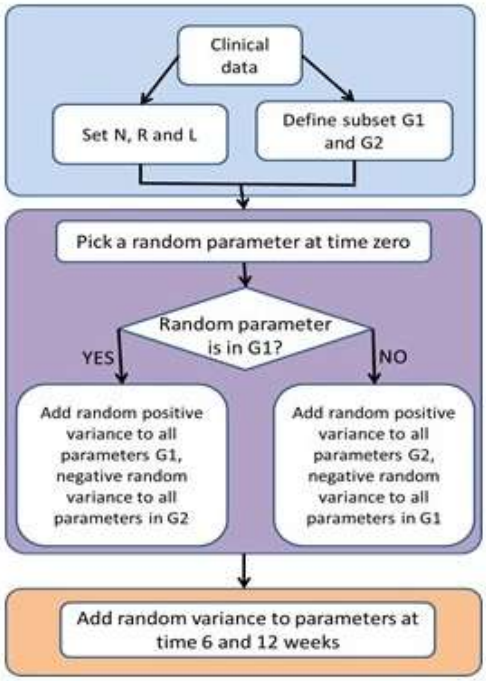


Algorithm:

GeneratingVirtualPatientPopulation
DF <- Clinical dataset
N <- set number of synthetic data created for each datum
R <- define the range of variance
L <- define the subset of parameters at T0
G1 <- define the subset of inflammatory parameters at T0
G2 <- define the subset of anti-inflammatory parameters at T0
SytheticPoulation <- define a matrix to save synthetic population
For i = 1 to number of row in DF
For j = 1 to N
RS <- randomly select one parameter from L
If RS in G1
Random variance added to par in G1 is positive, those in G2 is negative
else
Random variance added to par in G1 is negative, those in G2 is positive
For each parameter in G1/G2
Add a random variance
Add a random variance for the same parameter at T6 and T12

**Figure 4.3.** Flow chart and algorithm used for Generating a Synthetic CD Patient Population based on immunological parameter relationship matrix.

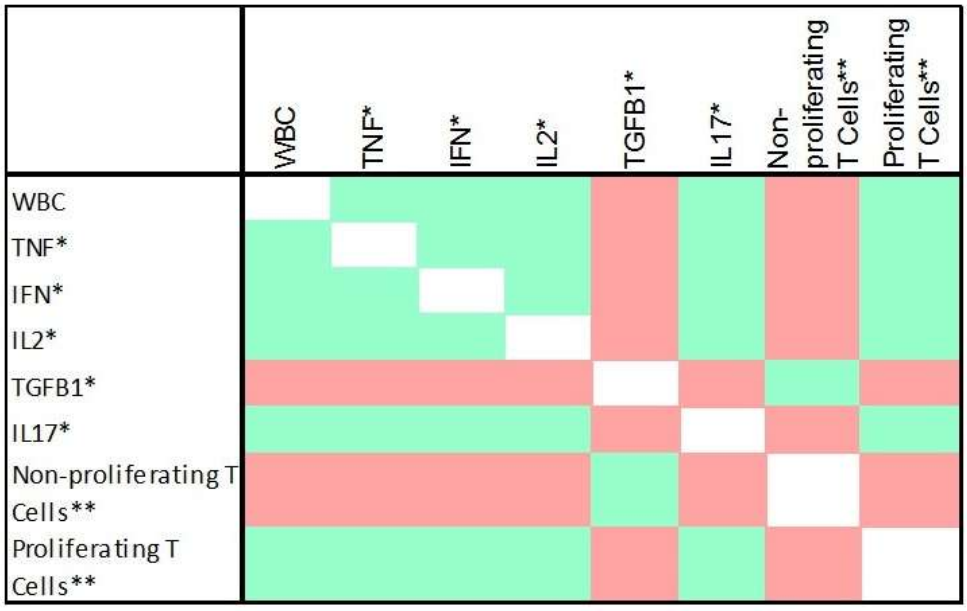

**Figure 4.4.** Parameter relationship matrix. Immunological parameters are used to create the synthetic population. The color of green indicates a positive relevance while the color of red represents negative relevance. The matrix is designed based on expert knowledge. * indicates CD4+ and CD8+ T cells; ** indicates CD3+, CD4+ and CD8+ T cells.

Virtual patients with placebo treatment were created based on the placebo data from two clinical trial studies. 1,000 CDAI scores were randomly generated, based on predefined mean and standard deviation or median and range, to represent disease activity index prior to treatment, 6 and 12 weeks following treatment. To assign CDAI scores of three time points to each virtual patient, the concept of moving window was applied (Figure 4.5). This step is crucial to generate patient data from population level data. The main assumption in this design is that patients that have higher than average initial score will also have higher than average initial score after treatment. However, because the windows can overlap between the different populations, the process will allow CDAI scores to slightly increase even after treatment for individual patients. This is shown in the five sub-panels of figure 4.5 (treatment time versus CDAI scores).

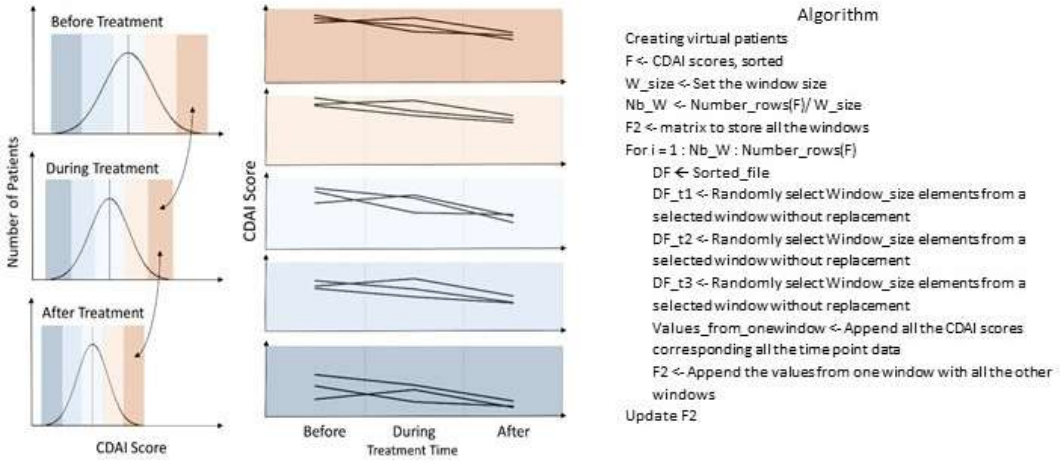


**Figure 4.5.** Assigning CDAIs at different time intervals to virtual patients based on population level data. First and second panels show a schematic representation and third panel describes the algorithm of the process; the code is implemented in R. The distributions at each of the time points as shown on the left were divided into the different colored windows. These windows are matched across the different time points, and one CDAI score is randomly selected from each group as shown by the windows of similar color connected by arrows to create a synthetic patient with three CDAI scores at their respective time points. Each connected data point on the line graph to the right represents one synthetic CD patient.

**3. Inclusion and exclusion criteria**

The inclusion and exclusion criteria are similar to the phase IIa clinical trial (11). In this *in silico* clinical trial, eighty percent of the patients enrolled have mild to moderately active CD (estimated CDAI > 150 - < 450), while 10% have an estimated CDAI score CDAI > 150 - < 150 (symptomatic remission), and 10% an estimated CDAI score CDAI > 450 - < 500 (Severe/Fulminant Disease). Patients are on stable medications two months prior to entry and could not be on prednisone at the time of screening. Patients were allowed to continue their baseline CD medications with the exception of oral prednisone and oral dietary supplements.

**4. *In silico* therapeutic interventions**

Four treatments (Placebo, CLA, GED-0301, and LANCL2 Ligand) were given to 10,000 virtual patients based on the working definition of CD activity corresponding to the computational equivalent to a Phase III clinical trial. Crohn's disease includes four levels. 1) *Symptomatic remission* CDAI <150; 2) *Mild to Moderate Disease* CDAI 150-220; 3) *Moderate to Severe Disease* CDAI 220-450; and 4) *Severe/Fulminant Disease* CDAI >450 (34). Initial CDAIs were randomly assigned to the 10,000 virtual patients following the ratio, 1:4:4:1, for the level of CD activity. Furthermore, *IFN-γ* and *TNF-α* are considered as molecular markers of CD, which are further confirmed by the PCA analyses on the clinical data from the CLA study (11). Thus, the efficacy of four treatments on CD could be indirectly reflected by how they could regulate *IFN-γ* and *TNF-α*, which is determined either by extracting information from publication or by predictions based on changes of CDAI scores. In the following section, the design of the four different *in silico* treatments is described (see Table 4.1). The simulation scores obtained following treatment, were then mapped to experimental scores prior to analysis of variance.

**Placebo:** The changes of *TNF-α* and *IFN-γ* led by placebo were predicted by using CDAIs of virtual patients. Machine learning procedure is especially valuable in this design due to the lack of mechanistic understanding on the effect that the placebo could

have on *TNF-α* and *IFN-γ* level. In particular, a random forest model was built for prediction of the two biomarkers. The placebo treatment causes the *IFN-γ* level to decrease by 17 percent; however, the *TNF-α* level shown a significant increase of 58 percent.

**CLA:** The two biomarkers, *TNF-α* and *IFN-γ*, were monitored in the clinical study of CLA (11). CLA is considered a nutritional intervention and the expected change in the levels of biomarkers could be less significant than more potent drugs. Nonetheless, the average decrease of *IFN-γ* level led by CLA is 24 percent; however, CLA caused an upregulation of *TNF-α* level by 25 percent.

**GED-0301**: The gut inflammation associated with CD is mainly characterized by the decreased activity of the immunosuppressive cytokine transforming growth factor *TGF-β1*. The increased level of *Smad7* that inhibits the *TGF-β1* receptor contributes mainly towards the decrease. Consequently, an antisense oligonucleotide *Smad7* inhibitor GED-0301 was designed for the phase 1 clinical trial wherein it was delivered primarily in the lumen of terminal ileum and right colon (28). The study provided us with valuable data regarding the pro-inflammatory cytokine levels of *IFN-γ*. A decrease of 30 percent in *IFN-γ* expressing cells was observed. The data for *TNF-α* levels was extrapolated from the phase 2 clinical trials(30), with 40mg of GED-0301, same antisense oligonucleotide used for the phase 1 trials. A decrease of 41 percent was observed in *TNF-α* expressed by the peripheral blood mononuclear cells.

**LANCL2 Therapeutics:** *LANCL2*, a potentially novel therapeutic target alternative for CD, can be modulated to reduce the levels of the two pro-inflammatory cytokines, *TNF-α* and *IFN-γ*. Data published in (25), using *LANCL2* ligands as a treatment regime on human peripheral blood mononuclear cells showed that the *IFN-γ* levels dropped by 75 percent and the *TNF-α* levels dropped by 55 percent following the treatment.

**Table 4.1:** The treatment design strategy.

| TREATMENT | TNF-A CHANGE (T0 TO T6) | IFN-Γ CHANGE (T0 TO T6) |
|---|---|---|
| **PLACEBO** | -0.58 | 0.17 |
| **LANCL2-LIGAND** | 0.55 | 0.75 |
| **GED-0301** | 0.41 | 0.3 |
| **CLA** | -0.25 | 0.24 |

**Data Analytics**

Statistical analyses were used to evaluate the efficacy of *LANCL2* ligands on virtual population with different severity level of Crohn's disease. Determination of statistically significant differences was made using analysis of variance (ANOVA) on changes of CDAIs, with $P < 0.05$. Two factors were considered in ANOVA test, treatments and initial CDAIs.

**4.4 Results**

Building a synthetic CD patient population from a small scale clinical trial resulted in generating 100 patients for each seed population for a total of 1,100 patients. A principal component analysis (see Figure 4.6) verified that the key biomarkers of the disease are captured from the larger *in silico* population, thus confirming the authenticity of the synthetic CD patients.

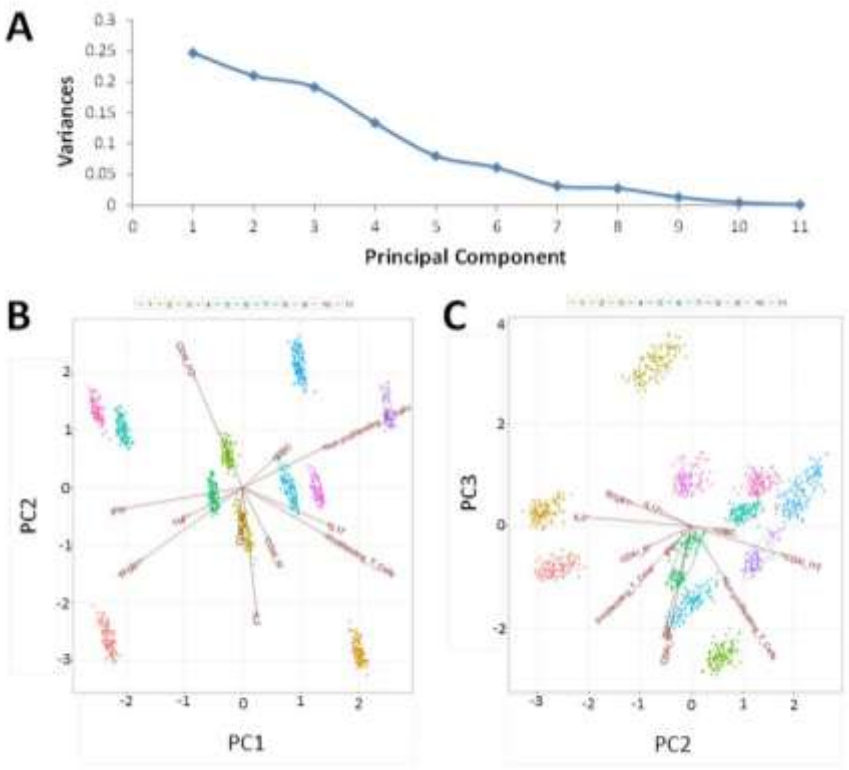


**Figure 4.6.** Principal Component Analysis (PCA) on synthetic population created based on clinical data from CLA study. A) Plot of the variances (y-axis) associated with the PCs (x-axis). B) Biplot of PC1 and PC2. The data are projected on PC1 and PC2, which show that IFN-γ plays an important role in explaining the variation on PC1. C) Biplot of PC2 and PC3. The data are projected on PC2 and PC3 showing that TNF-α plays an important role in explaining the variation on PC3. Clusters of data represent a synthetic CD population created from a seed patient group from the CLA clinical trial study.

A comparative analysis was performed on the 10,000 synthetic patients treated with four alternative therapies. Overall 20% of the patients are from initial CDAI score less than 150 or more than 450. The remaining 80% are from CDAI scores between 150 and 450. However, different treatment regimens show different efficacy based on the initial CDAI score. In the placebo group, the patients show significant differential response depending on their initial CDAI score. Specifically, the CDAI drop is lower for patients with moderate disease level (initial CDAI score of 150-220). See Figure 4.7.

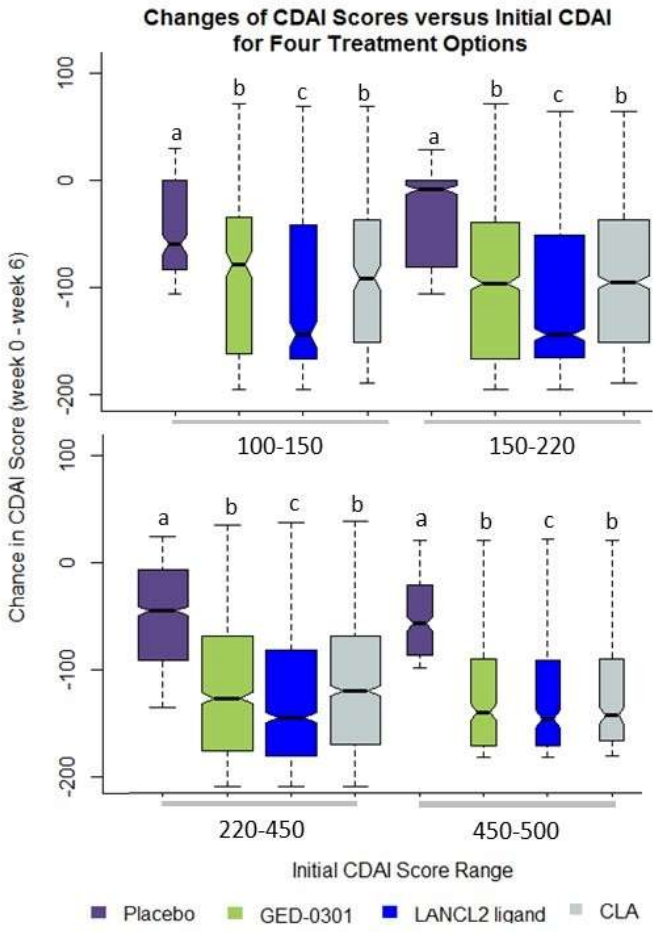


**Figure 4.7**. Changes of CDAIs during the first stage of treatment, led by four treatments strategies. Drop in CDAIs at week 6 was predicted for four treatments; LANCL2 Ligand, Placebo, CLA and GED-0301. Drop of CDAIs was plotted for four groups of patients with different levels of initial CDAIs. The width of the boxes is proportional to the square-roots of the number of patients in the groups. Across each CDAI range, the conditions that did and did not differ from one another are identified by subscripts. Those conditions that share a superscript letter (a, b, or c) did not differ from one another; those conditions that do not share a superscript were significantly different from one another ($P < .05$). Table 4.2 summarizes the statistical test results and shows significance between groups.

A two-way ANOVA was performed to analyze the effect of two factors, treatments (placebo, CLA, Smad7 therapeutics and LANCL2 therapeutics) and initial CDAIs, on the drop in CDAI. Furthermore, the interaction effect of treatments and initial CDAIs on drop in CDAI was also evaluated. The *P*-values for both treatments and initial CDAIs are less than 0.001, indicating that the kinds of treatments given to patients and the initial CDAIs of patients are both associated with how well a patient will respond to treatment.

The *P*-value for the interaction between treatments and initial CDAIs is 0.03, thus, indicating that the relationship between treatments and drop in CDAIs is dependent on the initial CDAIs.

Since ANOVA test was significant for both variables (treatments and initial CDAIs) and interaction effect between treatments and initial CDAIs was also present, Tukey test was further applied to test the main effect and interaction effect in pairwise comparisons. Results of Tukey test indicate that there are statistically significant ($P < 0.001$) pairwise differences between each treatment and placebo group. In addition, statistically significant ($P < 0.05$) pairwise differences also exist between higher and lower initial CDAIs groups except for 150-220 and 100-150. Tests on interaction effects show that treatments have statistically significant differences in their efficacy; in fact, the drop in CDAIs compared with placebo for all levels of initial CDAI ($P < 0.001$) are significant. Also, oral treatment with *LANCL2* ligand shows stronger effects than CLA and GED-0301 for patients with initial CDAIs between 150 and 220. Table 4.2 summarizes the statistical test results and shows significance between groups.

**Table 4.2:** Statistical analysis results comparing different treatment and initial CDAI range.

| STATISTICAL TEST | SIGNIFICANCE LEVEL (*P*-VALUE) |
|---|---|
| ANOVA: CDAI range | <2E-16 |
| ANOVA: Treatment | <2E-16 |
| ANOVA (2-way): CDAI range & treatment | 0.0301 |
| tukey multiple comparison test: ged-0301 & cla | 0.9637 |
| tukey multiple comparison test: LANCL2 & cla | 0.0000 |
| tukey multiple comparison test: placebo & cla | 0.0000 |
| tukey multiple comparison test: ged-0301 & lancl2 | 2E-07 |
| tukey multiple comparison test: PLACEBO & ged-0301 | 0.0000 |
| tukey multiple comparison test: placebo & LANCL2 | 0.0000 |

### 4.5 Discussion

Treatment options for patients with CD show limited efficacy and significant adverse side effects. In fact, the global CD market can be divided into five segments: 5-ASA,

Antibiotics, Biologics, Corticosteroids, and Immunomodulators. Even with today's aggressive treatments, still 75% of CD patients and 20-40% of UC patients cannot be effectively managed through medication and progress to needing surgery. Biologics seem to be a promising therapeutic option for severe cases of disease; however, many clinical studies have failed to provide a strong supporting evidence for further research. There is a continuous effort to provide a safer and more effective treatment that addressed the unmet clinical need of CD patients. Most clinical trials have used a 100 or 150 drop in the CDAI as quantitative measure of effectiveness. In addition to the CDAI scores, there is the new alternative, Patient Reported Outcomes (PRO), also known as health measures, which may represent a valuable tool to better understand the quality and efficacy of a given treatment (35, 36). PRO that are derived from CDAI diary items may be appropriate for use in clinical trials for CD. This practice could also represent tools that patients as well as medical teams can use to assess and track health over time and monitor changes. We have used published information on CDAI and immunological markers of disease to create a large synthetic population of CD patients. For this Phase III clinical trial, synthetic CD patients have then been randomized to placebo, CLA, GED-0301 or LANCL2 therapeutic interventions with oral routes of administration.

GED-0301 is an inhibitor of *Smad7*, which functions by restoring the *TGF-β*1 signaling in chronic IBD. The gut of patients affected with CD has high levels of *Smad7* that blocks the immune-suppressing activity of transforming growth factor *(TGF)-β1*. The blockage of the immune suppressive activity, thereby contributes towards increased levels of pro-inflammatory cytokines such as *IFN-γ* and *TNF-α*. *IFN-γ* and *TNF–α* being the major biomarkers in CD, are therefore indirectly targeted via *Smad7* inhibitor. The mechanism of action of *GED-0301* (antisense oligonucleotide - *Smad7* inhibitor) is the restoration of *TGF-β1* signaling, thereby suppressing the inflammatory cytokine production. The phase I and phase II clinical trials were based on the animal studies (37) wherein *Smad7* was knocked-down *in vivo* in mice with a *Smad7* antisense oligonucleotide, which attenuated the experimental colitis (37). The decrease in the percentage drops of *IFN-γ* and *TNF-α* from the human clinical studies were used in the data extraction process for this *in silico* clinical trial study. A recent Phase II clinical

study reported that the average drop in CDAI score following full treatment regimen (84 days) with 40 mg dose was 116 points (or 122 points at maximum dose of 160 mg); however, the median and range of CDAI score prior to treatment and following treatment were [223 – 368] and [16 – 436], this highlights that the drug can increase the CDAI score significantly in some cases. The results from our placebo-controlled, randomized, Phase III *in silico* clinical trial at 6 weeks following the treatment shows a positive correlation between the initial disease activity score and the drop in CDAI score. This observation highlights the need for precision medicine strategies for IBD.

Oral CLA supplementation was shown to modulate immune responses in patients with mild to moderately active CD (11). The CLA phase IIa clinical trial was based on a small number of patients; however, the quality and availability of data facilitated this larger *in silico* study. CLA is a nutritional intervention with anti-inflammatory properties (38, 39). However, oral CLA administration was shown to be well tolerated and suppressed the ability of peripheral blood T cells to produce pro-inflammatory cytokines, decreased disease activity and increased the quality of life of patients with CD. Overall, only one patient had an increase in CDAI score following treatment (<10%). The results from in *silico* clinical trials at 6 weeks post treatment also highlight a positive correlation between the initial disease activity score and the drop in CDAI score. In addition, this Phase III clinical trial highlights the potential of CLA as an adjunct nutritional intervention especially for the moderate/severe cases of CD. In fact, in the phase IIa clinical trials, the patients that responded the best to the intervention were those with initial CDAI > 220. However, the average CDAI score prior to the treatment was 245. The study could have been more successful if more severe cases had been enrolled.

IL-10 and TNF-α represent antagonistic functional behaviors during the onset of CD in the colon. IL-10 has an anti-inflammatory role and has been shown to down-regulate expression of MHC class II and B7 molecules, as well as IL-12 and IFN-γ production (40). In contrast, TNF-α is a pro-inflammatory marker involved in systemic inflammation and activation of pro-inflammatory mucosal cell subsets (41). Based on our preliminary results in mouse models of IBD, activation of the LANCL2 pathway upregulates the

levels of IL-10 in the colon while suppressing TNF-α colonic levels, both at the gene expression and cellular level in animal models and human cells (25). LANCL2 ligands can be a superior alternative treatment for CD patients. In fact, the results of the Phase III *in silico* clinical trial predict that LANCL2-based treatment can produce the significantly largest drop of CDAI scores of all treatments tested, consisting on an average drop of 126 points of CDAI for severe cases. Moreover, the results of this study suggest that the efficacy of LANCL2 therapeutics extends to all stages of disease. Thus, orally active, locally acting LANCL2-based drugs have the potential to disrupt the CD treatment paradigm.

Finally, the placebo results also show interesting and unexpected behavior. From this analysis, the placebo is most effective in patients with initial CDAI scores less than 150 or more than 220. Patients with mild to moderate disease levels tend to benefit least from the placebo effect. This is especially important since in some studies the distribution of patients in the placebo group can be biased and this may cause artifacts in the results. For instance, the number of patients with a severe disease activity could be lower than the number of patients with moderate disease activity level. Understanding the placebo effect is essential for disentangling drug effects from placebo effects, more truly capturing therapeutic efficacy in humans, and could possibly allow better designed clinical trials to maximize therapeutic outcomes and move towards informed precision medicine strategies guided by data (see a recent review (42)).

Future studies will investigate the therapeutic effects of longer-term therapeutic interventions. We will also expand the patient level data from existing clinical trials when such data become available. Given the importance of biologics in the current treatment paradigm for CD, we will also examine the effect of treating our synthetic population with biologics such as anti-*TNF-α* antibodies, as well as combinatorial interventions (i.e., nutritional adjuncts along with therapeutics) to the virtual patients for comparative analysis. For instance, we will identify possible interactions between diet, genetic makeup, microbiome populations, baseline medications, and response to treatment to advance personalized medicine interventions. Future studies will also apply multiscale

modeling by using ENISI MSM, a high-performance computing-driven tool with scalability of $10^9$-$10^{10}$ agents (43, 44), and in memory databases to integrate population level data with cellular and molecular procedural knowledge that explains response to treatment outcomes.

### 4.6 Acknowledgements

This work was supported by funds from the Nutritional Immunology and Molecular Medicine Laboratory (www.nimml.org).

### 4.7 References

1. Molodecky NA, Soon IS, Rabi DM, Ghali WA, Ferris M, Chernoff G, et al. Increasing incidence and prevalence of the inflammatory bowel diseases with time, based on systematic review. Gastroenterology. 2012;142(1):46-54 e42; quiz e30.
2. Baumgart DC, Sandborn WJ. Crohn's disease. Lancet. 2012;380(9853):1590-605.
3. Barrett JC, Hansoul S, Nicolae DL, Cho JH, Duerr RH, Rioux JD, et al. Genome-wide association defines more than 30 distinct susceptibility loci for Crohn's disease. Nature genetics. 2008;40(8):955-62.
4. Papadakis KA. Chemokines in inflammatory bowel disease. Current allergy and asthma reports. 2004;4(1):83-9.
5. Marks DJ. Defective innate immunity in inflammatory bowel disease: a Crohn's disease exclusivity? Current opinion in gastroenterology. 2011;27(4):328-34.
6. Lawrance IC, Radford-Smith GL, Bampton PA, Andrews JM, Tan PK, Croft A, et al. Serious infections in patients with inflammatory bowel disease receiving anti-tumor-necrosis-factor-alpha therapy: an Australian and New Zealand experience. Journal of gastroenterology and hepatology. 2010;25(11):1732-8.
7. Khan KJ, Dubinsky MC, Ford AC, Ullman TA, Talley NJ, Moayyedi P. Efficacy of immunosuppressive therapy for inflammatory bowel disease: a systematic review and meta-analysis. The American journal of gastroenterology. 2011;106(4):630-42.
8. Auer K, Trachter R, Van den Bogaerde J, Bassaganya-Riera J, Sorrentino D. Translational research and efficacy of biologics in Crohn's disease: a cautionary tale. Expert review of clinical immunology. 2014;10(2):219-29.
9. Danese S. New therapies for inflammatory bowel disease: from the bench to the bedside. Gut. 2012;61(6):918-32.
10. Rutgeerts P, Vermeire S, Van Assche G. Biological therapies for inflammatory bowel diseases. Gastroenterology. 2009;136(4):1182-97.
11. Bassaganya-Riera J, Hontecillas R, Horne WT, Sandridge M, Herfarth HH, Bloomfeld R, et al. Conjugated linoleic acid modulates immune responses in patients with mild to moderately active Crohn's disease. Clinical nutrition. 2012;31(5):721-7.
12. Romero K, Ito K, Rogers JA, Polhamus D, Qiu R, Stephenson D, et al. The future is now: model-based clinical trial design for Alzheimer's disease. Clinical pharmacology and therapeutics. 2015;97(3):210-4.

13. Brown D, Namas RA, Almahmoud K, Zaaqoq A, Sarkar J, Barclay DA, et al. Trauma in silico: Individual-specific mathematical models and virtual clinical populations. Sci Transl Med. 2015;7(285):285ra61.
14. Buczak AL, Babin S, Moniz L. Data-driven approach for creating synthetic electronic medical records. BMC medical informatics and decision making. 2010;10:59.
15. Eekhout I, de Boer MR, Twisk JWR, de Vet HCW, Heymans MW. Missing Data A Systematic Review of How They Are Reported and Handled. Epidemiology. 2012;23(5):729-32.
16. Wendelsdorf K, Bassaganya-Riera J, Hontecillas R, Eubank S. MODEL OF COLONIC INFLAMMATION: IMMUNE MODULATORY MECHANISMS IN INFLAMMATORY BOWEL DISEASE. Journal of theoretical biology. 2010;264(4):1225-39.
17. Carbo A, Hontecillas R, Kronsteiner B, Viladomiu M, Pedragosa M, Lu P, et al. Systems modeling of molecular mechanisms controlling cytokine-driven CD4+ T cell differentiation and phenotype plasticity. PLoS computational biology. 2013;9(4):e1003027.
18. Carbo A, Hontecillas R, Andrew T, Eden K, Mei Y, Hoops S, et al. Computational modeling of heterogeneity and function of CD4+ T cells. Frontiers in cell and developmental biology. 2014;2:31.
19. Lu P, Abedi V, Mei Y, Hontecillas R, Hoops S, Carbo A, et al. Supervised learning methods in modeling of CD4+ T cell heterogeneity. BioData Min. 2015;8:27.
20. Lu P, Abedi V, Mei Y, Hontecillas R, Philipson C, Hoops S, et al. Supervised Learning with Artificial Neural Network in Modeling of Cell Differentiation Process. In: QN T, Arabnia H, editors. Emerging Trends in Computational Biology, Bioinformatics, and Systems Biology. 1st ed: Elsevier; 2015. p. 674.
21. Clermont G, Bartels J, Kumar R, Constantine G, Vodovotz Y, Chow C. In silico design of clinical trials: a method coming of age. Critical care medicine. 2004;32(10):2061-70.
22. Monteleone G, Neurath MF, Ardizzone S, Di Sabatino A, Fantini MC, Castiglione F, et al. Mongersen, an oral SMAD7 antisense oligonucleotide, and Crohn's disease. N Engl J Med. 2015;372(12):1104-13.
23. Lu P, Hontecillas R, Philipson CW, Bassaganya-Riera J. Lanthionine synthetase component C-like protein 2: a new drug target for inflammatory diseases and diabetes. Current drug targets. 2014;15(6):565-72.
24. Magnone M, Sturla L, Jacchetti E, Scarfi S, Bruzzone S, Usai C, et al. Autocrine abscisic acid plays a key role in quartz-induced macrophage activation. FASEB journal : official publication of the Federation of American Societies for Experimental Biology. 2012;26(3):1261-71.
25. Carbo A. HR, Cooper J., Gandour R., Ehrich M., Bassaganya-Riera J. Lanthionine Synthetase C-like Receptor 2 (LANCL2): A Novel Therapeutic Target for Inflammatory Bowel Disease. Gastroenterology. 2015;148(4):S686-S7.
26. Plevy SE, Landers CJ, Prehn J, Carramanzana NM, Deem RL, Shealy D, et al. A role for TNF-alpha and mucosal T helper-1 cytokines in the pathogenesis of Crohn's disease. J Immunol. 1997;159(12):6276-82.

27. Nakao A, Afrakhte M, Morn A, Nakayama T, Christian JL, Heuchel R, et al. Identification of Smad7, a TGFβ-inducible antagonist of TGF-β signalling. Nature. 1997;389(6651):631-5.
28. Monteleone G, Fantini MC, Onali S, Zorzi F, Sancesario G, Bernardini S, et al. Phase I clinical trial of Smad7 knockdown using antisense oligonucleotide in patients with active Crohn's disease. Molecular Therapy. 2012;20(4):870-6.
29. Magnone M, Ameri P, Salis A, Andraghetti G, Emionite L, Murialdo G, et al. Microgram amounts of abscisic acid in fruit extracts improve glucose tolerance and reduce insulinemia in rats and in humans. The FASEB Journal. 2015.
30. Monteleone G, Neurath MF, Ardizzone S, Di Sabatino A, Fantini MC, Castiglione F, et al. Mongersen, an oral Smad7 antisense oligonucleotide, and Crohn's disease. New England Journal of Medicine. 2015;372(12):1104-13.
31. Sandborn WJ, Schreiber S, Feagan BG, Rutgeerts P, Younes ZH, Bloomfield R, et al. Certolizumab pegol for active Crohn's disease: a placebo-controlled, randomized trial. Clinical Gastroenterology and Hepatology. 2011;9(8):670-8. e3.
32. Günther F, Fritsch S. neuralnet: Training of neural networks. The R journal. 2010;2(1):30-8.
33. Liaw A, Wiener M. Classification and regression by randomForest. R news. 2002;2(3):18-22.
34. Lichtenstein GR, Hanauer SB, Sandborn WJ. Management of Crohn's disease in adults. The American journal of gastroenterology. 2009;104(2):465-83.
35. Khanna R, Zou G, D'Haens G, Feagan BG, Sandborn WJ, Vandervoort MK, et al. A retrospective analysis: the development of patient reported outcome measures for the assessment of Crohn's disease activity. Aliment Pharmacol Ther. 2015;41(1):77-86.
36. Williet N, Sandborn WJ, Peyrin-Biroulet L. Patient-Reported Outcomes as Primary End Points in Clinical Trials of Inflammatory Bowel Disease. Clin Gastroenterol H. 2014;12(8):1246-+.
37. Boirivant M, Pallone F, Di Giacinto C, Fina D, Monteleone I, Marinaro M, et al. Inhibition of Smad7 With a Specific Antisense Oligonucleotide Facilitates TGF-β1–Mediated Suppression of Colitis. Gastroenterology. 2006;131(6):1786-98.
38. Bassaganya-Riera J, Reynolds K, Martino-Catt S, Cui Y, Hennighausen L, Gonzalez F, et al. Activation of PPAR gamma and delta by conjugated linoleic acid mediates protection from experimental inflammatory bowel disease. Gastroenterology. 2004;127(3):777-91.
39. Bassaganya-Riera J, Hontecillas R. CLA and n-3 PUFA differentially modulate clinical activity and colonic PPAR-responsive gene expression in a pig model of experimental IBD. Clinical nutrition. 2006;25(3):454-65.
40. van Deventer SJ, Elson CO, Fedorak RN. Multiple doses of intravenous interleukin 10 in steroid-refractory Crohn's disease. Crohn's Disease Study Group. Gastroenterology. 1997;113(2):383-9.
41. Nielsen OH. New strategies for treatment of inflammatory bowel disease. Frontiers in medicine. 2014;1:3.
42. Colagiuri B, Schenk LA, Kessler MD, Dorsey SG, Colloca L. The placebo effect: From concepts to genes. Neuroscience. 2015;307:171-90.

43. Abedi V, Hontecillas R, Hoops S, Carbo A, Lu P, Philipson C, et al. ENISI Multiscale modeling of mucosal immune responses driven by high performance computing

IEEE International Conference on Bioinformatics and Biomedicine (BIBM); Nov 9-12, 2015; Washington, D.C.2015. p. in press.
44. Mei Y, Abedi V, Carbo A, Zhang X, Lu P, Philipson C, et al. Multiscale modeling of mucosal immune responses. BMC Bioinformatics. 2015;16 Suppl 12:S2.

## Chapter 5. Conclusions

The LANCL protein family represents an evolutionary adaptation of a prokaryotic enzyme responsible for intramolecular thioether formation into a regulatory protein that controls mammalian signal transduction, neural and immunoregulatory processes. LANCL2 is required for binding of ABA and other small molecules to immune and pancreatic cells for the transduction of the LANCL2 ligand signaling into cell-specific functional responses that result in immune modulatory and anti-diabetic effects. The therapeutic functions of LANCL2 have been identified, including increasing cellular sensitivity to the anticancer drug and mediating inflammation in different cellular and environmental conditions, anti-diabetic, and immune modulatory actions. The novel regulatory mechanism of the LANCL2 pathway includes intracellular cAMP elevation and activation of protein kinase A, but many downstream signals remain to be discovered. Our case of LANCL2-based drug discovery has been presented, which supports the feasibility of developing novel therapeutics targeting LANCL2 (1).

In Chapter 2, a three-dimensional structural model of LANCL2 was built to identify the binding site of ABA in LANCL2. We generated the model of LANCL2 by homology modeling, to which ABA was docked. Furthermore, pioglitazone and rosiglitazone bound to the same site as ABA on LANCL2. On the basis of these findings, we propose a novel mechanism by which PPAR γ agonists can elicit their biological effects (2).

The studies described in Chapter 3 employed an integrated drug discovery pipeline consisting of molecular modeling approaches followed by experimental validation. We performed large-scale screening of compound libraries based on predicted binding to an LANCL2 binding site that was obtained from Chapter 2. NSC61610, the top ranked lead compound based on binding free energy, significantly ameliorated experimental IBD in mice in a LANCL2- and PPAR γ-dependent manner. These results confirm that LANCL2 is a novel therapeutic target for inflammatory diseases and NSC61610 is a potential new drug (3).

In Chapter 4, LANCL2-based treatment identified from the Chapter 3 was tested using *in silico* clinical studies. Advanced machine learning methods were used to generate virtual patients based on data from clinical studies on CD. In particular Artificial Neural Network and Random Forest Models are built from clinical data and used to generate population level features. Treatment regimens were also designed based on clinical data and applied to the large virtual population to quantify and compare different treatments in the context of a randomized, placebo-controlled Phase III *in silico* clinical trial, which indicates that LANCL2 ligands can be a superior alternative treatment for CD patients (4).

**Reference**


1. Lu P, Hontecillas R, Philipson CW, Bassaganya-Riera J. Lanthionine synthetase component C-like protein 2: a new drug target for inflammatory diseases and diabetes. Current drug targets. 2014;15(6):565-72.
2. Lu P, Bevan DR, Lewis SN, Hontecillas R, Bassaganya-Riera J. Molecular modeling of lanthionine synthetase component C-like protein 2: a potential target for the discovery of novel type 2 diabetes prophylactics and therapeutics. Journal of molecular modeling. 2011;17(3):543-53.
3. Lu P, Hontecillas R, Horne WT, Carbo A, Viladomiu M, Pedragosa M, et al. Computational modeling-based discovery of novel classes of anti-inflammatory drugs that target lanthionine synthetase C-like protein 2. PloS one. 2012;7(4):e34643.
4. Abedi V[1], Lu P[1], Hontecillas R, Verma M, Vess G, Philipson CW, et al. Phase III Placebo-Controlled, Randomized Clinical Trial with Synthetic Crohn's disease Patients to Evaluate Treatment Response. Emerging Trends in Computational Biology, Bioinformatics, and Systems Biology-–Systems & Applications: Elsevier; In Press.